UNLEASHING THE PROPER MOTIONS:

REVOLUTION IN THE INNER GALAXY

Felipe Eduardo Gran Merino

UNLEASHING THE PROPER MOTIONS: REVOLUTION IN THE INNER GALAXY

BY

Felipe Eduardo Gran Merino

Thesis submitted to the Faculty of Physics at
Pontificia Universidad Católica de Chile in partial fulfillment
of the requirements for the degree of *Doctor of Philosophy*

Thesis Advisor

Manuela Zoccali

Thesis Co-advisor

Ivo Saviane

Santiago de Chile, February 2022

PONTIFICIA
UNIVERSIDAD
CATÓLICA
DE CHILE

FACULTAD DE FÍSICA

INSTITUTO DE ASTROFÍSICA

UNLEASHING THE PROPER MOTIONS: REVOLUTION IN THE INNER GALAXY

BY

Felipe Eduardo Gran Merino

Members of the Committee

Manuela Zoccali	(PUC, MAS)
Ivo Saviane	(ESO Chile)
Márcio Catelan	(PUC, MAS)
Julio Chanamé	(PUC)
Ricardo R. Muñoz	(UChile)

Santiago de Chile, February 2022

ACKNOWLEDGEMENTS

To everyone who made this possible.

CONTENTS

LIST OF TABLES

LIST OF FIGURES

ABSTRACT

Globular clusters (GCs) are dense agglomerations of stars that were formed roughly at the same time and constitute an important part of galaxies over the full mass range. The presence of several stars with a range of mass but the same age and distance allow us to measure the latter two quantities, which would be impossible for individual stars. Therefore, they are key tracers of the structure, time of formation and chemical composition of the Galaxy as a whole, and of its individual components.

GCs were discovered and catalogued principally through visual inspection of astronomical images. By this method, however, some of the low mass ones were lost. In the inner region of the Milky Way (the inner disk and bulge), characterised by large extinction and crowding, there are reasons to believe that only the brightest clusters have been detected. Precisely these GCs in the inner Galaxy, though, are crucial to decipher the early stages of our Galaxy, since they are a group that was born *in-situ* and have evolved with the Milky Way across cosmic time.

Recently, upon extensive studies on a star-by-star basis, GCs turned out to be much less homogeneous than previously thought, in terms of chemical abundances and, probably, age of individual stars. They therefore depart from the historical concept of "simple stellar populations".

In order to both detect new low mass GCs in regions with a high density of field stars, and to study internal dispersion in age and chemical composition of stars in known GCs, it is crucial to assess the membership of a given star to the cluster or to the field. By the definition of a cluster as a group of stars born together and still bound by gravity, the only way to establish the existence of a cluster and assess the membership of a given star to it, is by means of kinematics. A cluster exist as such only if a group of stars move together in space. This is why we address the study of GCs by means of proper motions.

Initially, the main goal of this thesis was the analysis of APOGEE high-resolution stellar spectra of the innermost parts of the Milky Way, as part of a Chilean contributed

programme to the SDSS-IV survey. By characterising the velocity dispersion of the sample in addition to the precise metal content and elemental abundance determinations, we would be able to make links within the heart of the Milky Way to its surroundings with a statistical significance not seen before. Unfortunately, the observations were not carried out in time for this thesis, and for three years in a row we clouded out. Because of this reason during the first year of the thesis project, I was dedicated to get familiar with the APOGEE data. This exercise resulted in a publication related to the globular cluster NGC 6544. In the meantime, the second data release of the Gaia catalogue was published and motivated by the lack of intermediate- and small-size globular clusters towards the Galactic bulge, I started to modify an existent clustering algorithm in order to detect at the same time all the known clusters. Then the primary goal of this thesis switched to confirm literature cluster candidates and search for new globular clusters towards the Galactic bulge area using data mining (clustering) algorithms. A more complete sample of globular clusters belonging to the bulge would allow us to put new constraints on the cluster survivability within a hostile environment like the inner Galaxy.

Within the framework of this thesis, five new globular clusters were found and characterised in terms of their positions, complete phase-space motions and metal content. Orbital properties for all of them were determined, describing which substructure from the early Milky Way they belong to. Two were classified as bulge members and three as halo clusters with distances up to 14 kpc behind the Galactic centre. Additionally, all but two of the globular cluster candidates present in the literature towards the Galaxy bulge were discarded for dynamical reasons. Finally, a few open clusters not present in any catalogue up to date were isolated from field stars and analysed.

We conclude that an automatic implementation of the clustering algorithm is an efficient way to search for clusters in the multidimensional space created by sky positions, proper motions and magnitudes. Although the algorithm is conceptually simple to understand and implement, we discovered and characterised globular clusters towards the Milky Way bulge for the first time. We uncovered a new population of globular clusters buried in the inner parts of the Galaxy that survived its accretion, which could be one of the keys to studying the early stages of the Milky Way. Finally, within the data-dominated Gaia

era already taking place, these studies are crucial to establish which algorithms are more efficient dealing with huge amounts of data, and what kind of filters and parameters are preferred to find clusters. In the long term, we hope to answer the question of how many globular clusters there are in the Galaxy.

RESUMEN

Los cúmulos globulares son densas aglomeraciones de estrellas que fueron formadas aproximadamente al mismo tiempo y constituyen una parte importante galaxias en todo el espectro de masas. La presencia de estrellas de distinas masas pero a la misma edad y distancia nos ha permitido medir estas dos cantidades, tarea imposible para estrellas individuales. Por lo tanto, ellas son trazadoras cruciales de la estructura, tiempo de formación y composición química de la Galaxia entera, y sus componentes individuales.

Cúmulos globulares fueron descubiertos y catalogados principalmente en imágenes astronómicas a través de inspección visual. Por este método, sin embargo, algunos de los cúmulos de baja masa no fueron descubiertos. En las regiones centrales de la Vía Láctea (disco interno y bulbo), caracterizadas por grandes cantidades de extinción y multitud de estrellas, hay razones para creer que sólo los cúmulos más brillantes han sido detectados. Precisamente estos cúmulos globulares en hacia el centro de la Galaxia, y aunque son cruciales para decifrar las etapas tempranas de la Galaxia, ya que ellos nacieron *in-situ* y han evolucionado con la Vía Láctea todo este tiempo.

Recientemente, estudiando exhaustivamente una a una las estrellas, los cúmulos globulares han resultado mucho menos homogéneos y simples de lo que se tenía inicialmente, ya sea en términos de abundancias químicas y probablemente edad de estrellas individuales. Ellos entonces salen del concepto histórico de lo que se denominó una "población estelar simple".

Para detectar nuevos cúmulos globulares de baja masa en regiones con una densidad estelar de estrellas de campo alta además de estudiar su dispersión interna en edad y composición química de estrllas de cúmulos globulares conocidos, es crucial evaluar la pertencia de una estrella dada al campo o al cúmulo en cuestión. Por definición un cúmulo de estrellas que nacen como un grupo están unidas por gravedad, y la única manera de establecer la existancia de un cúmulo es por medio de la dináminca de ellas. Un cúmulo sólo existe como tal si sus estrellas se mueven juntas en el espacio. Es por esto que analizamos

y estudiamos los cúmulos globulares por medio de sus movimientos propios.

Inicialmente el objetivo principal de esta tesis se centraba en el análisis de espectros APOGEE de alta resolución en las partes centrales de la Vía Láctea, como parte de un proyecto Chileno contribuído al survey SDSS-IV. Caracterizando su velocidad de dispersión, en conjunto con la metalicidad y abundancias químicas de cada estrella esperábamos conectar el corazón de nuestra Galaxia con sus otros componentes con una significancia estadística nunca vista con anterioridad para esta zona. Desafortunadamente, las observaciones no se realizaron a tiempo, ya que por tres años consecutivos se nubló en los días asignados. Por esta razón, y durante el primer año de esta tesis se dedicó a familiarizarme con los datos de APOGEE, dando lugar al estudio del cúmulo globular NGC 6544. Durante este mismo período se hizo publica la segunda entrega del survey Gaia, lo que derivó en el estudio de cúmulos globulares de tamaño intermedio y pequeño localizados hacia el bulbo Galáctico.

Se comenzó por modificar un algoritmo de agrupamiento automático para detectar todos los cúmulos al mismo tiempo. Es así que luego el objetivo principal cambió a confirmar confirmar cúmulos globulares de la literatura además de buscar nuevos dentro del área delimitada por el bulbo Galáctico usando algoritmos de minería de datos. Una muestra más completa de estos cúmulos nos permitirá colocar nuevos límites en cómo sobrevivieron en este hostil ambiente como lo son las partes centrales de la Vía Láctea. Dentro del marco de esta tesis, cinco nuevos cúmulos globulares fueron encontrados y caracterizados en térmios de sus posiciones, sus velocidades en tres dimensiones y su metalicidad. Parámetros orbitales para todos ellos fueron determinados, describiendo también de qué subestructura que formó la Vía Láctea pertenecen. Dos de estos cúmulos fueron casificados pertenecientes al bulbo y tres al halo, con distancias que llegan hasta los 14 kpc detrás del centro Galáctico. Adicionalmente, todos menos dos candidatos a cúmulo globular presentes en la literatura dentro del área estudiada fueron descartados por razones dinámicas. Varios cúmulos abiertos no presentes en otros catálogos también fueron descubiertos y analizados. Concluímos que la implementación automática del algoritmo de agrupamiento es una manera eficiente de buscar cúmulos en el espacio multidimensional creado por sus posiciones en el cielo, sus movimientos propios y magnitudes o brillo

medido. Pese a que el algoritmo es conceptualmente simple de entender e implementar, se han descubierto y caracterizado cúmulos globulares ubicados hacia el bulbo de la Vía Láctea. Demostramos que una nueva población de cúmulos globulares que sobrevivió este tiempo está enterrada en las partes centrales de la Galaxia, pudiendo ser una de las varias claves que tendremos para estudiar las etapas tempranas de la Vía Láctea. Finalmente, y dentro de la era dominada por los datos del satélite Gaia, estos estudios son cruciales para sentar precedente a futuros astrónomos de qué algoritmos fueron más eficientes analizando grandes cantidades de datos, qué tipo de filtros y parámetros fueron preferidos para encontrar cúmulos y en un tema relevante astrofísicamente hablando, cuál es el número total de cúmulos globulares en la Galaxia.

1

Introduction

1.1 The Milky Way in motion

Astrometry is defined as the astronomical discipline that studies the changes in the positions of celestial objects. Even before the invention of the telescope, humans have realised that the daily changes in the sky are driven by Earth processes like rotation and translation (Perryman, 2012). However, with the steady improvement of the telescopes and their associated instruments, preciser measurements have possibly reached uncertainties within the microarcsecond regime. Since the confirmation and measurement of the first proper motion (Halley, 1717), several observational efforts have been executed from the ground and space to deliver as much information as possible to study the nearby stars.

A massive improvement was accomplished by the Hipparcos satellite (*The HIPPAR-COS and TYCHO catalogues. Astrometric and photometric star catalogues derived from the ESA HIPPARCOS Space Astrometry Mission* 1997) increasing the number of available measurements of stellar proper motions, limited at that time to only ground-based observations from over 8.000 samples (van Altena et al., 1995) to more than 117.950 at the end of its mission. From there on, only incredible achievements have been made to explore the dynamics of the Milky Way stars. Initially limited to the nearby stars within the Solar neighbourhood, but then reaching stars up to the Magellanic clouds and beyond. The Gaia satellite (Gaia Collaboration, Brown, et al., 2021) has dramatically contributed to this expanded coverage with proper motions, allowing to performing studies from Solar system discoveries to distant catalogues of galaxies (Brown, 2021).

1.2   The Galaxy evolution told by its globular clusters

When trying to observe and understand the galaxy evolution, globular clusters are one of the most valuable stellar tracer available. Specifically in our Galaxy, their location within the Milky Way allows us to derive and constrain ages, masses and distances with great precision, being the primary laboratory of stellar evolution, including its chemical evolution and enrichment processes.

The contribution of globular clusters to the Milky Way stellar content is indisputable. A wide variety of numerical simulations (Kruijssen, 2019; Kruijssen et al., 2019a; Carlberg, 2020, and references therein) show that most of the proto-globular clusters stars have been dissolved in the inner Galaxy (Baumgardt et al., 2019). From the observational point of view, it is clear that the properties of nowadays globular clusters differ from those of their progenitors formed at high redshift (Renzini, 2017; Carlberg, 2020). A similar hypothesis is needed to explain several observed features related to the multiple stellar populations in globular clusters, whereby the very first generation of stars must have been much more massive than currently observed, to enrich the subsequent generations (see, e.g. Bastian and Lardo, 2018; R. A. Gratton et al., 2019, for recent reviews).

On a similar observational topic, globular clusters can be used to trace the different components assembled during the history of our Galaxy. Since the work of D. A. Forbes and Bridges (2010), a tentative separation was proposed trying to classify globular clusters (Leaman et al., 2013) by their origin using age and metallicity measurements. Various groups were later confirmed using dynamical and chemical information of the whole set of available globular clusters (Massari et al., 2019; Myeong et al., 2018). These groups can be broadly separated by one simple orbital criteria: the accreted and *in situ* components. The first one comprises those globular clusters formed within dwarf galaxies, then accreted by the Milky Way (Mackey and Gilmore, 2004; Myeong et al., 2019). One of the most important implications of these results is that all of the bulge and disk globular clusters

comprise the *in situ* component that evolved with the Galaxy. They have an essential role in the characterisation of the Milky Way formation, as they can trace the fossil record of its early stages (Barbuy et al., 2018; Zoccali, 2019).

1.3 Opening the Box of Pandora: multiple stellar populations of globular clusters

Considered to be "simple stellar populations", globular clusters have revealed a much more complex composition of their member stars. In-depth photometrical and spectroscopic analysis of larger samples of stars per cluster allows differentiating one or more stellar generations within a large group of globular clusters. Each generation with its own characteristic star-to-star abundance variations in both light- and heavy-elements that even varies within similar globular clusters (Gratton et al., 2012; Bastian and Lardo, 2018, and references therein). These multiple populations within a globular cluster refer basically to a first (or primordial) and at least a second generation of stars (see Bellini et al., 2017, for the extreme case of 15 sub-populations). Theoretically, the first generation pollutes the second one with processed material, and in this way, different sub-populations arise in the cluster. The composition of the second group or generation varies almost at an individual cluster level, determining the presence of several sequences in colour-magnitude diagrams, as well as light-element variations within the clusters (C, N, O, Na, Mg, Al, Si, among other elements, see Bastian and Lardo, 2018; R. A. Gratton et al., 2019, for recent reviews).

In what follows, we will focus on the light-element variations, since they appear on a broader range of clusters. Iron spread, on the other hand, is limited to a few massive clusters that we will not study on this thesis (Carretta et al., 2009a, and references therein). We will enumerate and briefly describe the most common abundance trends and their corresponding chemical reactions that are present in clusters with multiple stellar populations for the near-infrared APOGEE spectra:

- Magnesium-Aluminium (Mg-Al) cycle: is a complex set of proton capture reactions (Prantzos et al., 2007; Carretta et al., 2009b; Cassisi and Salaris, 2013). This cycle needs high temperatures to trigger ($\sim$ 50 MK), the reason why the anticorrelation between Mg and Al cannot occur inside low-mass stars. Massive enough stars are thought to be the cause of producing and transporting the observed pattern into the surface of low-mass red giant branch stars (Renzini et al., 2015; Bastian and Lardo, 2018).

- Carbon-Nitrogen anticorrelation: this observed abundance pattern is the product of the so-called CNO cycle that happens in the stellar interiors. This process depletes C and O and enhances N while the H is burning (Cassisi and Salaris, 2013). These products may be carried to the upper stellar layers by extra mixing phenomenon along the red-giant branch or due to other mechanisms like winds of high-mass asymptotic giant branch.

- The Sodium-Oxygen anticorrelation: this prominent feature is one of the first to be analysed in detail with statistical significance across many globular clusters (Gratton et al., 2004; Carretta et al., 2009b). It originates with the combination of both the CNO cycle while burning, simultaneously, the products of the Neon-Sodium cycle to increase the Sodium concentration. These cycle combinations require lower temperatures than the Magnesium-Aluminium cycle (around 40 MK). They are only efficient in intermediate-mass stars during the thermal pulses of the asymptotic giant branch stage. However, it can also be achieved sub-optimally at the bottom of the convective envelope in red-giant branch stars.

- Other important elements are Potassium, an odd-Z element produced by proton capture reactions. Nevertheless, its temperature requirement is so high (around 120-180 MK) that it cannot be produced in low-mass atmospheres (Ventura et al., 2012; Iliadis et al., 2016). Calcium will also be analysed, and the only significant contribu-

tion of its element comes from supernovae explosions, therefore not affected by the H-burning processes, nor other stellar polluters. Finally, Cerium and Neodymium, two neutron-capture elements, can only be produced in burning shells of massive stars or during the thermal pulses of asymptotic giant branch stars (Sneden et al., 2008; Bisterzo et al., 2011; Bisterzo et al., 2014).

1.4 Proper motions as a tool to isolate different stellar populations

During the last few years, the Gaia satellite has revolutionised our understanding of the Milky Way, giving crucial dynamical information (proper motions) to more than 1.8 billion stars in the sky. The proper motions have been used in a extremely wide variety of ways to analyse every piece of sky available. Enhanced with the last two data releases (Lindegren et al., 2018; Gaia Collaboration, Brown, et al., 2018; Lindegren et al., 2021; Gaia Collaboration, Brown, et al., 2021), several key discoveries have been made thanks to Gaia, namely:

- Discovery of a major Milky Way merger, triggered by the use of orbital parameters derived mainly from Gaia data (Fernández-Alvar et al., 2018; Helmi et al., 2018; Belokurov et al., 2018).

- Anticentre science demonstration that considers the Sagittarius dwarf galaxy, the anticentre stream and two open clusters (Gaia Collaboration, Antoja, et al., 2021; Laporte et al., 2022).

- Isolation of the Sagittarius dwarf galaxy across the entire sky (Ruiz-Lara et al., 2020; Ramos et al., 2021)

- Star formation history of the Milky Way (Gallart et al., 2019).

Of course, the topics mentioned above are only the tip of the iceberg in terms of the Gaia contribution to the Milky Way understanding.

In terms of young star clusters, several efforts have been made to ensure the reliability of the new discoveries, since most of the open clusters are located on the Galactic plane. The contributions of Castro-Ginard et al. (2020), Cantat-Gaudin et al. (2020) and Hunt and Reffert (2021) to the census of open clusters are without a doubt one of the major achievements in young cluster science, not only for the discovery and characterisation of new groups, but for the reliability of its conclusions (Cantat-Gaudin and Anders, 2020; Hunt and Reffert, 2021). Finally, old star cluster science was greatly benefited by the derivation of membership criteria for a large number of stars around the globular cluster that Gaia gives by using the proper motions. That is why the work of Baumgardt and Vasiliev (2021) and Vasiliev and Baumgardt (2021) quickly replaced the Harris (2010) catalogue, given that there is available an homogeneous astrometrical and photometrical source to derive positional, structural and orbital properties a vast majority of the Milky Way Globular clusters.

1.5 Missing low-luminosity globular clusters towards the Galactic bulge

Despite the relevant role that the bulge globular clusters play in the characterisation of the early Galaxy, no consensus has been achieved on the absolute number of clusters belonging to this component. Significant amount of (differential) extinction towards the disk and bulge together with considerable contamination by field stars are the most relevant barriers that do not allow us to properly study this area. Both causes hinder our ability to recognise clusters, blurring colour-magnitude diagram features so strongly that we cannot differentiate cluster from field stars without other diagnostic. A similar scenario occurred and was reported in the most distant regions of the Milky Way halo in which the same

uncertainty is inferred (Webb and Carlberg, 2021). According to the comprehensive analysis presented in Baumgardt et al. (2019, see their Figure 8), we are only detecting the high-mass end of the bulge globular clusters. In the same article the authors derive a minimum globular cluster mass (close to the $10^5 M_\odot$) required to survive the dynamical processes going on in the early inner Galaxy. The question that arise from this scenario is how many clusters we are missing from current catalogues in between that limiting mass and the observed high-mass clusters.

Trying to overcome this scenario several observational efforts have been done towards the Galactic bulge that include the near-infrared surveys 2MASS and VISTA Variables in the Vía Láctea (Skrutskie et al., 2006; Minniti et al., 2010). More recently, and despite being an optical survey, the Gaia satellite (Gaia Collaboration, Prusti, et al., 2016; Lindegren et al., 2018; Gaia Collaboration, Brown, et al., 2018; Gaia Collaboration, Brown, et al., 2021) have greatly contributed to uncover the gas and dust veil through the inclusion of stellar proper motions derived from its very precise astrometry, permitting the dynamical isolation of clusters by their movements over time.

This only addition of all-sky proper motions dramatically improves the cluster (whether old or young) detection capabilities.

Thanks to the mentioned efforts, in the last few years the number of publications reporting the discovery of candidate globular clusters has risen significantly (e.g., Minniti et al., 2011a; Moni Bidin et al., 2011; Borissova et al., 2014; Minniti et al., 2017b; Minniti et al., 2017a; Minniti et al., 2017c; Gran et al., 2019; Palma et al., 2019; Garro et al., 2020).

Recently, more pieces of evidence of the globular cluster contribution to the stellar content of the disk (Price-Jones et al., 2020) and bulge (Hughes et al., 2020; Horta et al., 2021; Kisku et al., 2021) have been revealed and demonstrated. It is also clear that globular cluster are dissolved when they are under the strong gravitational potential of the Milky Way, producing extended stellar tails or streams. Nevertheless, those remnants are extremely difficult to isolate in crowded fields with only a few documented exceptions of

massive satellite companions towards the inner Galaxy (Ibata et al., 2001; A. M. Price-Whelan et al., 2016; Ibata et al., 2018; Price-Jones et al., 2020). Despite the relevance for the Galactic environment of these structures, we will focus on the compact cores or remnants of these tidal processes. The clusters we are looking for need to be dynamically bound as we can identify them as an overdensity using various stellar tracers (e.g., star counts, variable star content, proper motion clusters, among others). In fact, the only way to confirm the cluster nature of an overdensity is by using the dynamical information given by the radial velocities, proper motions, or a combination of both especially when there is a substantial background/foreground contamination. However, a major fraction of the candidate clusters listed in the literature in recent years lack this proper motion or radial velocity check, which is one of the thesis core topics. A similar approach is given in Cantat-Gaudin and Anders (2020) in which the authors note that a high percentage of the literature open clusters were not dynamically bound and end up being classified as asterisms.

High-resolution spectroscopic analysis of the globular cluster NGC 6544

2.1 APOGEE view of the globular cluster NGC 6544[1]

Given the importance of a complete study of the Galactic bulge and the active partici-
pation of the Chilean Participation Group (CPG) within the SDSS-APOGEE2S (Eisenstein
et al., 2011; Blanton et al., 2017) survey, I started my PhD learning how to analyse and
process the data from the APOGEE survey. Within this catalogue composed of chemical
abundances, radial velocities and fundamental stellar parameters, I started with a globular
cluster (NGC 6544) that was dynamically studied in R. Contreras Ramos et al. (2017) by
another member of our research group. Taking advantage of the APOGEE high spectral
resolution, the large number of stars targeted within this cluster (23 members), and the
precise results derived from the data, we decided to complete the analysis and publish the
following article.

2.1.1 Introduction

As the oldest objects in our Galaxy, Galactic globular clusters (GCs) play a crucial role
in the characterisation of the early phases of its formation. While most halo clusters have
been extensively studied, GCs close to the plane of the Milky Way (MW) have not been
equally explored. The variable amount of gas and dust and the contamination by disk and

---

[1]Based on the article published by Gran et al. (2021a)

bulge stars in the disk and bulge line-of-sights were the main reasons to evade observations in this area. Bulge GCs, in particular, that can be associated with this Galactic component based on their positions, kinematics and metallicities (e.g. Minniti, 1995; Pérez-Villegas et al., 2020), have been avoided until recently, when near-infrared (near-IR) detectors and spectrographs allowed us to reduce the effect of extinction e.g. Valenti et al., 2007; Valenti et al., 2010; Bica et al., 2016; Cohen et al., 2017; Cohen et al., 2018.

NGC 6544 ($\ell = 5.83$, $b = -2.20$; Cohen et al., 2014) is a perfect example of a poorly studied GC, despite being at a distance of only ~ 2.5 kpc in the bulge direction. The first attempt to characterise NGC 6544 come from 160 stars measured with photographic plates, Alcaino (1983) reported a very reddened cluster, with E($B-V$) = 0.70 mag, at a distance of 2.8 kpc. During the last decade, Valenti et al. (2010) analysed the first near-IR CCD photometry of the cluster and used the slope of the red-giant branch (RGB) to derive a metallicity of [Fe/H]=-1.36 dex. Based on low-resolution spectroscopy, Carretta et al. (2009a) and Saviane et al. (2012) found consistent results of the cluster metallicity with [Fe/H] of -1.47 and -1.43 dex, respectively, both slightly lower than the photometric determination. Recently Cohen et al. (2014) combined near-IR photometry from the VISTA Variable in the Vía Láctea survey (VVV; Minniti et al., 2010; Saito et al., 2012) with optical photometry from the Hubble Space Telescope, deriving $d = 2.46$ kpc, E($B-V$) = 0.79 mag, and constraining the tidal radius with a lower limit of $r_t = 19$ arcmin. They also concluded that the cluster is likely to have undergone a tidal stripping process, under the assumption that NGC 6544 is a halo cluster currently passing close to the Galactic disk, and projected towards the bulge (Bica et al., 2016).

Recently, R. Contreras Ramos et al. (2017), Pérez-Villegas et al. (2020), and Massari et al. (2019) confirmed that the cluster origin was not the bulge based on absolute proper motions (PMs), from which they derive the orbit of NGC 6544. Interestingly, R. Contreras Ramos et al. (2017) found a remarkable elongation of the shape of the cluster in the direction of the Galactic centre, unfortunately without any tidal tail signature. Finally, and as a side product of the numerous efforts to characterise the GC content in the Gaia Data

Release 2 (DR2) catalogue (Gaia Collaboration, Brown, et al., 2018; Gaia Collaboration, Helmi, et al., 2018; Lindegren et al., 2018), Vasiliev (2019a), Baumgardt and Hilker (2018), and Baumgardt et al. (2019) derived several structural and photometric properties for NGC 6544. This is how very precise estimates, based solely on cluster members, of the distance, PMs, core, tidal and half-light radius, and mass were derived.

This section presents the first high-resolution spectral analysis of 23 NGC 6544 cluster members, to characterise its internal chemical composition and compare it with other globular clusters and the bulge field. The structure of this paper is the following: subsection 2.1.2 describes the used data, subsection 2.1.3 describes cluster members selection process, subsection 2.1.4 provides the metallicity determination for the cluster, subsection 2.1.5 refers to the chemical abundances of the individual stars and its variations within the cluster, subsection 2.1.6 gives a context of our findings within a sample of GCs, subsection 2.1.7 presents our concluding remarks, and finally, Appendix 5.1.1 contains a table with all the abundances used within this section.

2.1.2   APOGEE survey data

The APOGEE survey (Majewski et al., 2017) is one of the projects carried out within the SDSS-III (Eisenstein et al., 2011) and the SDSS-IV (Blanton et al., 2017) Collaboration. APOGEE uses a multi-fiber spectrograph (Wilson et al., 2010; Wilson et al., 2012; Wilson et al., 2019) to obtain high-resolution ($R \sim 22,000$) high-SNR (>100) spectra in near-IR wavelengths (H band; $1.51 - 1.69 \mu$m) in order to observe all the components of the MW (halo, disk, bar, and bulge) from the Apache Point Observatory (APO; Gunn et al., 2006) and Las Campanas Observatory (LCO; Bowen and Vaughan, 1973). The survey targets mainly giant stars imposing a colour cut in the dereddened near-IR colour-magnitude diagram (Zasowski et al., 2013; Zasowski et al., 2017). After the observations, all the data collected are processed by the APOGEE pipeline (Nidever et al., 2015) to extract and co-add multiple visits of the same target and calculate accurate radial velocities to the
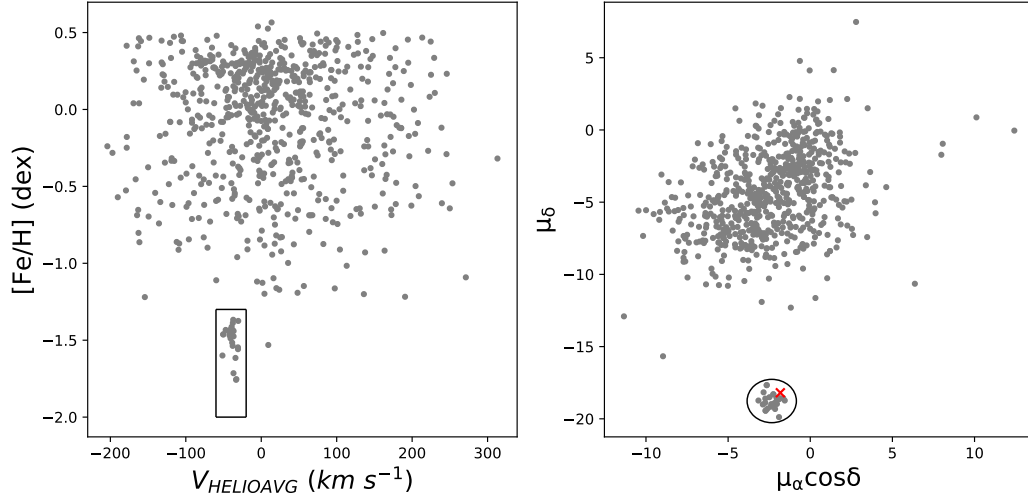
Figure 2.1: (**Left panel**): Heliocentric radial velocity versus [Fe/H] for all the APOGEE targets within 45 arcmin from the centre of NGC 6544. A group of stars, candidate cluster members, clearly separate from the bulk of field (bulge) stars. See text for the box limits. (**Right panel**): VPD for the same field around the cluster. A small concentration of stars can be seen as a coherent group isolated from the bulge field stars. We choose the radius of the circle as 1.5 mas yr^{-1}. Note that the RR Lyrae star used to derive the distance to the cluster is marked with a cross.

level of 0.1 km s^{-1} for an SNR > 20 star with at least three observations. Finally, all the individual and co-added spectra are processed by the APOGEE stellar parameter and chemical abundance pipeline (ASPCAP; García Pérez et al., 2016) to derive abundances for up to 26 chemical elements (Shetrone et al., 2015; Smith et al., 2021) in the publicly available Data Release 16 (DR16; Ahumada et al., 2020). The DR16 version of the APOGEE catalogue is presented by Jönsson et al. (2020), and it includes data for more than $\sim 437,000$ stars across all the components in the MW.

2.1.3   NGC 6544 in the APOGEE DR16

We searched for stars that might belong to known globular clusters in the APOGEE public DR16, restricted to the bulge area observed by the VVV survey footprint. Origi-
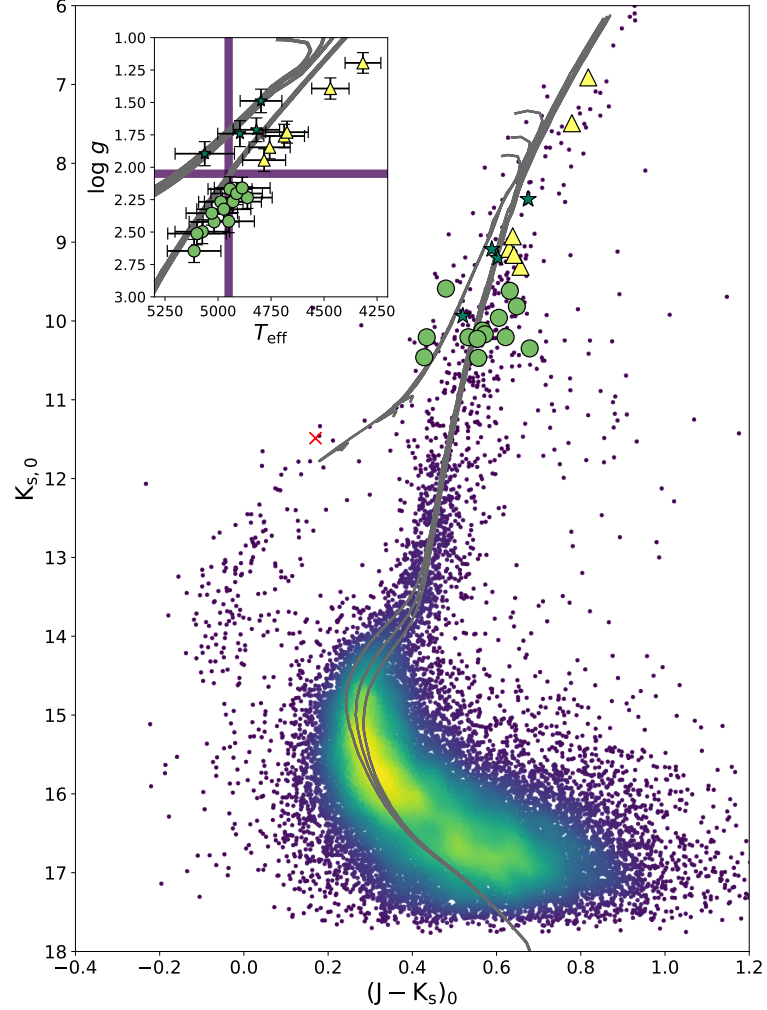
Figure 2.2: Dereddened (J-K_s) $\times$ $K_s$color-magnitude diagram of NGC 6544 members from VVV ($K_s \gtrsim$ 11 mag, R. Contreras Ramos et al., 2017) and 2MASS ($K_s \lesssim$ 11 mag Skrutskie et al., 2006; Valenti et al., 2007). As mentioned in the text, different symbols were used to differentiate within stellar stages. Circles, triangles, and stars were used to highlight different evolutionary stages based on their positions on the T_{eff} -$\log g$ diagram (see section 2.1.3 for definitions). Subsequent figures will use the same markers. The RR Lyrae star analysed in section 2.1.4 is marked with a cross. (**Inset**): T_{eff} -$\log g$ diagram of the 23 APOGEE cluster candidates together with the same three PARSEC isochrones. All of them for the same metallicity and α-enhancement values of the cluster, for ages of 10, 12 and 14 Gyr. The RGB bump is marked at the intersection of the two shaded areas.

nally, NGC 6544 was not part of the APOGEE-1 calibration set of clusters (observational campaign form APO), and targeting efforts of cluster members started with APOGEE-2 (APO and LCO observations). In total, more than 690 stars lie within 45 arcmins of the cluster centre. The spatial selection cut was performed using the cluster centre derived by Cohen et al. (2014), as listed in Table 2.1, which centre is shifted by 7 arcsecs with respect to the value provided by the Harris (1996, 2010 edition) catalogue. Most of the stars within this radius are bulge stars, although 26 stars group around a V_{HELIO} and [Fe/H] loci far from the main field distribution, as shown in Figure 2.1 (left panel). Note that of the 26 stars selected, there are three with repeated observations from both hemispheres (APO and LCO).

From here on, we will merge the entries selecting the ones with lower overall errors (APO). Shown here are the heliocentric velocity and iron abundance derived from the APOGEE reduction pipeline and ASPCAP, respectively. The cluster members tend to agglomerate in a region of the V_{HELIO}-[Fe/H] space marked with a box with [Fe/H]$_{\mathrm{median}}$ = -1.46 dex and $V_{\mathrm{HELIOmedian}}$ = -38.17 km s^{-1}. The radial velocity limits of the box have been set as the maximum dispersion found in massive GCs (McLaughlin and van der Marel, 2005; Watkins et al., 2015) of $\lesssim 20$ km s^{-1}, while for the iron content, we select all the stars with $-2.0 \lesssim$ [Fe/H] (dex) $\lesssim -1.4$ because there are no more stars in this range to be considered cluster members.

As an additional test, we crossmatch the same bulge field stars around NGC 6544 with the Gaia DR2 to obtain PMs with the idea of applying a kinematic cut in our sample. For all the cluster candidates we found a match which gives us the PMs ($\mu_{\alpha} \cos \delta$ and μ_{δ} in mas yr^{-1}), which we show as the vector-point diagram (VPD) in Figure 2.1 (right panel). We select a boundary limit of 1.5 mas yr^{-1} to select cluster members within the VPD. The median PM of the matched APOGEE stars shows a perfect agreement with the value published by Vasiliev (2019a) and Baumgardt et al. (2019). We want to perform the cluster selection process as blind as possible, therefore we do not put additional parameter constraints.

In total, the same initial 23 stars were selected as probable NGC 6544 members. The final selection of cluster candidates is also showed on their position in the dereddened (J-K_s) *vs* $K_s$color-magnitude diagram (CMD), using the 2MASS magnitudes (Skrutskie et al., 2006) transformed to the VISTA filters[2]. Figure 2.2 shows the CMD of NGC 6544 with the selected APOGEE targets shown with symbols. For stars with $K_s >$ 12 mag, VVV dereddened magnitudes come from the PM selected cluster members, according to R. Contreras Ramos et al. (2017). However for $K_s <$ 12 mag, stars are saturated in the VVV survey, and therefore we perform a dynamical selection (with 1.5 mas yr^{-1} tolerance) based on the Gaia DR2 PMs to select 2MASS members (Skrutskie et al., 2006; Valenti et al., 2007). Three isochrones from the PARSEC library (Bressan et al., 2012; Y. Chen et al., 2015; Y. Chen et al., 2014; Tang et al., 2014; Marigo et al., 2017; Pastorelli et al., 2019), were overplotted to the data. The predefined parameters were used to retrieve the isochrones in the version 1.2S. We choose ages of 10, 12, and 14 Gyr, that can be noticed from left to right in the turnoff area. As expected for the given ages, all the isochrones follow an almost identical line in the main-sequence, RGB and asymptotic giant-branch (AGB). The same metallicity and α-enhancement derived for the cluster (see section 2.1.5 for the exact values) were used.

The inset in Figure 2.2 also shows the T_{eff} -$\log g$ diagram for the observed stars with the isochrones mentioned above. The isochrones help identify the RGB bump in the inset panel, highlighted with two intersecting shaded areas at $T_{eff} \sim$ 4950 K and $\log g \sim$ 2.0 dex, splitting the RGB sample into two. Note that all the stars in the T_{eff} -$\log g$ diagram appear to be shifted to the respective isochrones towards cooler temperatures or higher gravities. The shift is small, and similar to the total error on the parameters, with values of $\Delta T_{eff} \sim$ 100 K and $\Delta \log g \sim$ 0.2 dex in the uncorrelated case and half of them if we consider a simultaneous shift on both measurements. Despite this fact and as expected for a single GC, stars follow the evolutionary sequences, confirming that the stellar surface

---

[2]http://casu.ast.cam.ac.uk/surveys-projects/vista/technical/
photometric-properties

parameters are rather well determined. On the contrary, the targets are more spread out in the observed colour-magnitude diagram because of the large differential reddening along the line-of-sight: up to $\Delta E(J\text{-}K_s) \sim 0.4$ mag within arcmin scales around the cluster centre, as already noted by R. Contreras Ramos et al. (2017). It is for this reason that we only use the position of the stars in the T_{eff} -$\log g$ diagram to classify the cluster members into three groups: the main two in the RGB evolutionary phase, below and above the bump and the third one, associated to the AGB phase. Take in consideration that the RGB-bump might differ whether we select a stellar model or perform an empirical estimate, as shown in Cohen et al. (2017) for NGC 6544. The shift in magnitudes can be as large as $\Delta K_s \sim 0.2 - 0.3$ mags for this cluster, depending on the derived distance, α-enhancement, and to a lesser extent by age (Salaris et al., 2007).

As Figure 2.2 suggests, we split the cluster sample into three groups: stars below and above the RGB bump (lower RGB or lRGB as circles, and upper RGB or uRGB as triangles), and the AGB group (as stars). Each group consists of 13, 6 and 4 stars for the lRGB, uRGB, and AGB, respectively, with a total of 23 observed cluster stars. These groups were also marked with different symbols according to APOGEE derived T_{eff} and $\log g$ values.

In section 2.1.4 and 2.1.5, abundance differences will be reviewed, but as expected from an evolutionary point of view, stars below the RGB bump will be Carbon-enhanced and Nitrogen-depleted, and the contrary for the stars above the bump.

2.1.4 NGC 6544 fundamental parameters

Metallicity and α-enhancement values

From the photometric point of view, some of the most uncertain parameters to determine from a CMD are the metallicity, α-enhancement, and age of a stellar population. Even a slight change in the first two affects the main-sequence turnoff point location, and therefore the estimated age of a stellar population (e.g. Oliveira et al., 2020; Souza et al., 2020).

Table 2.1: NGC 6544 coordinates (J2000), tidal radius and distance from the Sun (Cohen et al., 2014), heliocentric radial velocity, metallicity (Harris, 1996, 2010 edition), and PMs (Baumgardt et al., 2019).

RA	Dec	ℓ	b	$r_{\rm t}$
(hh:mm:ss)	(dd:mm:ss)	(deg)	(deg)	(arcmin)
18:07:20.12	-24:59:53.6	5.8365	-2.2024	$\simeq 19$
$V_{\rm HELIO}$	$d_{\odot}$	[Fe/H]	$\mu_{\alpha}\cos\delta$	μ_{δ}
(km s^{-1})	(kpc)	(dex)	(mas yr^{-1})	(mas yr^{-1})
-27.3 ± 3.9	2.46 ± 0.09	-1.4	-2.34 ± 0.04	-18.66 ± 0.04

Here the cluster metallicity is known in great detail even across different stages of stellar evolution, and the combination of PMs and radial velocities ensures that all the analysed stars move coherently in space and form part of the cluster.

One of the first striking results that the spectra present is the systematic difference between the DR16 derived metallicity of the RGB (both groups) and that of the AGB. The marked difference between populations of a globular cluster was not present in previous studies, while using APOGEE spectra but applying different reduction methods (García-Hernández et al., 2015; Masseron et al., 2019; Mészáros et al., 2020). In this cluster we are finding that the median metallicity with its standard error for the entire RGB is [Fe/H]=-1.44 ± 0.04 dex, that is composed of a lower and upper part with -1.44 ± 0.05 dex and -1.46 ± 0.04 dex, respectively. RGB metallicities agrees within its errors, nevertheless are systematically higher than those of AGB stars of [Fe/H]=-1.66 ± 0.10 dex. Across the paper we use the standard deviation of the median as a statistically significant measurement on the errors.

The discrepant values of iron content for stars in different evolutionary stages (RGB and AGB in this case) is not a new finding. Indeed, Ivans et al. (2001) found that AGB stars in M5 had [FeI/H] lower than RGB stars, by 0.15 dex. They concluded that this

finding was in agreement with the prediction of Thévenin and Idiart (1999), i.e., that in the atmosphere of metal poor, late type stars, most FeI lines are formed out of local thermal equilibrium (LTE), and therefore by assuming LTE, derived FeI abundances are lower than real. This is due to the fact that in thin, transparent atmospheres, some of the Fe is ionised by UV radiation coming from the stellar interior. The effect is larger for less dense atmospheres at a given T_{eff} , and also larger for higher T_{eff} at a given luminosity, therefore it is expected to be larger in AGB stars than in RGB stars. According to Thévenin and Idiart (1999), FeII lines are not affected by this NLTE effect. More recently and using optical spectra, Lapenna et al. (2014), Lapenna et al. (2015), Mucciarelli et al. (2015b), and Mucciarelli et al. (2015a) all confirmed that the putative spread in the iron abundance of stars in 47 Tuc, M 62, M 22, NGC 3201, reported in previous studies, was due to the same effect. Namely, FeI abundances in AGB stars were lower than those of RGB stars. On the contrary, iron abundances derived from FeII lines showed a very good agreement in both evolutionary phases. However, converging metallicities between the RGB and AGB stages were found by García-Hernández et al. (2015), Masseron et al. (2019), and Mészáros et al. (2020) when characterising APOGEE near-IR spectra that uses only FeI lines. With these conflicting evidence in context, it is clear that we have no clear explanation of the phenomena that NGC 6544 AGB stars exhibit, giving that they are dynamically confirmed cluster members. For that reason, we have isolated the behaviour of the different evolutionary stages to compute the median [Fe/H].

A max-to-mean difference of 0.23 dex is observed in [Fe/H] (or 0.17 dex within each RGB subdivision), a value that exceeds the observational errors in NGC 6544 (typically ±0.02 dex), and in other GCs (Carretta et al., 2009a). It will be evident from Section 2.1.5 that the star-to-star variations exceed the observational error, even among the RGB and AGB stars themselves. We cannot exclude that extra-enrichment processes happened in NGC 6544 (as explained in Renzini, 2008), or even that this trend is the result of the interaction with the MW (Rodrigo Contreras Ramos et al., 2018; Kundu et al., 2019a; Kundu et al., 2019b). Given the absolute *V* magnitude (M_{V_t}) of -6.94 mags as a proxy of

the total mass, no other cluster with similar M_{V_t} shows an [Fe/H] dispersion greater than ~ 0.07 dex (Harris, 1996; Bailin, 2019). Up to now, we do not have a clear explanation of the origin of the [Fe/H] spread of NGC 6544, considering the limited number of stars observed.

Finally, the ASPCAP pipeline returns an estimation for the $[\alpha/\text{Fe}]$ content of each analysed star. Following the description in García Pérez et al. (2016), this contribution is measured using O, Mg, Si, S, Ca, and Ti from the spectra. The median $[\alpha/\text{Fe}]$ value obtained from cluster combined RGB stars is 0.20 ± 0.04 dex, matching canonical values for GCs. If we separate stars in the lower and upper part of the RGB, we find medians of 0.22 ± 0.04 dex and 0.19 ± 0.03 dex, respectively. The same deviation from the RGB values is found in the AGB stars, with a median of 0.25 ± 0.08 dex. We present median observed quantities, instead of mean, because of a significant spread in the [Fe/H] and $[\alpha/\text{Fe}]$ of cluster stars.

Distance to NGC 6544

Distance is a crucial parameter that is often derived from CMD fitting. Although it degenerates with reddening and metallicity. A CMD-independent measurement of the distance can be sought to confirm that the isochrone parameters were accurate enough. Figure 2.2 uses a reddening value of E(J-K$_s$) = 0.36 mags (R. Contreras Ramos et al., 2017) in the VISTA filters or 0.40 mags in the 2MASS system and a distance modulus of $dm = 11.92$ found in this work, which is consistent with the distances derived by Cohen et al. (2014) and R. Contreras Ramos et al. (2017) of $dm = 11.96$ mag.

Although only one RR Lyrae star has been detected to move along with the cluster (see Figure 2.1 right panel), it can be used to verify the assumed distance modulus. The RR Lyrae is listed in the online catalogue of Clement et al. (2001), it was also detected by the Optical Gravitational Lensing Experiment (OGLE) survey Soszyński et al. (2014) and

Soszyński et al. (2019, OGLE-BLG-RRLYR-13867[3]), and by the VVV survey (Contreras Ramos private communication). Its main properties are presented in Table 2.2, yielding a distance modulus of $dm = 11.92 \pm 0.18$ mag (2.43 ± 0.20 kpc) using the Muraveva et al. (2015) period-luminosity relation for the K_s band, an intrinsic (J-K_s) RR Lyrae colour of 0.17 ± 0.03 (Navarrete et al., 2015; Contreras Ramos et al., 2018) and the Cardelli et al. (1989) extinction law, which is comparable to other distance measurements. We also report the near-IR reddening and extinction values given by the RR Lyrae star in Table 2.2. Consider that all the near-IR measurements presented here are in the 2MASS filter system. Note that E(J-K_s) and E(V-I)derived are consistent within errors with R. Contreras Ramos et al. (2017) and Cohen et al. (2014), respectively. To calculate E(V-I), we use the same derivation described by Pietrukowicz et al. (2015), considering the actual metallicity of the cluster derived above and the Catelan et al. (2004) period-luminosity relations. There is also a discrepancy in the E(J-K_s) value derived by Cohen et al. (2014) which is ~ 0.1 mags shifted towards higher reddening. This shift will be addressed in the next subsection as a VVV survey calibration issue discovered in Hajdu et al. (2020).

Finally, Vasiliev and Baumgardt (2021) recently derived a parallax-driven value of $d = 2.54 \pm 0.07$ kpc ($\overline{\varpi} = 0.394 \pm 0.011$ mas) to NGC 6544. This is an independent distance determination, which is also in agreement with all of the previous measurements showed in this section.

Reddening Law towards NGC 6544

Given the multi-survey synergies that we have presented until this point, the final quantity that we want to constraint is the reddening law towards NGC 6544. Using the spectroscopic data that we are analysing, it is possible to derive isochrone-based or synthetic colours for all the stars in the cluster. We will consider, however, only the RGB stars, given the uncertain nature of the AGB stars as discussed in Section 2.1.4. We crossmatch the star

---

[3]Available: `http://ogledb.astrouw.edu.pl/~ogle/OCVS/o.php?OGLE-BLG-RRLYR-13867`

Table 2.2: RR Lyrae star used to verify the NGC 6544 distance modulus. Magnitudes in each filter corresponds to the mean quantity. J- and H-band values were derived from only a few epochs, as described in Saito et al. (2012).

Stellar parameters from Gaia DR2	
Source ID	4065784375110674176
RA (J2000)	271.868215
Dec (J2000)	-25.031377
ℓ (deg)	5.8226
b (deg)	2.2458
G (mag)	14.5874 ± 0.0311
BP (mag)	15.2310 ± 0.1308
RP (mag)	13.6256 ± 0.0770
$\mu_\alpha \cos\delta$ (mas yr^{-1})	-1.821 ± 0.074
μ_δ (mas yr^{-1})	-18.195 ± 0.061
Stellar parameters from OGLE survey	
OGLE ID	OGLE-BLG-RRLYR-13867
V (mag)	13.584
I (mag)	15.048
P (days)	0.5723310 ± 0.0000001
$I_{\mathrm{amplitude}}$ (mag)	0.777
Stellar parameters from VVV survey	
VVV ID	VVV180728.37-250153.1
J (mag)	12.164 ± 0.02
H (mag)	11.932 ± 0.03
K_s (mag)	11.694 ± 0.01
Derived stellar parameters	
E(V-I)	0.98 ± 0.07 mag
E(J-K_s)	0.31 ± 0.03 mag
A_{K_s}	0.25 ± 0.02 mag
dm (mag)	11.92 ± 0.18
Distance (kpc)	2.43 ± 0.20

positions to a list of surveys that have observed the area with 1 arcsec tolerance, founding that there are observations from the ultraviolet (UV) to the mid-IR for part of the stars in our sample. Photometric information from SWIFT (Roming et al., 2005), PanStarrs DR2 (Chambers et al., 2016; Flewelling et al., 2020), Gaia DR2 (Gaia Collaboration, Brown, et al., 2018; Lindegren et al., 2018), 2MASS (Skrutskie et al., 2006), Spitzer/GLIMPSE (Benjamin et al., 2003; Churchwell et al., 2009) and AllWISE (Wright et al., 2010; Mainzer et al., 2011) was collected. In total, 20 filters (UVOT/UVW2; g, r, i, z, y; G, BP, RP; J, H, K_s; $[3.6], [4.5], [5.8], [8.0]$; and $W1, W2, W3, W4$) contain fluxes for our stars. Given the crowded nature of a GC, even with the radius tolerance of 1 arcsec, surveys with large pixel scale will often present incorrect or blended magnitudes for the analysed stars. Note also, that we retrieve Swift matches for only five stars in the NGC 6544 sample, in contrast to all the other surveys in which we obtain a high counterpart recovery percentage ($\sim 95\%$ or 18 out of 19 possible matches in the worst case). Considering the relevance of the B and V filters in the extinction characterisation, to obtain these magnitudes we apply a colour transformation present in Tonry et al. (2012) to the PanStarrs g and r bandpasses.

To derive synthetic magnitudes we interpolate the T_{eff} and $\log g$ from the APOGEE DR16 into a PARSEC isochrone of 12 Gyr and the cluster metallicity to obtain the absolute magnitudes in different filters. With the absolute theoretical magnitudes, we are able to calculate the colour excess term just subtracting to the observed colour term. This step is necessary to compare with other results, like the one that we derive from the RR Lyrae colours, or the canonical E(B-V) value. Indeed, it is important to mention that there should be statistical and systematic errors not considered here, like the isochrone election or additional differential reddening effects.

Our results for the E(B-V) $= 0.77 \pm 0.19$ mag coincides with the one derived by Cohen et al. (2014) of 0.79 ± 0.01 mag. However, the E$(g - r) = 1.19 \pm 0.16$ value from our method is greater than previously published values. Extinction maps released[4] by G. M. Green

---

[4]Available at the website: `http://argonaut.skymaps.info/`

et al. (2014) and G. M. Green et al. (2019) account for a value of E($g - r$) = 0.58 ± 0.03 mag at the cluster distance.

In parallel, Cohen et al. (2014), R. Contreras Ramos et al. (2017), and Surot et al. (2019) and Surot et al. (2020) give values of the E(J-K$_s$) of 0.43 ± 0.03 mag, 0.40 mag, and 0.47 ± 0.09 mag respectively, for which we agree with our method. Is important to note that to produce the best fit for the Figure 2.2 CMD we use the E(J-K$_s$) value present in the R. Contreras Ramos et al. (2017) article (0.36 mags). This value is provided in the VISTA system of magnitudes, and it is affected by the VISTA-2MASS colour transformations, and the correction to the zero-point calibration published by Hajdu et al. (2020). After transformation to the 2MASS framework, the R. Contreras Ramos et al. (2017) value of E(J-K$_s$) = 0.40 mag, is consistent with our results. The small discrepancy that is still remains of the order of ∼ 0.04 with our E(J-K$_s$) derived value can be explained by the strong differential reddening of the cluster, with have amplitudes of up to ΔE(J-K$_s$) = 0.33 mags depending on the spatial location across the cluster area (Contreras Ramos private communication). Another possible explanation is possibly the recalibration process proposed by Hajdu et al. (2020), however, this effect should be an order of magnitude less prominent than the last one. With this analysis, we have settled the near-IR reddening discrepancy, preferring the value given by Cohen et al. (2014) and this work of E(J-K$_s$) = 0.44 ± 0.01.

Finally, we take the difference within the observed star magnitudes and the theoretical absolute magnitude, shifted to the cluster distance (*dm* = 11.92 from Table 2.2). The difference corresponds to the total extinction A$_\lambda$ present in the line of sight per filter, which is presented in Table 2.3. Giving the positive physical nature of the extinction values, we have not considered some slightly negative results as a product of statistical fluctuations in the data, which were probably caused, as we commented earlier, by the differential reddening not taken into account in this step. As expected, a monotonic decrease trend is observed as the wavelength increases, only interrupted by the reddest filters W2, $[8.0]$ and W3 for which we assume that several stars contribute to the matched magnitude in

its corresponding catalogues. Note also that W4 shows a very high dispersion compared to the others near- and mid-IR filters that follow the overall trend. Figure 2.3 shows the inverse wavelength and normalised extinction values with respect to the V-band in the same format as in Cardelli et al. (1989). We use the `dust_extinction` python package to reproduce the MW RV extinction curve at different $R_V = A_V/E(B-V)$ values. As it is clear from the Figure, total-to-selective extinction ratio of $R_V = 3.5 \pm 0.19$ deduced from the data is enough to reproduce the overall optical trend ($0.4 \lesssim \lambda$ (nm) $\lesssim 1.0$). However, this value present inconsistencies with the UV and mid-IR data. We attribute this discrepancy to the source confusion caused by the combined effect of the crowding level typical of GCs and the lower spatial resolution (i.e., larger pixel size) of these photometric surveys. The Figure also shows an extreme case with $R_V = 5.9$ that fits solely the UV observation, not reproducing any other available filters to illustrate the the erroneous status of the measurement. Given the similarities in the optical and IR parts of the spectral energy distribution within the $R_V = 3.1$ and $R_V = 3.5$ curves of less than $\sim 5\%$, we are not able to differentiate the preferred model, both being consistent with the current data.

As a final caveat on this procedure, all of the extinction derivation relies on the fact that isochrones are model independent, which is not completely accurate in this case. The PARSEC set of isochrones uses the Cardelli et al. (1989) recipe to apply the interstellar extinction to their data, adopting a canonical value of $R_V = 3.1$. Nevertheless, given the short distance of the cluster this effect should not represent a dramatic change in our results.

2.1.5   Fingerprint of an elusive cluster

As a result of the earliest star formation in galaxies GCs are one of the main tools that we have to unveil the early stages and evolution of the Milky Way. Long considered as simple stellar populations, GCs have revealed a more complex composition of their stars, which appears to belong to different generations, each one with star-to-star abundance variations, visible at photometric and spectroscopic scale Gratton et al. (2012) and Bastian

Table 2.3: Median extinction coefficients per bandpass derived for the NGC 6544 stars.

Filter	x	Wavelength	A_λ	A_λ/A_V
	(μm^{-1})	(μm)	(mag)	
UVW2	4.67	0.21	4.51 ± 0.90	1.69
B	2.30	0.44	3.42 ± 0.28	1.28
g	2.08	0.48	3.12 ± 0.19	1.17
BP	1.88	0.53	2.55 ± 0.10	0.96
V	1.83	0.55	2.72 ± 0.14	1.02
r	1.62	0.62	2.35 ± 0.10	0.88
G	1.49	0.67	1.93 ± 0.08	0.72
i	1.33	0.75	1.90 ± 0.13	0.71
RP	1.25	0.80	1.44 ± 0.06	0.54
z	1.15	0.87	1.46 ± 0.12	0.55
y	1.04	0.96	1.16 ± 0.05	0.43
J	0.81	1.24	0.40 ± 0.03	0.15
H	0.60	1.66	0.19 ± 0.03	0.07
K_s	0.46	2.16	0.16 ± 0.03	0.06
W1	0.30	3.32	0.03 ± 0.03	0.01
[3.6]	0.28	3.52	0.06 ± 0.02	0.02
[4.5]	0.22	4.45	0.11 ± 0.03	0.04
W2	0.22	4.56	0.15 ± 0.02	0.05
[5.8]	0.18	5.61	0.06 ± 0.03	0.02
[8.0]	0.13	7.70	0.08 ± 0.18	0.03
W3	0.09	10.79	0.31 ± 0.04	0.12
W4	0.05	21.91	0.00 ± 0.09	0.00
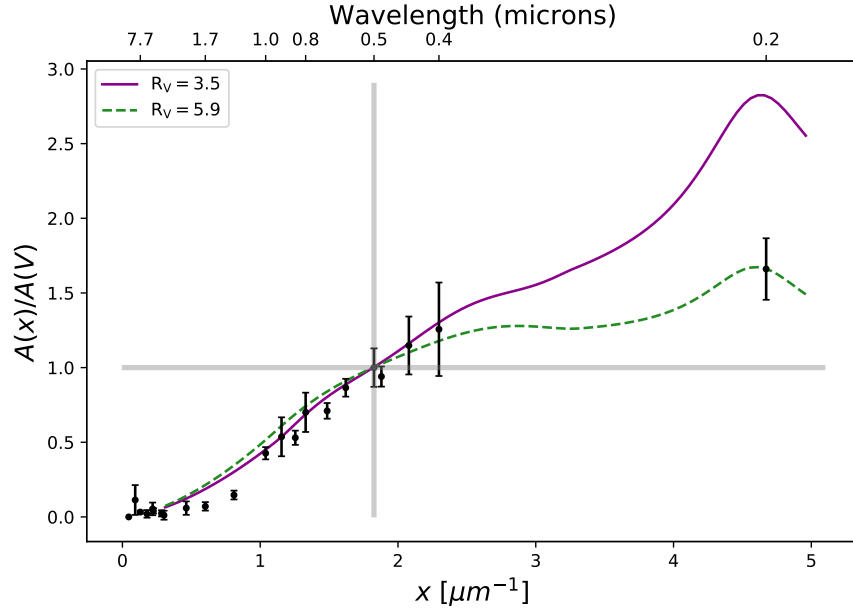
Figure 2.3: Wavelength (as $x \equiv \lambda^{-1}$[nm^{-1}] and λ [nm]) against the normalised extinction values with respect to the V-band A(x)A(V). The two extinction curves shown represents the total-to-selective ratio of $R_V = 3.5$ (continuous), and $R_V = 5.8$ (dashed) between 0.3 and 5.0 nm. In total, 20 filters from the UV to the mid-IR with its derives extinction values are shown. The V-band is highlighted with a shaded area because, by definition, all the extinction curves pass through this point.

and Lardo (2018, and references therein).

In this sense, these multiple populations (MPs) within a GC refer basically to a first (or primordial generation, FG) and at last a second generation (SG) of stars. The FG of stars pollutes the SG with processed material, and in this way different sub-populations arise in the cluster. The composition of the SG stars varies almost at an individual cluster level, manifested through several sequences in CMDs, as well as light-element variations within the clusters (C, N, O, Na, Mg, Al, Si, among other elements, see Bastian and Lardo, 2018, for a recent review).

We want to extend this background to NGC 6544 if possible, trying to search for MPs within the member stars through light-element abundances. In order to interpret NGC 6544 chemical properties, we compare its abundance patterns with other GCs observed by APOGEE, and with nearby bulge field stars. All the abundance comparisons were performed with the APOGEE DR16 values. Crossmatched stars from other GCs were located in the DR16 using the `APOGEEID` available for all the recent APOGEE publications.

Abundance analysis and element variations

The present analysis adds a substantial contribution to the chemical characterisation of NGC 6544. Our sample of cluster members ascends to 23 and allows us to observe intracluster abundance variations comparatively. In previous publications, Nataf et al. (2019) and Mészáros et al. (2020), only found 2 and 7 stars in the APOGEE DR14 and 16, respectively. This difference is originated because of the growing number of observations produced by the APOGEE survey over time, and the fact that we not use the GC flag that is present in all the APOGEE DRs (`TARGFLAGS={APOGEE_SCI_CLUSTER,` `APOGEE2_SCI_CLUSTER}`). Recently, Horta et al. (2020) analysed most of the GCs present in the APOGEE catalogue including NGC 6544, in a broad approach to compare the accreted and *in situ* classification given by Massari et al. (2019). They calculated mean metallicities, radial velocities and [Si/Fe] abundances to derive general GCs properties

of the MW, but without detailing any other cluster features. The paper indicates that 21 NGC 6544 stars were recovered from the cluster reaching identical results than the ones presented here. We estimate that the different number of stars analysed originated on the automatic elimination of stars, which removes two of the most metal-poor AGB stars (see Figure 2 in the Appendix of Horta et al., 2020)

Table 5.1 contains the abundance values, derived by the ASPCAP pipeline, for a subset of all the elements reported in the DR16. Specifically, we select the following elements: [C/Fe], [N/Fe], [O/Fe], [Na/Fe], [Mg/Fe], [Al/Fe], [Si/Fe], [K/Fe], and [Ca/Fe], together with $\left[\alpha/\text{Fe}\right]$, and [Fe/H], in order to analyse known (anti) correlations for other GCs and to insert NGC 6544 within the scenario proposed by Jönsson et al. (2018) and Zasowski et al. (2019) and Masseron et al. (2019) for the bulge and GC samples, respectively.

Figure 2.4 shows the abundance of each element as a function of iron, for all the cluster members. Nevertheless, we will base the discussion on RGB stars only, because of the metallicity offset of AGB stars mentioned in section 2.1.4. Figure 2.4 shows a slight trend in sections showing the evolution of T_{eff} , $\log g$, and $\left[\alpha/\text{Fe}\right]$ with metallicity for lRGB stars, but the trend vanishes as stars cross the RGB bump. A clear dichotomy for stars in the lRGB and uRGB is present in the [C/Fe] abundances as expected from stellar evolution with C-enhanced stars below the RGB bump and C-poor stars above the same point (Iben, 1968; Cassisi and Salaris, 2013; Lardo et al., 2012).
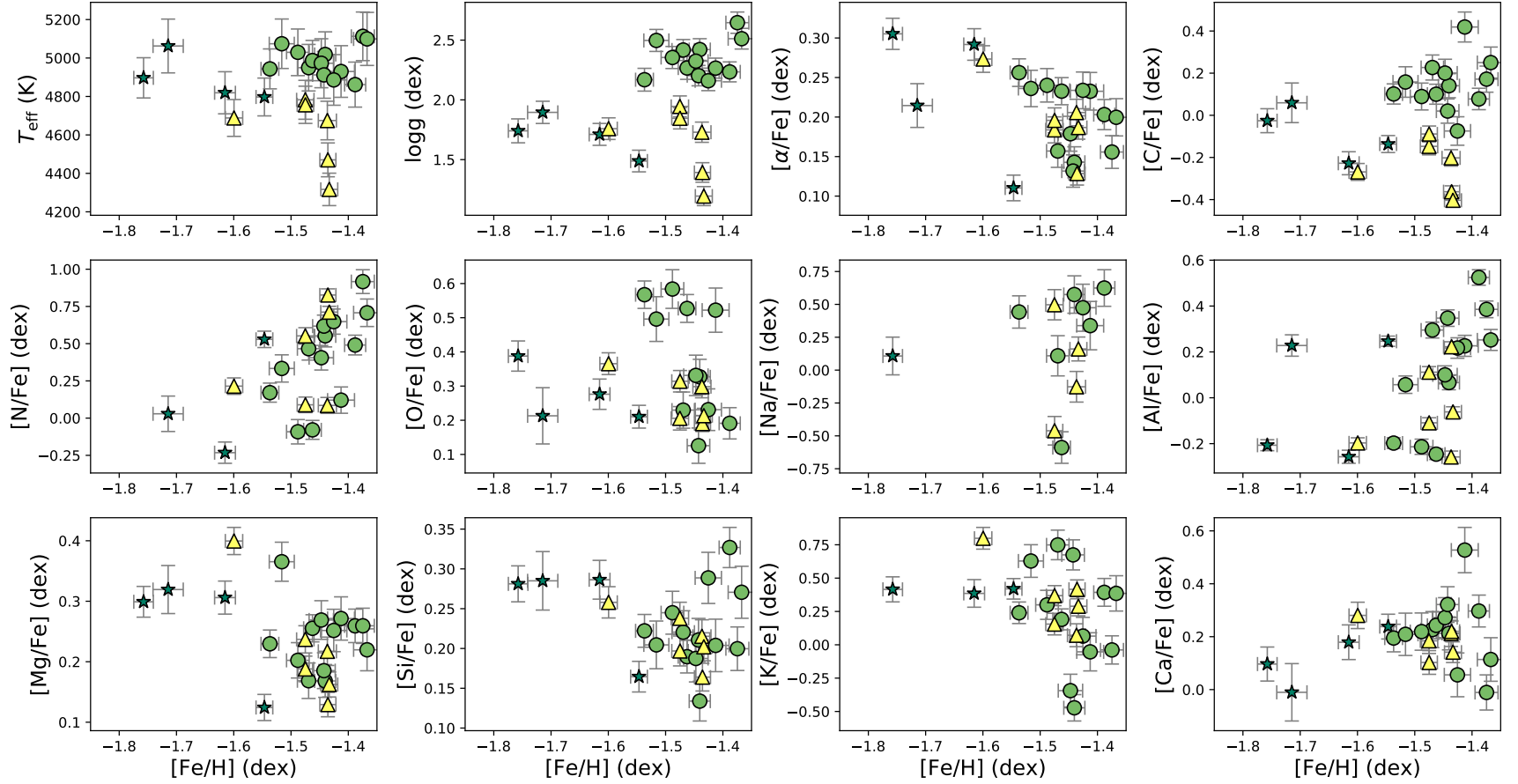
Figure 2.4: T$_{\text{eff}}$, log$g$, and [X/Fe] for surface parameters and abundances in Table 5.1. It can be noticed from the Figure, for a given metallicity there is a large spread for certain elements ([N/Fe], [C/Fe], [Na/Fe], and [Al/Fe]). The AGB group (green stars) and one uRGB star (yellow triangle) is completely offset from the global [Fe/H] trend. This variety of [Fe/H] values was the main reason which led us to consider and publish the median over the mean values for the elemental abundances.

Even if there are only a few Na lines in the APOGEE H-band spectra, only half of the cluster sample has measured abundances from the ASPCAP pipeline. They show a wide spread of Na abundance that resemble the trend presented in Masseron et al. (2019) and Carretta et al. (2009b). A detailed discussion of known (anti)-correlations will be given in the next subsections.

The Mg-Al anticorrelation and the non-existent Si-leakage

The Mg-Al chain is a complex set of proton capture nuclear reactions that need high temperatures (50 MK) to trigger (Prantzos et al., 2007; Carretta et al., 2009b; Cassisi and Salaris, 2013). For this reason, the anticorrelation between Mg-Al that is naturally produced through this chain, cannot happen inside low mass stars. Massive stars are thought to be responsible for producing the observed anticorrelations, with some external mechanism needed to transport processed material to the surface of low mass RGB stars (Renzini et al., 2015; Bastian and Lardo, 2018).

Upper left panel in Figure 2.5 shows the comparison of our [Mg/Fe] and [Al/Fe] abundances with stars of other APOGEE observed GCs (Schiavon et al., 2017; Masseron et al., 2019; Mészáros et al., 2020) from the Galactic bulge to the halo. For both catalogues, its stars were matched with the DR16, resulting in more than 680 stars in total. Overall the red-giant stars in NGC 6544 follow the same trend that other globular clusters at the same metallicity as M13, M2, and M3 with [Fe/H] equal to -1.53 dex, -1.65 dex, and -1.50 dex, respectively. For a cluster as low-mass as NGC 6544, an approximate mono abundance of [Mg/Fe] is expected. Despite that, we found that there is some spread around the median [Mg/Fe] value of 0.24 ± 0.07 dex. Nevertheless, this spread is well within two times the observational error, that also depends on the evolutionary stage marked with different symbols on the Figure. A clear sign of the Mg-Al anticorrelation is more evident in the [Al/Fe] abundances, in which we observe a high amplitude of almost Δ[Al/Fe]~ 0.8 dex. The same result was reported by Carretta et al. (2009b), also observing a [Mg/Fe]-depletion
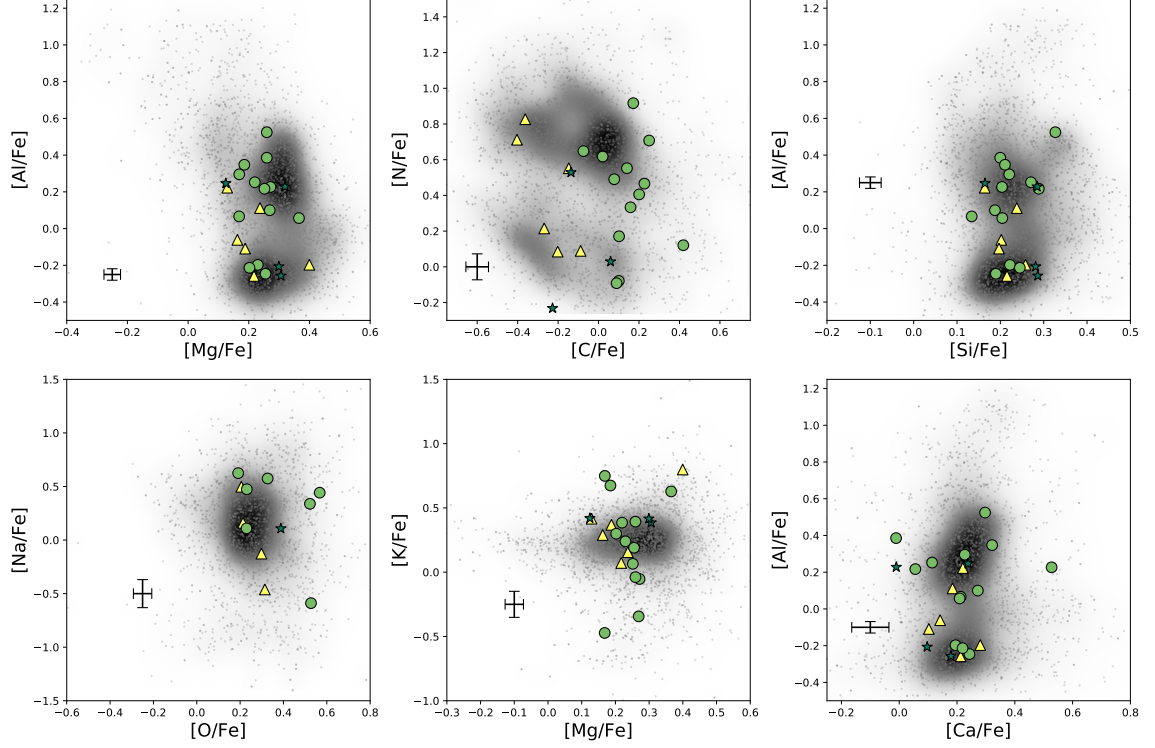
Figure 2.5: Known Mg-Al, C-N, and O-Na anticorrelations, along with other discussed abundance planes in section 2.1.5: Si-Al, Mg-K, and Ca-Al. This Figure uses the same background and symbols described Figure 2.4, and for the background the matched APOGEE stars from the Schiavon et al. (2017), Masseron et al. (2019) and Mészáros et al. (2020) analysed cluster stars. We also apply a Gaussian smoothing to this sample, shown as the coloured background, to emphasise the high-density areas of the distributions.

for stars with [Al/Fe] $\geq$ 0.8 dex in massive and/or metal-poor globular clusters. We report a maximum [Al/Fe] abundance of 0.52 dex, which agrees with the results of Carretta et al. (2009b). There appears to be a gap around [Al/Fe]= 0 dex, and even AGB stars appear to split in two groups. Often, a large Al-spread and decrease in the [Mg/Fe] for stars with [Al/Fe]$\leq$ 0.8 dex, could suggests a possible Si-leakage from the Mg-Al chain, that should be seen as an enhancement in the [Si/Fe] abundance. We do not detect any sign of [Mg/Fe] depletion. Indeed, although the Mg-Al knee is observable in the APOGEE data, none of the cluster members shows an evident Mg-poor, Al-rich behaviour. In fact, there is only a few clusters observed with APOGEE in which this effect have been documented (see Masseron et al., 2019; Mészáros et al., 2020, for more details). Another observable consequence of the Mg-depletion would be the increase of the [Si/Fe] spread among individual stars in a GC, also known as Si-leakage, which is also not observed. This effect have been observed and described in depth in GCs more metal-poor than NGC 6544 (Mészáros et al., 2020), like NGC 6341/M92 ([Fe/H]= -2.31 dex) and NGC 7078/M15 ([Fe/H]= -2.37 dex). Within the cluster, the [Si/Fe] abundances remain constant, with a median value of 0.22 ± 0.05 dex, for cluster stars showing large differences in [Al/Fe]. Two groups of stars with different [Al/Fe] abundances can be identified, with separation around [Al/Fe]$\sim$ 0 dex. We will assign the labels of FG, and SG to the groups depending on the [Al/Fe] abundance lower, and greater than 0.0 dex, respectively. These two groups, FG and SG, median [Al/Fe] values have a total difference of 0.42 dex and a standard deviation of 0.23 dex, without counting the AGB stars. Both values agrees with the results of Mészáros et al. (2020) for other APOGEE observed clusters around the metallicity that we derive for NGC 6544. Similarly, we can separate FG and SG stars in the C-N plane.

The C-N anticorrelation

The C-N anticorrelation is a natural consequence of the CNO cycle, which depletes C and O and enhances N in the H-burning (Cassisi and Salaris, 2013). These products may

be carried to the upper layers of the star either through some extra mixing phenomenon along the RGB, or because of pollution of the stellar atmosphere by the winds of high mass AGB stars. The central upper panel in Figure 2.5 shows the anticorrelation for NGC 6544 in comparison with the globular clusters analysed by Schiavon et al. (2017), Masseron et al. (2019), and Mészáros et al. (2020). Notice that we must be careful with the [C/Fe] values derived by ASPCAP. The value represents the best fit value for the whole spectrum, and according to Mészáros et al. (2015), only upper values can be measured below [Fe/H] = -1.7 dex. Fortunately, only two AGB stars fall under this metal-poor regime, and only one does not return any value in the DR16. A clear separation between pre and post-RGB-bump is seen through the [C/Fe] abundances.

The Na-O anticorrelation

The Na-O anticorrelation is produced by oxygen and sodium, produced by the combined action of the CNO and Ne-Na cycles (Gratton et al., 2004; Cassisi and Salaris, 2013). While the CNO cycle decreases the O abundance (maintaining the C+N+O overall count), the Ne-Na cycle produces Na, creating the anticorrelation. The latter cycle is efficient in intermediate-mass stars during the thermal pulses of the AGB phase, but can also be active at the bottom of the convective envelope in RGB stars, since it requires lower temperatures compared with the Mg-Al cycle (around 40 MK). Observationally, Na is difficult to measure in APOGEE spectra, because its two lines are very weak in the H-band. That is the reason that all the [Na/Fe] quantities reported (and its associated errors) must be considered with caution, as the most uncertain values presented in this work. On the same behaviour, O can be difficult to detect for metal-poor stars (see the previous subsection, and Masseron et al., 2019). As a result, only a few cluster stars have both elements measured, and are shown in the lower-left panel of Figure 2.5. As a broad overview, NGC 6544 stars follow the expected anticorrelation, like other APOGEE clusters, with a large [Na/Fe] spread of Δ[Na/Fe]~ 1.1 dex. This is in agreement with the results from other clusters (Gratton

et al., 2004), which also shows a larger spread in [Na/Fe] with respect to [Al/Fe].

The Odd-Z element K

Finally, we analyse an element that present strange patterns in the NGC 6544 APOGEE DR16 data. Potassium, as an odd-Z element, is produced from Argon by a proton capture reaction. It needs a much higher temperature than other cycles reviewed in this section, with 120-180 MK to trigger (Ventura et al., 2012; Iliadis et al., 2016). There are available only a few lines in the APOGEE spectra, but as shown in Masseron et al. (2019), [K/Fe]was successfully recovered and reported a negligible K production over all the GCs analysed.

Contrary to the results for other GCs, we observe a broad [K/Fe] spread, with up to ~ 1.25 dex in range. This abundance variation matches the values reported by Carretta et al. (2013) and Mucciarelli et al. (2017) with high [K/Fe] variance. The central lower panel in Figure 2.5 shows the Mg-K plane. As seen in the background for other GCs observed by APOGEE (Schiavon et al., 2017; Masseron et al., 2019; Mészáros et al., 2020), a constant value around solar composition was reported, i.e., no K-production was found. K-enhanced stars are indeed expected in globular clusters if the polluters achieve high temperatures to create Potassium. Like K-rich stars, subsequent generations will also show Mg-depleted and Si-enhanced stars due to the lower temperature barrier of the Mg-Al-Si cycle, as shown in Mészáros et al. (2020) for some APOGEE GC stars.

With the present observations, we cannot determine the origin of the peculiar K-enhancement, which is not compatible with a constant value given the significant star-to-star variations. Optical follow-up is necessary to constraint the discrepancy extent of our measurements.

The α-element Ca

Most of the Calcium that we can measure in GCs stars is produced by supernovae, and therefore not affected by the H-burning processes neither of the stars nor of the polluters.

Mészáros et al. (2020) reported constant [Ca/Fe] values for APOGEE GCs, though warning about the weakness of the Ca lines in the near-IR at low metallicities. Their results are shown in the lower right panel of Figure 2.5 as background, along with the NGC 6544 stars.

In general, cluster stars follow the overall trend of constant Calcium abundance, centred at [Ca/Fe]= 0.21 ± 0.09 dex. There is a deviation of this behaviour, but only for stars with [Al/Fe]$\lesssim 0.15$ dex. These four stars, (3 lRGB and 1 AGB), however, also present large [Ca/Fe] errors according to ASPCAP. If we do not take into account these four outliers, the Calcium abundance can be described as a constant, with stat-to-star deviations within the errors.

Neutron-capture elements: Ce and Nd

Neutron capture elements, like Cerium and Neodymium, can be formed by a wide variety of channels in different contexts within the Galaxy (Sneden et al., 2008). However in a GC, the possible scenarios that can occur can be limited to a few like a burning shell in a massive stars or an evolved AGB star in the thermally pulsating phase (Bisterzo et al., 2011; Bisterzo et al., 2014). Within the APOGEE survey, multiple measurements of Ce and Nd have been reported since its characterisation and inclusion in subsequent DRs (Hasselquist et al., 2016; Cunha et al., 2017). Given the limited range of temperatures in which Ce can be reliably fitted and measured ($T_{\text{eff}} < 4400$ K according to Mészáros et al., 2020), all of the ASPCAP [Ce/Fe] abundances reported here and in the DR16 not in this temperature range, can be considered only as upper limits. ASPCAP García Pérez et al. (2016), as an automatic abundance pipeline, cannot handle correctly the difference between an upper limit and a non-detection in which the line is absent from the spectra. This is the case of all the Ce abundance measured and reported in this section. Moreover, to better constraint the Ce abundances, the BACCHUS (Masseron et al., 2016) code was used to properly account for the non-detections, even including more Ce lines to the fitting
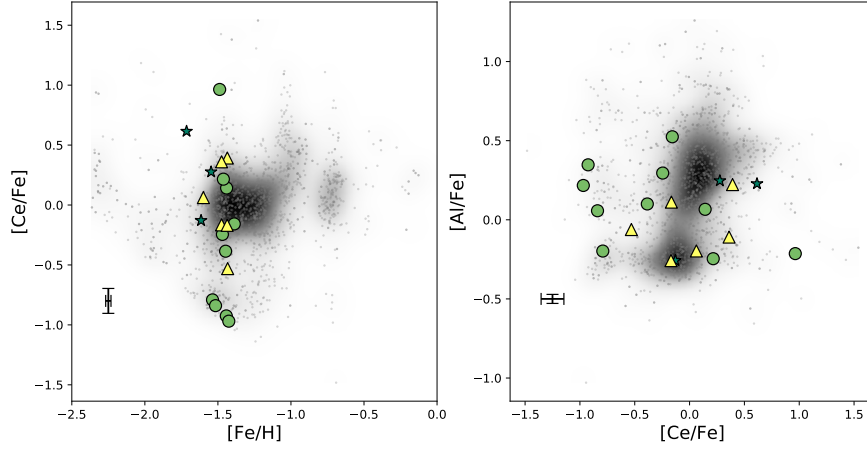
Figure 2.6: Upper limits for the [Ce/Fe] detections vs [Fe/H] (**Left panel**) and [Al/Fe] (**Right panel**) for the APOGEE observed clusters present in the DR16. NGC 6544 stars are colour-coded with the same markers as in Figure 2.4 and 2.5. A spread of almost ~ 2 dex in [Ce/Fe] can be explained by the inability of the ASPCAP pipeline to treat upper limits in the analysed spectra (see text).

procedure(Masseron et al., 2019; Mészáros et al., 2020).

Given that information, we can explain the behaviour of the [Ce/Fe] within the cluster. Figure 2.6 shows the [Ce/Fe] abundance as a function of the metallicity and [Al/Fe] for NGC 6544 and other APOGEE observed clusters. The wide range of [Ce/Fe] of 1.9 dex are solely explained by the fact that ASPCAP is not able to correctly fit the Ce line. As showed in Mészáros et al. (2020), ω Cen presents the most dramatic Ce enrichment of ~ 1 dex across ~ 1 dex of [Fe/H] enrichment, followed by NGC 1851/47Tuc. This marked difference exemplifies how our measurements do not represent the actual state of NGC 6544 [Ce/Fe]. Further analysis with cooler stars within the cluster are necessary before reliably establish the Ce status of NGC 6544.

Finally, no [Nd/Fe] have been reported for the selected NGC 6544 stars due to the combination of T_{eff} and [Fe/H] that the spectra of the GC presents. According to Hasselquist et al. (2016), only a fraction close to the $\sim 20\%$ of the total APOGEE spectra will show

Nd variations that are strong enough to be detected at a high-SNR.

Al-N correlation and its relation with NGC 6544 mass

Finally, and with the aim to check the consistency of the previous APOGEE results, we perform the same analysis of Nataf et al. (2019) that relates the amplitude of the Al- and N-spread with the cluster mass. This relation was built in the past DR14 version of the APOGEE database, however considering that the calibrations within DRs consists only in shifts on the abundance plane, we can assume that is still valid within errors. To built the relation, we need first to define the Δ[X/Fe] quantity, which is defined as

$$\Delta\left[\text{X/Fe}\right]_i = \left[\text{X/Fe}\right]_{\text{Gen II,i}} - \left\langle\left[\text{X/Fe}\right]_{\text{Gen I}}\right\rangle,$$

which relates the difference within the [X/Fe] value of each *i*-star with SG abundance patterns with the mean value of [X/Fe] but measured for FG stars. As derived in equation 6 of Nataf et al. (2019), we apply the relation within [Fe/H] and Δ[N/Fe] of the individual SG stars, and the cluster mass $\log\text{M/M}_\odot$ to derive the total Δ[Al/Fe] of the same stars. Given that the only unknown quantity is the total cluster mass, we can apply this relation to constraint the possible NGC 6544 mass values. The procedure is performed by comparing the reason of both Δ[Al/Fe] quantities, derived from Aluminum abundances, and from fixing the cluster mass. After calculating the median of all the stars, the most accurate mass will produce a value of $\Delta\text{Al} = \Delta[\text{Al/Fe}]_{\text{spectra}}/\Delta[\text{Al/Fe}]_{\text{fixed mass}}$ closer to 1. The results shown in Figure 2.7 correlates well with the statements of Nataf et al. (2019) in both the [Al/Fe]-[N/Fe] correlation (left panel) and the Δ[Al/Fe]-Δ[N/Fe] plane. Note that there are two different NGC 6544 total masses in the literature which differs by a factor of ~ 2, one listed in the Harris (1996) catalogue and used by Nataf et al. (2019) of $\log\text{M/M}_\odot = 5.05$, and the other one derived by Baumgardt and Hilker (2018) of $\log\text{M/M}_\odot = 4.80$. Also is important to highlight that at the time of fixing the cluster mass from the relation to calculate the trend line, we also fixed the metallicity of the cluster to [Fe/H] = -1.44 dex,
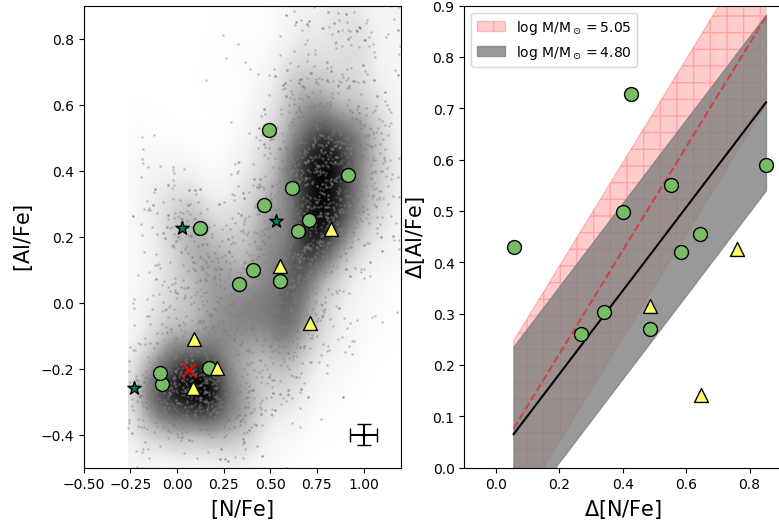
Figure 2.7: (**Left panel**): [Al/Fe]-[N/Fe] correlation for the cluster stars. A clear separation between FG and SG at [N/Fe]< 0.4 dex and [Al/Fe]< 0 dex for both abundances, respectively. Same symbols were used than in other figures for the different evolutionary stages. The red cross indicate the mean value of the FG stars, used later in the Δ[X/Fe] values. (**Right panel**): Δ[N/Fe]-Δ[Al/Fe] diagram as is shown in Nataf et al. (2019), with the continuous solid line representing the best fit using the lower mass value indicated in the legend, with its corresponding error as shaded area. Additionally, we include the fit as a dashed line (and hatched area for the error) with the mass value used by Nataf et al. (2019) to derive this relation. Note that only SG stars are showed in this panel for which Δ[X/Fe] can be measured.

as is stated in subsection 2.1.4. We use both masses and conclude that the Baumgardt and Hilker (2018) fully agrees within the errors the Al-N-Mass relation, which is showed as a continuous line in the right panel of Figure 2.7. To quantify this statement, both fixed masses produces a value of ΔAl equal to 0.82 and 1.00, for the Nataf et al. (2019) and Baumgardt and Hilker (2018) masses, respectively.

2.1.6   Galactic context

NGC 6544 is projected on the sky towards the bulge area in a very crowded region at $(\ell, b) \sim (5.8°, -2.2°)$. The first comprehensive observations describe the cluster as a relatively metal-poor one, unlike most other inner Galactic GCs (Cohen et al., 2014; Cohen et al., 2017; Cohen et al., 2018, and clusters there in). Indeed, Bica et al. (2016) and R. Contreras Ramos et al. (2017) classify NGC 6544 as a halo intruder in the bulge region based on metallicity estimates and simple orbital constraints. More recently, Pérez-Villegas et al. (2020) derived a more robust probability-based membership based on state of the art Galactic potentials for GCs in the inner Galaxy. With a very high percentage (within $\sim$80 to 97% depending on the Galactic bar parameters), NGC 6544 was classified as thick disk GC. Based on its [Fe/H] we can state that the cluster is consistent with the metal-poor tail of the canonical thick disk. In order to contextualise the present results for the cluster, we built a catalogue of GCs observed by APOGEE (Schiavon et al., 2017; Masseron et al., 2019; Mészáros et al., 2020). The median metallicity and total α-enhancement, as measured by ASPCAP in the DR16, were calculated. Figure 2.8 shows the chemical neighbourhood of NGC 6544, together with other clusters in the halo (NGC 7078/M 15, NGC 6341/M 92, NGC 5024/M 53, NGC 5466, NGC 7089/M 2, NGC 5272/M 3, NGC 6205/M 13 and NGC 5904/M 5), thick disk (NGC 6171/M 107, Pal 6, and NGC 6838/M 71), and bulge (NGC 6522, Ter 5, NGC 6528, and NGC 6553). We have also added a sample of randomly selected field stars from APOGEE DR16, representing 10% of the total catalogue, as comparison.

As a detailed comparison between the abundances of cluster stars and those of its spatial neighborhood, we show in Figure 2.9 the abundances of several elements in the cluster and in a sample of 3731 field stars located within 2° from the cluster centre, which are mostly bulge stars. The normalised abundance distribution are shown as a density estimation for both bulge and cluster population, whereby the median, min and max of the measurements of each element are marked. As it is clear from the Figure, cluster stars show a wider
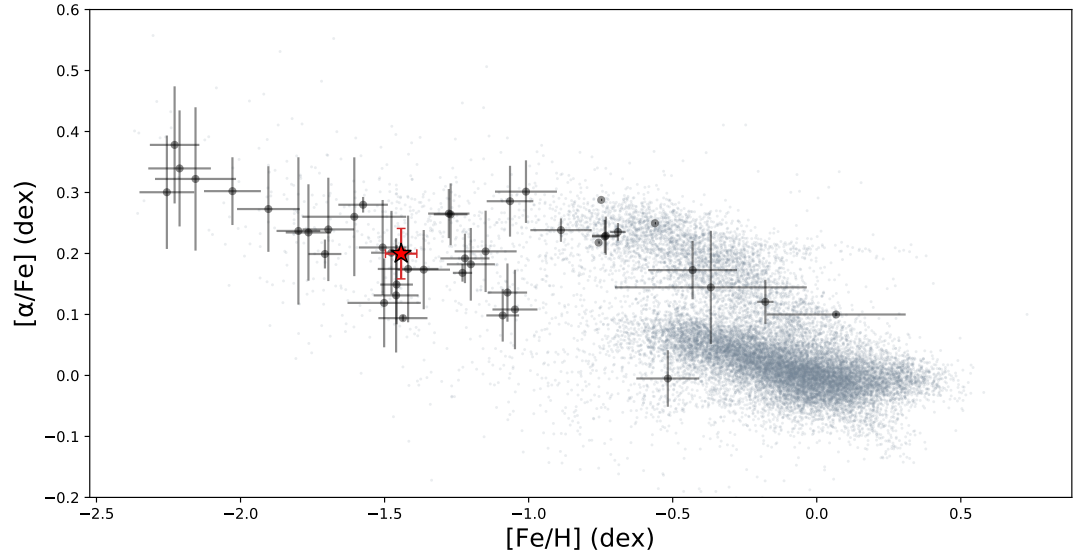
Figure 2.8: Tinsley diagram of the $[\alpha/\text{Fe}]$ enrichment across metallicity for the observed globular clusters by APOGEE (Schiavon et al., 2017; Masseron et al., 2019; Mészáros et al., 2020). Despite being in a similar position of some halo globular clusters (NGC 5272/M 3, NGC 7089/M 2, and NGC 6205/M 13 with [Fe/H] = -1.49, -1.56, and -1.60 dex, respectively), NGC 6544 (shown as a red star) was classified as thick disk GC by orbital reasons. As a background reference (small points), we place a randomly selected 10% of the whole APOGEE catalogue. The bulge, disk, and halo are visible, even showing the sequence of anomalous stars at $[\alpha/\text{Fe}] \sim 0.2$ dex, described by Zasowski et al. (2019).

range of abundances than field stars, for all the elements except Mg and Si. The effect is especially clear in [C/Fe], [N/Fe], [Na/Fe], [Al/Fe] (with hints of the bimodality reported in section 2.1.5), and [K/Fe]. Compared with previous results for field stars that may belong to GCs (Fernández-Trincado et al., 2016; Fernández-Trincado et al., 2017), we do not find any unusual abundance ratios in the nearby bulge stars that can be directly linked to NGC 6544.

Finally, given the remarkable elongation displayed by NGC 6544 caused by the Galaxy (R. Contreras Ramos et al., 2017), we also search for extra tidal stars within the APOGEE DR16. We use the derived metallicity and space velocity for the cluster within this work as a first guess. Unfortunately, we did not find additional members within $\sim 10°$ from the cluster centre. The use of more extended and deep data is mandatory to constrain the expected tidal tails of NGC 6544. Upcoming releases of the APOGEE data, and also forthcoming stellar wide-field multi-object spectroscopic surveys like 4MOST (de Jong et al., 2019) and MOONS (Cirasuolo et al., 2011), will help to identify extra tidal members, if they exist, as it was strongly suggested by previous studies (Cohen et al., 2014).

2.1.7 Concluding remarks

We have performed a near-IR high-resolution spectral analysis for the reddened GC NGC 6544. With 23 confirmed members in the APOGEE DR16 data, this is the most complete study up to date, to characterise the abundance patterns of this cluster. Across the RGB (below and above the bump) and AGB, the abundances derived by the ASPCAP pipeline were presented and discussed in the context of other Galactic GCs. Known anticorrelations (Mg-Al, C-N, Na-O) were used to isolate two generations of stars, a FG with 9 members and a SG with 14 members. For a random targeting, these numbers are in very good agreement with predictions about the number of FG stars that still remain in GCs (close to ~ 13 of the total population).

A large [Al/Fe] spread of 0.78 dex, negligible [Mg/Fe] dispersion, a significant variation
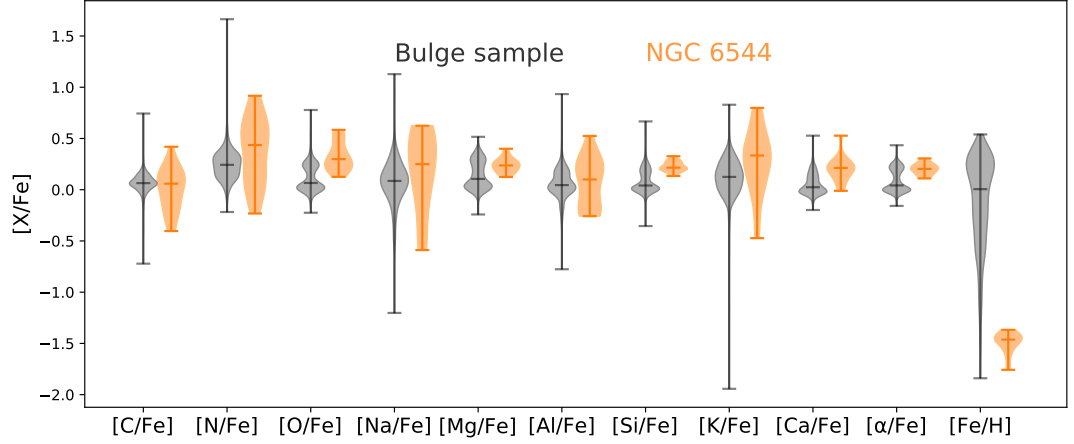
Figure 2.9: [X/Fe] abundance density estimation comparison between bulge (left grey symbols) and cluster (right orange symbols) stars. Each violin representation was normalised, and indicates with horizontal lines the median and limits of the distribution.

of CNO, across all the sampled evolutionary phases was a pivotal factor to divide different generations of stars. The metallicity and α-element abundances for RGB stars, from which we have a bonafide abundance determination, are -1.44 ± 0.05 dex and 0.20 ± 0.04 dex, respectively. Using a correlation within the cluster Aluminium, Nitrogen, and metallicity we were able to constraint the NGC 6544 mass, favouring the less massive proposed scenario with $\log M/M_\odot = 4.80$.

Multi-survey synergies were used to derive other cluster properties, such as the distance, reddening law towards the cluster and confirming its Galactic classification. Finally, no extra tidal or chemically peculiar stars were found around the cluster, using data from the APOGEE DR16. Still, this picture could change with future and deeper spectroscopic surveys, which might explain the spatial elongation of NGC 6544.

3

Dynamical analysis of the Galactic bulge globular cluster candidates

3.1 Globular cluster candidates in the Galactic bulge: Gaia and VVV view of the latest discoveries[1]

Given the importance of the dynamical information when describing a stellar population in the Gaia era, and driven by the results of R. Contreras Ramos et al. (2017) deriving the VVV proper motions, we start exploring the bulge area, trying to confirm a large number of globular clusters candidates. Additionally, using the Gaia and VVV proper motion catalogues, we start a blind search for groups of stars within the bulge area with cluster-like patterns. During this section, we present one of the five newly discovered globular clusters (`Gran 1`), which was later confirmed by a subsequent spectroscopic follow up.

3.1.1 Introduction

Star clusters are invaluable astrophysics tools for a number of reasons. In addition to being a laboratory for stellar evolution, including chemical evolution and self-enrichment, they are among the few objects for which a rather precise age can be measured. If young and massive, their mass function closely resembles the initial mass function (N. Leigh et al., 2012; Webb and N. W. C. Leigh, 2015). For all the others, the radial variation of the

---

[1]Based on the article published by Gran et al. (2019)

43

present-day mass function allows us to quantify the internal dynamical evolution, while the global present-day mass function is related to the dynamical interaction of the cluster with its environment. Although we do not know exactly how and where massive clusters form (Duncan A. Forbes et al., 2018), we know that stars do not form in isolation. Most of them form in groups, if not in massive clusters, and therefore the struggle to get a census of the cluster population of a galaxy is motivated by their relevance for building up the field star population (Kruijssen et al., 2019b).

In recent decades, the number of candidate star clusters reported in the literature has increased significantly, thanks to wide area photometric surveys that allowed to literally scan the sky in search of groups (S. Koposov et al., 2007; Belokurov et al., 2010; Muñoz et al., 2012; Ortolani et al., 2012; Belokurov et al., 2014; Laevens et al., 2014; Bechtol et al., 2015; Kim and Jerjen, 2015; Laevens et al., 2015a; Laevens et al., 2015b; S. E. Koposov et al., 2017; Luque et al., 2017; Ryu and Lee, 2018, and references therein). In the direction of the Galactic bulge only, from VISTA Variables in the Vía Láctea (VVV; Minniti et al., 2010) survey images, Minniti et al. (2011a) reported the discovery of the candidate globular cluster (GC) VVV CL001, Moni Bidin et al. (2011) identified two more candidate clusters CL002 and CL003, Borissova et al. (2014) listed 58 new infrared star cluster candidates, and another cluster candidate, already catalogued as cluster candidate, was further analysed in search for variables by Minniti et al. (2017b). Another 84 old cluster candidates were reported by Minniti et al. (2017a), Minniti et al. (2017c), and Minniti et al. (2017d) based on detection of spatial overdensities, projected overdensities of RR Lyrae variables, and projected overdensities of RR Lyrae and type II Cepheids, respectively. Finally, another five GC candidates were identified by Camargo (2018) by visual inspection Wide-field Infrared Survey Explorer (WISE) images.

Although new star clusters can be initially identified as overdensities, the only way to confirm their cluster nature is to verify that their stars move coherently in space, i.e., they are gravitationally bound. This can be done by measuring either radial velocities or proper motions (PMs) of stars in a region centred at the centre of the spatial overdensity.

In the present paper, we describe a method to identify unusual concentrations of stars simultaneously in the plane of the sky, vector point diagram (VPD), and colour-magnitude diagram (CMD).

The data used in this work come mostly from the second data release (DR2) of the Gaia mission (Gaia Collaboration, Prusti, et al., 2016; Gaia Collaboration, Brown, et al., 2018), including positions, PMs (Lindegren et al., 2018), and magnitudes in three photometric bands for all of the stars (Riello et al., 2018; Evans et al., 2018). The work of Pancino et al., 2017, Gaia Collaboration, Helmi, et al., 2018, and Vasiliev, 2019b illustrates the potential of Gaia to characterise the GCs known up to date. In the region close to the Galactic plane, at latitudes $|b| < 3°$ the Gaia catalogue is highly incomplete owing to the large interstellar extinction affecting optical fluxes, and, to a minor extent, to the higher stellar surface density coupled with the limited transmission bandpass of the satellite. In this region, Gaia detects almost exclusively the brightest blue disk stars, while it is virtually blind to the bulge red giants. On the contrary, the near-infrared (near-IR) VVV observations are optimised for the reddest bulge giants, and the PM catalogues obtained with the method described in R. Contreras Ramos et al. (2017) are both deeper and more precise than the Gaia catalogue. We use the VVV PMs, in addition to Gaia to analyse candidate clusters at latitudes $|b| < 3°$.

The section is organised as follows: subsection 3.1.2 describes the automated method to detect –and simultaneously confirm– new star clusters, including the detection of a new old star cluster labeled `Gran 1`. Subsection 3.1.3 presents an analysis of the PM of stars within 1 arcmin from the nominal position of a sample of 93 old cluster candidates reported by Minniti et al. (2011a), Moni Bidin et al. (2011), Minniti et al. (2017a), Minniti et al. (2017c), Minniti et al. (2017d), Camargo (2018), and Bica et al. (2018). The present clustering method was then applied, with relaxed parameters, within a region of 2 arcmins across the centre of each cluster candidate, to double check against possible errors in the candidate estimated centres. Finally, subsection 3.1.4 summarises our results. The VPDs and CMDs of all the unconfirmed candidate clusters are included in Appendix 5.1.2.

3.1.2   Method to detect coherent groups

The region selected to search for star clusters was the whole bulge area within $-10°\,(\ell,\,b)\,10°$. This region was divided in small circles of $0.8°$ radius, centred on every integer degree in Galactic latitude and longitude. An algorithm was developed to search for stars that have an unusually large number of neighbours in a five-dimensional phase-space including coordinates, colour, and PMs. For each star with complete information, the algorithm counts the number of neighbours within 1 arcmin in space, one mas/yr in PM, and 1 mag in colour using the K-Dimensional Tree (KDTree) implementation on `scikit-learn` (Pedregosa et al., 2011). For each given field, a minimum threshold of 10 neighbours per star was imposed to ensure statistical significance of the results. Stars with more than 10 neighbours within the complete magnitude range were then searched for groups, in the phase-space mentioned above, with the Density-Based Spatial Clustering of Applications with Noise (DBSCAN) algorithm (Ester et al., 1996) also implemented in the `scikit-learn` package. Groups were kept as candidate clusters and then visually inspected only if they contained at least 20 members. We note that a group of neighbour stars define "a neighborhood" that may end up being significantly larger than the phase-space radius (1 arcmin, 1 mas yr^{-1}, 1 mag) used for the initial search around each star.

It should be noted that several false positives are detected by the algorithm, that is, close to the mean PM of bulge $(-6, -0.2)$ and disk $(-2, -0.5)$ field stars, in the VPD. After visual inspection, however, we keep only clusters that define narrow sequences in the CMD that are significantly different, by shape and/or tightness, from the main branches of the bulge+disk CMD.

A very first step for the validation of the algorithm described above is that it must be able to rediscover all the clusters known to exist in the area explored. In order to verify this, the catalogue of overdensities was cross-matched with the latest version of the `Global survey of Milky Way star clusters` (MWSC; Kharchenko et al., 2016) catalog to identify all the clusters that were previously known. Indeed, we detected all the 45 known

bulge GCs in this region and $\sim 17\%$ (22/129) of the open clusters up to 5 arcmins from their nominal centre. Five known GCs located in the region $|b| < 2.5°$ (Terzan 4, Terzan 6, Terzan 10, 2MASS-GC002, and Djorg 2) were not detected in Gaia, but they were detected in VVV. Another 4 that are listed in the MWSC catalogue as candidate GCs, namely ESO 456-09, ESO 373-12, FSR 0019, and FSR 0025, were not detected in either of the two surveys. Based on our data, we do not find any evidence allowing us to confirm their cluster nature.

Figure 3.1 shows the detection of Terzan 1 ($\ell = -2.44°$, $b = 0.99°$, Ortolani et al., 1999). The mean PM of this cluster is very similar to the mean PM of bulge stars (lower left panel). Nonetheless, the algorithm detects a higher concentration of stars, in the VPD, with respect to a smoother background. Of course, the detection is also triggered by the clustering of Terzan 1 stars both in the plane of the sky (upper left) and in the CMD (right). We note that, as explained above, the algorithm can detect compact sequences of stars, in addition to roundish groups. We overplot a PGPUC isochrone (Valcarce et al., 2012) for a [Fe/H] = -1 dex, 12 Gyr simple stellar population, at the cluster distance quoted in Kharchenko et al. (2016), to confirm that the overdensity is indeed Terzan 1.

The algorithm is also able to detect open star clusters. As an example, Fig. 3.2 shows the recovery of ESO-589-26, a young star cluster reported at RA=18:02:14, DEC=-21:54:54 (l,b)=(7.9517°, 0.3279°), which our code independently detected 7 arcsec away from its nominal position. A total of 62 cluster members were identified with our method, defining a narrow main sequence in the CMD and a very coherent group in the VPD. A 3 Myr PARSEC (Bressan et al., 2012) isochrone of solar metallicity is included in the CMD to guide the eye. The isochrone was shifted to a distance of ~ 2.4 kpc, as reported in Kharchenko et al. (2016).

Application of this neighbour algorithm to the selected bulge area yielded several cluster candidates not listed in the MWSC catalogue. We visually inspected the region within a radius of 5 arcmins from the centre of each of these cluster candidates and ended up with at least seven new GCs. The new clusters will be published in dedicated forthcoming
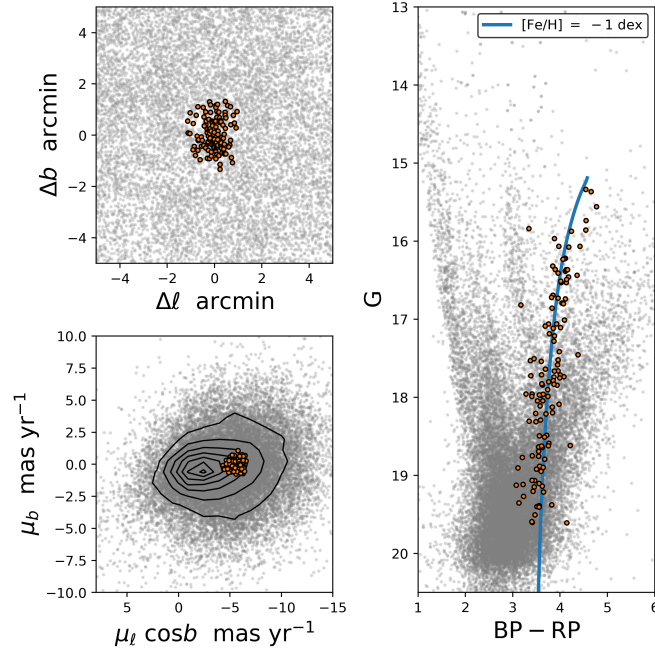
Figure 3.1: Globular cluster Terzan 1 as detected by our algorithm. The orange points represent the detected overdensity along with background stars (grey points) within 15 arcmins from the detected cluster centroid. The grey stars define three populated sequences from left to right: the disk MS, disk red clump (both spread along the line of sight), and the bulge upper red giant branch with a PGPUC isochrone overplotted.
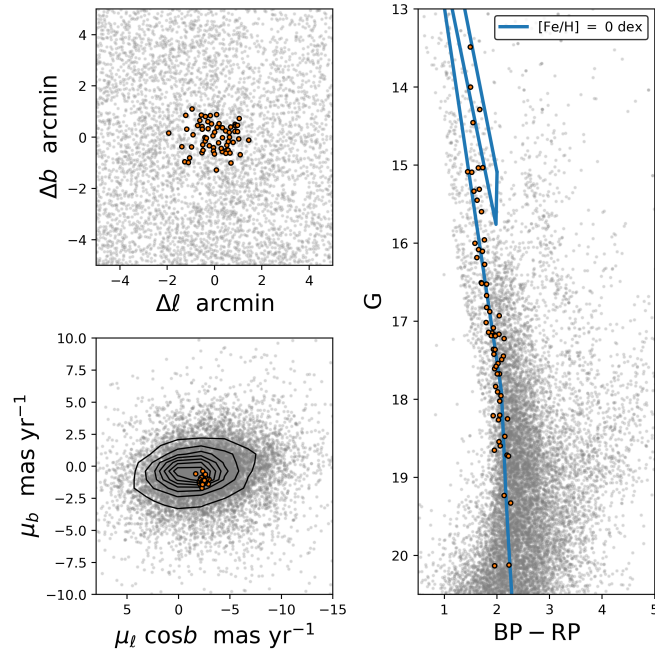
Figure 3.2: Open cluster ESO 589-26 as detected by our algorithm. The background sequences are the same as in Fig. 3.1, although the bulge red giant branch is highly incomplete because this cluster is located very close to the Galactic plane ($b = 0.33°$) in a region of the sky with large interstellar extinction.

papers once they have been spectroscopically confirmed. We show in this paper only one of the new GCs, which we name `Gran 1`, as an example of the ability of the algorithm to find new clusters. Further, we examine the candidate cluster VVV CL001 (Minniti et al., 2011a), VVV CL002, VVV CL003, and VVV CL004 discussed in Moni Bidin et al. (2011), the 84 candidate clusters published in the series of papers by Minniti et al., 2017a, Minniti et al., 2017c, and Minniti et al., 2017d, plus another five candidates presented in Camargo, 2018, one of which is further analysed by Bica et al., 2018.

New globular cluster Gran 1

A new cluster, not present in the MWSC catalogue, was initially detected as a group of 24 stars within 0.731 arcmins from $(\ell, b) = (-1.22°, -3.98°)$ (RA=17:58:36.61 DEC=-32:01:10.72). As we believe that this is the first detection of a cluster in this position, we name it `Gran 1`. The plots that triggered its discovery are shown in Fig. 3.3. The 24 clustered stars initially found by the code were used to define a cluster centre, both in the plane of the sky and in the VPD. These positions were used to select all the stars included both within 2 arcmin in the sky and within 2 mas yr^{-1} in the VPD, which yielded 95 stars, shown as filled orange circles in Fig. 3.3. The CMD in the right panel demonstrates that they are compatible with the RGB and horizontal branch (HB) of a cluster with [Fe/H]=-1 dex, located at a distance of ≈ 8.8 kpc, or m$-$M+A$_{K_s}$= 15 mag, i.e., within the Galactic bulge. We emphasise that the cluster metal content, distance, and age cannot be constrained by the present data, as the turnoff cannot be identified in the CMD, future spectroscopic follow-up will derive more precise parameters of this cluster. As a reference, we show a 12 Gyr PGPUC isochrone overplotted to the data, using the putative red clump and HB stars (J-K$_s$ ~ 0.25 mag and K$_s$ ~ 15 mag) as an anchor to estimate a reddening of E(J$-$K$_s$) and, adopting the extinction law by Nishiyama et al., 2009, a total extinction of A$_{K_s}$. The age was assumed to be larger than 10 Gyr, owing to the presence of the two blue HB stars, whose nature would need confirmation. If these two stars are proved to be field

stars, the age of the candidate cluster could be lower than the estimate we give in Table 3.1.

It should be noted that Gran 1 would not have been discovered as a high spatial concentration only because this cluster has an overdensity of only 3.4 sigma above the mean stellar density of the field in this region. Gran 1 is detected in this case because the selected cluster member stars are simultaneously clustered in the plane of the sky and they share a coherent motion with a median value of $(\mu_\ell \cos b, \mu_b) = (-11, +3)$ mas yr^{-1}, which is off-centred with respect to the mean PM of field stars. The integrated magnitude of Gran 1, down to the limit magnitude of the VVV catalogue is $K_s = 8.07$ mag, while that of Terzan 1 in the same range is $K_s = 5.24$ mag. Gran 1 is similar in luminosity to Whiting 1, AM 4, or Koposov 1 (Harris, 2010). A JYZ colour image of the newly discovered cluster is shown in Fig. 3.4.

3.1.3 Application to candidate globular clusters in the literature

Hereafter we examine various sets of candidate clusters recently published in the literature. Specifically, Minniti et al. (2011a) reported on the discovery of a low mass GC, named VVV GC001, at coordinates $(l, b)=(5.25°, 0.78°)$, (RA=17:54:42.5, DEC=-24:00:53), that is, approximately 10 arcmins away from the known GC UKS 1. In the same year, Moni Bidin et al. (2011) detected three new candidate clusters tentatively named VVV GC002, GC003, and GC004. Upon analysis of their CMD, the same authors concluded that they were most likely a GC, a stellar association, and an overdensity whose nature could not be established, respectively.

In 2017, Minniti et al. compiled a catalogue containing 84 GC candidates based on overdensities of stars in the plane of the sky (Minni 1 to Minni 21; Minniti et al., 2017a) and on the coincidence in the plane of the sky of a couple or more RR Lyrae (Minni 22 to Minni 60; Minniti et al., 2017c) and/or Type II Cepheids (Minni 61 to Minni 84; Minniti et al., 2017d) within 2 arcmins. In the latter two papers, these authors checked that at least two of the variables within each group had magnitudes consistent with
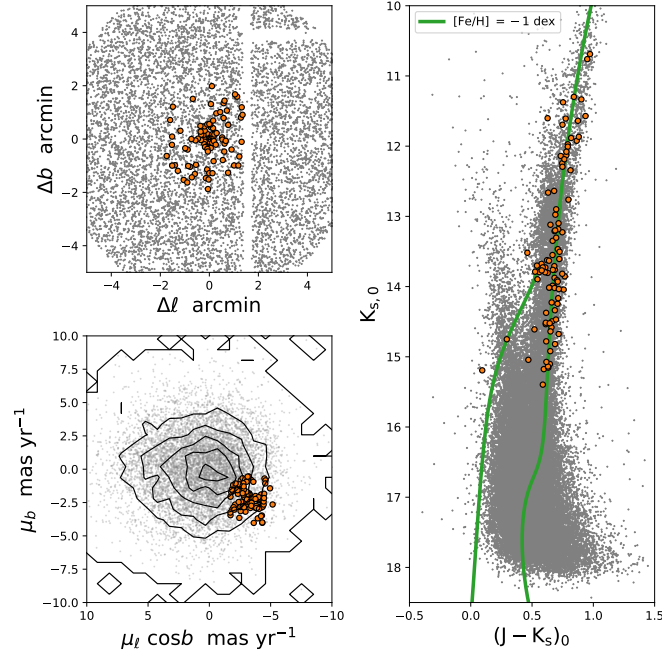
Figure 3.3: New GC Gran 1 as detected in the plane of the sky (upper left), in the VPD (lower left), and in the dereddened CMD (right). All data are from VVV, using the dereddened PSF photometry by Surot et al. (2019) and the PMs from R. Contreras Ramos et al. (2017). Small, light grey dots are field stars within 5 arcmin from the cluster centre given in Table 3.1, while large orange dots are bonafide cluster members. Blank stripes in the upper left panel denote the chip separations where stars were rejected because the PM values were not well constrained (R. Contreras Ramos et al., 2017).

Table 3.1: Basic parameters for the newly discovered GC Gran 1, derived from the present analysis. We emphasise that the metallicity, age, and distance for the cluster are very uncertain, as they were derived using 76 stars by comparing the observed CMD with a PGPUC isochrone.

Parameter	Value	Unit
ℓ	-1.2320	deg
b	-3.9776	deg
RA (J2015.5)	17:58:36.61	hh:mm:ss
Dec (J2015.5)	$-32:01:10.72$	dd:mm:ss
E(J-K$_{\rm s}$)	~ 0.45	mag
$A_{K_{\rm s}}$	~ 0.24	mag
$d_\odot$	~ 8.8	kpc
$\mu_\ell \cos b$	-10.9426	mas yr^{-1}
μ_b	3.0252	mas yr^{-1}
$\mu_\alpha \cos \delta$	-8.0583	mas yr^{-1}
μ_δ	-8.0833	mas yr^{-1}
Age	$\sim 8 - 12$	Gyr
[Fe/H]	~ -1	dex
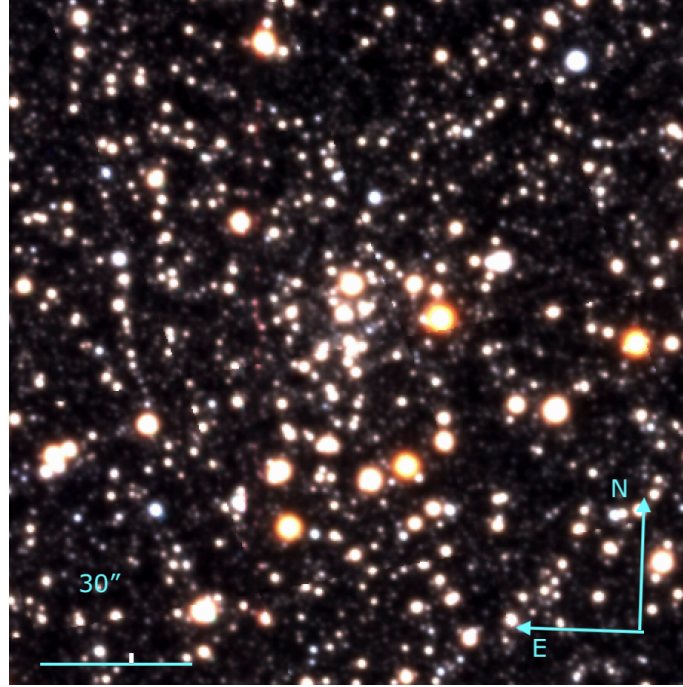
Figure 3.4: JYZ color image of the new GC Gran 1 from the VVV Data Release 4.

similar distances. Finally, Camargo (2018) published a list of 5 clusters visually selected in multicolour images from the WISE satellite, and then analysed these sources using 2MASS photometry and Gaia DR2 PMs.

The algorithm developed in this work, which were applied to the Gaia PM catalogue, did not blindly detect any of the 93 cluster candidates mentioned above (4 VVV GCs, 84 Minnis, plus 5 Camargos) in the Gaia DR2 catalogue. Because of the much higher stellar density close to the plane, a blind search across the VVV area within $|b| \lesssim 3°$ yielded a large number of overdensities, which will be examined and validated in a forthcoming paper. For the present purpose, we only need to search in a very restricted area around their nominal centres to validate previously published candidate clusters. Therefore, we ran the original code, this time allowing for a lower minimum number of member stars (15 instead of 20) only in a region of 2 arcmins radius around the candidate centres for stars brighter than G = 19 mag. We ran this restricted search for all the 93 clusters, on the

Gaia catalogue, and for the 54 candidates (4 VVV GC, 46 Minnis, and 4 Camargos) within $|b| \lesssim 3°$ on the VVV PM catalogue.

As a result, only the candidates VVV GC001 and GC002 seem to be real clusters. Both of these lie relatively close to the plane, and nothing is detected in the Gaia catalogue. In VVV data, however, the algorithm picks up an overdensity of stars whose mean PM is offset with respect to the mean PM of field stars, and who define a rather narrower RGB sequence compared with that of field stars within the same spatial region. This is illustrated in Fig. 3.5 and Fig. 3.6.

For all the others, the algorithm either did not detect any overdensity nor did it detect a broad peak, but it was centred in the VPD at the same position of the median PM of field stars and the CMD did not show anything different from the CMD of field stars. Appendix 5.1.2 shows the spatial selection of stars within 1 arcmin from the candidate centre, together with their position in the VPD, compared to that of field stars within 10 arcmins of the published centre, and the CMD of both. For each cluster, we show these diagrams from Gaia data on the left and, if available, from VVV data on the right. We also include the two confirmed candidates VVV GC001 and VVV GC002 in order to demonstrate that we would have been able to confirm these even without using the clustering algorithm. In fact, by selecting stars within 1 arcmin from their centre in the VVV data the field contamination is larger, but a group of stars with a mean PM offset from that of field stars is visible in both of these. The offset is smaller for GC001, where the CMD is better defined; the offset is larger in GC002, where the CMD alone would be more ambiguous. On the contrary, by means of these plots, we reject all the clusters that were not the VPD nor the CMD, which allows us to see anything clearly different from the dominant field population. With this argument, we concluded that by means of the present data we cannot confirm the cluster nature of any of the other 91 candidates.

A few considerations are in order. First, it is expected that by pure Poisson statistics applied to the VPD, we would expect larger fluctuations where the density of stars is higher. That is, at the peak PM of field stars. In other words, we expect a large number of false

positives whose mean PMs are identical to those of the dominant population of field stars, whether bulge or disk. Second, we used the catalogue of 150 GC PMs provided by Vasiliev (2019b), together with the mean bulge PM from Reid and Brunthaler (2004)[2] to estimate what fraction of known clusters are expected to have a mean PM centred at the mean value for bulge stars. The result is that only 7 clusters have mean PM within 1 mas yr^{-1} from the mean bulge PM. Of those, only 3 are located within the area explored in this work, where there are in total 49 clusters. In other words, only 7% of the clusters located in the bulge are expected to have the same mean PM as bulge stars.

If the candidate clusters were massive enough, we would detect these clusters even if their PM would be identical to the peak of bulge stars, as we do for Terzan 1. Therefore, we can safely exclude that any of the 91 candidates that we do not confirm in this work are as massive as Terzan 1. In order for these candidates to be real, they must have a very low mass, and/or low central concentration and their PMs must be identical to those of bulge stars. This is expected to be true for at most 6 of these candidates.

3.1.4   Summary

We present a clustering algorithm that looks for overdensities simultaneously in a five-dimensional space including the two coordinates in the sky, the corresponding stellar PMs in each coordinate, and one colour. The algorithm was independently applied to the Gaia DR2 catalogue of a region of the sky within $-10° \leq \ell, b \leq 10°$, and to a VVV catalogue including point spread function (PSF) photometry and PMs for stars within $|b| < 3°$, where Gaia is highly incomplete for bulge stars owing to large interstellar extinction.

With the adopted parameters, discussed in Sec. 3.1.2 the algorithm is able to recover all the clusters known to be present in this area and to find several new young and old star

---

[2]The authors quote $(\mu_\ell \cos b, \mu_b)=(-6.379, -0.202)$ mas yr^{-1} as the absolute PM of Sagittarius A, which must coincide with the mean absolute PM of bulge stars. Converted to equatorial coordinates, this gives $(\mu_\alpha \cos \delta, \mu_\delta)=(-3.15, -5.55)$ mas yr^{-1}, which we subtract from the values in Table B1 from Vasiliev (2019b).
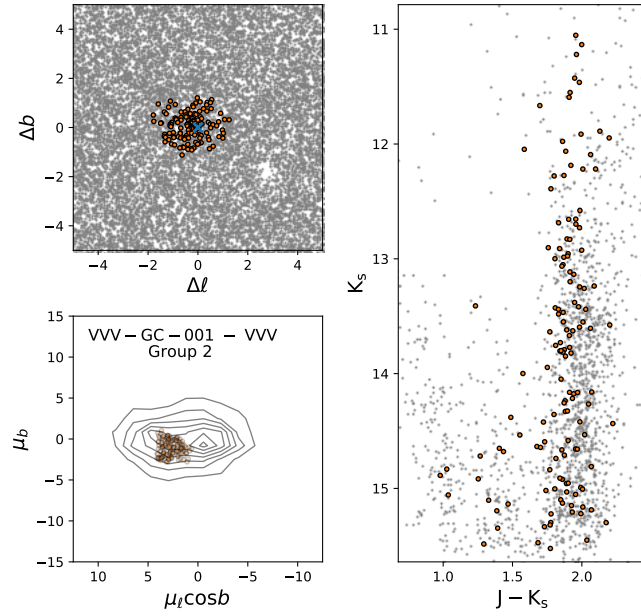
Figure 3.5: Diagnostic plots for the GC GC001 Stars within 2 arcmins from the nominal cluster centre were used to perform the clustering algorithm. The spatial distribution of stars (Group 2 defined by the code) that comprise the GC are shown in orange points (upper left), plotted in the VPD (bottom left) and in the CMD. We note that the distribution of cluster stars is shifted with respect to the contours of the total distribution of stars in the VPD.
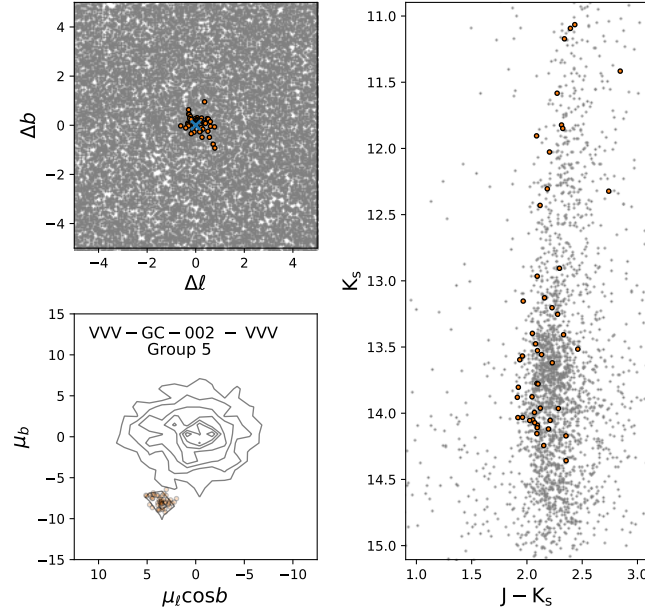
Figure 3.6: Same as Fig. 3.5 for the GC VVV GC002.

clusters. We presented the detection of one old cluster named `Gran 1` and deferred the discussion of the other new clusters to forthcoming, dedicated paper.

The PMs of Gaia and VVV were then used to confirm or dismiss the cluster nature of 93 cluster candidates recently presented in the literature. Based on the requirement that the putative cluster members must move coherently, we could confirm 2 of these candidate (VVV GC001 and VVV GC002) and discarded another 91.

The present result emphasises that statistical fluctuations of the projected stellar density in the plane of the sky or a chance alignment of a few variable stars can be relatively frequent in a huge survey such as Gaia and VVV. These statistical fluctuations can be easily mistaken for a star cluster for two reasons. First, the stellar population of the Galactic bulge has a (relatively low) spread in metallicity and age that makes its RGB only slightly wider than that of a GC. Second, when selecting stars in a small region of the sky, that is within a few arcmins from a spatial overdensity peak, the CMD sequences always appear narrower than those of a wider region because they are affected by a lower differential extinction.

For this reason, the list of candidate new star clusters published in the last few years has increased enormously. Only stellar motions, however, can confirm the real cluster nature of a detected overdensity and these have proven to dismiss the large majority of candidates. Given the present availability of Gaia PMs across almost the whole sky, the claimed detection of new candidate clusters should always be supported by kinematics analysis, proving that the cluster member stars move coherently in space.

By means of the present data, we cannot exclude that a few of the candidates are extremely low mass clusters that happen to have zero PM with respect to bulge stars, are located at a distance very close to 8 kpc, and present relatively broad CMD sequences possibly owing to differential extinction. We can only state that, because of these characteristics, they would be invisible to both Gaia and VVV. It is important to keep this in mind, however, when deciding whether to allocate telescope time to follow-up studies of such candidates.

Five new globular clusters in the Milky Way: from the bulge to the halo

4.1 Hidden in the haystack: low-luminosity globular clusters towards the Milky Way bulge[1]

As a natural continuation of the last section, we started a complete characterisation and analysis of the discovered clusters. After the photometrical and dynamical analysis with Gaia and VVV data, we secured a follow-up with the MUSE IFU to derive radial velocities, metallicities and orbital parameters of the clusters. We confirm all of the globular cluster nature, giving hints that a new population of clusters, not observed before, is present towards the Galactic bulge. From this analysis, we can infer a minimum mass of the clusters still in the bulge area, which is in the same order of magnitude as other studies.

4.1.1 Introduction

Globular clusters (GCs) represent one of the most valuable stellar tracers that can be observed to understand the Milky Way (MW) evolution. They allow us to constrain ages, masses and distances with unique precision, in contrast with most stars located in the Galaxy. Only recently and for a limited sample of stars, a more precise determination of those parameters became available in the second Data Release (DR) of the Gaia catalogue

---

[1]Based on the article published by Gran et al., 2021b

(Brown, 2021).

Their contribution to the MW assembly has been widely explored in numerical simulations (Kruijssen, 2019; Kruijssen et al., 2019a; Carlberg, 2020), presenting the proto-GCs properties and suggesting that most of their stellar content is now lost in the inner Galaxy (Baumgardt et al., 2019). From the observational point of view, it seems established that the properties of GCs observed today in the Galaxy are different from those that they had when they formed at high redshift (Renzini, 2017; Carlberg, 2020). A similar hypothesis is needed to explain the observations of multiple stellar populations in massive GCs, whereby the first generation of stars must have been much more massive than currently observed, to enrich the second generation (see, e.g. Bastian and Lardo, 2018; R. A. Gratton et al., 2019, for recent reviews).

Besides, GCs can be used to trace the different components that have been assembled during the history of the build-up of our Galaxy. A tentative separation of the Galactic GC population was proposed by D. A. Forbes and Bridges (2010), Leaman et al. (2013) and Myeong et al. (2018), the latter employing orbital energy criteria to classify the *in situ* and accreted GCs. The accreted group comprises those GCs formed within dwarf galaxies, then accreted by the MW (Mackey and Gilmore, 2004; Myeong et al., 2019). One of the most important implications of these results is that bulge GCs have an essential role in the characterisation of the early phases of the Galaxy formation, as they can trace the fossil record of its early stages (Barbuy et al., 2018; Zoccali, 2019).

Despite the critical role that the Galactic bulge GCs play in the characterisation of the early Galaxy, no consensus has been reached on the absolute number of clusters belonging to this component. This is primarily due to significant and differential extinction towards the disk and bulge and more considerable contamination by field stars. Both occurrences hinder our ability to recognise the cluster colour-magnitude diagram (CMD) sequences against the field stars. To complement this scenario, it was also reported that even in the most distant regions of the MW, the same uncertainty is observed (Webb and Carlberg, 2021).

According to the analysis of Baumgardt et al. (2019, see their Figure 8), we are only detecting the high-mass end of the bulge GCs. They also derive that a minimum mass was required for a given GC to survive the dynamical processes going on in the early inner Galaxy. Recent observational efforts to complete the census of bulge GCs include systematic searches in the near-infrared (near-IR) 2MASS (Skrutskie et al., 2006) and VISTA Variables in the Vía Láctea (VVV, Minniti et al., 2010) surveys, and more recently, in the Gaia survey (Gaia Collaboration, Prusti, et al., 2016; Lindegren et al., 2018; Gaia Collaboration, Brown, et al., 2018; Gaia Collaboration, Brown, et al., 2021). Despite the latter being an optical survey, its very precise astrometry permits to kinematically distinguish cluster from field stars, dramatically improving the cluster detection capabilities. Only in the direction of the Galactic bulge, in the last few years, the number of publications reporting the discovery of new GC candidates has risen significantly (e.g., Minniti et al., 2011a; Moni Bidin et al., 2011; Borissova et al., 2014; Minniti et al., 2017b; Minniti et al., 2017a; Minniti et al., 2017c; Gran et al., 2019; Palma et al., 2019; Garro et al., 2020).

Recently, a large body of evidence of the contribution of GCs to the star content of the disk (Price-Jones et al., 2020) and bulge (Hughes et al., 2020; Horta et al., 2021; Kisku et al., 2021) has been revealed. It is clear from that view that GCs will dissolve because of the strong MW gravitational potential, producing extended stellar tails or streams. Nevertheless, those remnants are extremely difficult to isolate from the field population, with only a few exceptions towards the inner Galaxy (Ibata et al., 2001; A. M. Price-Whelan et al., 2016; Ibata et al., 2018; Price-Jones et al., 2020).

We will focus our study on the compact cores or remnants of these processes, as we can identify them as overdensities in star counts, variable star content or any other dynamical tracer. However, by definition, a cluster needs to be dynamically bound. Thus the only way to confirm an overdensity detection as a real cluster is by verifying that the stars move coherently in space, using either radial velocities (RVs), proper motions (PMs), or both. In fact, a major fraction of the new bulge GC candidates that have been found based on star counts in previous studies were discarded by Gran et al. (2019) using dynamical constraints.

Specifically, the PM dispersion of the putative cluster members was comparable to that of the field stars in a spatial region near the centre of those cluster candidates. Similar issues arise from the Cantat-Gaudin and Anders (2020) analysis of open clusters candidates.

In the present paper, new GC candidates are presented based on a refined version of the technique introduced in Gran et al., 2019 to detect coherent groups of stars. The initial search was performed on the Gaia DR2 catalogue and later confirmed in the Gaia early-DR3 (EDR3) database. The detected clusters were also searched in the VVV PSF photometry (R. Contreras Ramos et al., 2017; Surot et al., 2019, Contreras-Ramos in prep.), which contains deeper and more precise photometry in the most extincted regions close to the Galactic plane. Finally, the possible presence of RR Lyrae was verified using the OGLE IV and Gaia catalogues (Soszyński et al., 2019; Gaia Collaboration, Eyer, et al., 2019) if the candidate GC exhibits a well-defined horizontal branch.

The section is organised as follows: subsection 4.1.2 describes the Gaia DR2/EDR3 catalogue that was used to search for new GCs and the algorithm adopted to detect clusters. subsection 4.1.7 presents the structural and dynamical analysis of the newly discovered GCs. subsection 4.1.11 presents the spectroscopic confirmation of four GCs, together with their RVs, mean metallicities and derived orbits. Finally, subsection 4.1.12 summarises the discoveries and state the prospects of this population. Appendix 5.1.3, 5.1.3, and 5.1.3 contain all the plots relative to each of the new GCs, while Appendix 5.1.3 and 5.1.3 contain the diagnostic plots for other analysed clusters.

4.1.2 Gaia DR2: bulge data and methodology

4.1.3 Gaia DR2: data selection

We follow the same method detailed in Gran et al. (2019), focusing our search on the Gaia DR2 catalogue (Gaia Collaboration, Prusti, et al., 2016; Gaia Collaboration, Brown, et al., 2018; Lindegren et al., 2018) which provides coordinates, proper motions and magnitudes for a large region of the sky in the bulge area. This area includes the

whole Galactic bulge within $|\ell, b| \lesssim 10$ deg with a complete photometric and astrometric solution.

We query for Gaia DR2 sources in the mentioned region, dividing it into small circles of 0.8 deg radius. This choice ensures that each coordinate within the selected area is included at least once and up to four times within the circles. This was done to optimise the clustering execution and avoid losing clusters that may appear close to the edges. Only the stars from the main `GAIA_SOURCE` catalogue with complete astrometric and photometric information about their positions (α, δ), PMs ($\mu_\alpha \cos\delta$, μ_δ) and magnitudes (G, RP, and BP) were kept.

4.1.4 A method to discover new GCs

For each star, the algorithm counts the number of neighbours within 1 unit in the phase-space defined by 1 arcmin in space, $1 \, \text{mas} \, \text{yr}^{-1}$ in PM, and 1 mag in $(BP - RP)$ colour. Then, we select stars with at least nine neighbours (i.e., a group with at least 10 members), trying to avoid the detection of false-positive clusters due to stochastic overdensities, common in the bulge area. This step was performed using the K-Dimensional Tree (KDTree) implementation on `scikit-learn` (Pedregosa et al., 2011). Then, we apply a clustering algorithm to the selected stars with more than 10 neighbours to search for their centroids on the sky if any. The latter task was performed with the DBSCAN (Ester et al., 1996) routine, also implemented in `scikit-learn`. We choose DBSCAN over other algorithms because it does not need an already known number of groups to be found in each region, different to the K-means behaviour, and it offers the possibility to apply physical constraints to the cluster determination, as the maximum separation within points of the same group. Note that the physical size of the resulting cluster may vary, as several groups of stars can form it within the separation constraints, in which DBSCAN will only recognise one cluster. In fact, a group of neighbours defines a "neighbourhood" that can be significantly larger than the minimum distance between a star and its neighbours. Finally, DBSCAN has been

intensively tested with Gaia data, especially to search for open clusters. For a complete DBSCAN description and comparison with other clustering algorithms, we point to the recent detailed studies by Cantat-Gaudin et al. (2019) and Cantat-Gaudin et al. (2020), Castro-Ginard et al. (2019) and Castro-Ginard et al. (2020), and Hunt and Reffert (2021, and references therein) for the use of DBSCAN to detect open clusters using Gaia DR2.

Then, an initial median centroid of the distribution of the candidate cluster stars in the sky and PM space was derived. In a second step, the resulting candidate cluster stars were compared with the surrounding stars within 5 arcmins of the derived centre, by means of the on-sky positions, PM diagram (also called Vector Point Diagram; hereafter VPD) and the (BP-RP, G) CMD.

The algorithm found 2614 cluster candidates, and for each one, a visual inspection was made to select groups whose members show outstanding coherence in position, motions and, particularly, the characteristic structures in the CMD of a single-age stellar population. In the present paper, we will focus on the old clusters; therefore, we selected candidates with a well-populated red giant branch (RGB), red-clump (RC) or hints of a horizontal branch (HB). We ended up with seven bonafide old star clusters and one candidate (C1), later discarded. Of those seven clusters, two match known objects (BH 261 and Djorg 1), and five are considered original discoveries, which we call `Gran 1, 2, 3, 4` and `5`. A possible identification of Gran 1 with ESO 456-29 is later addressed (see Sec. 4.1.5).

Because this work considerably improves their parameters, we decided to retain Djorg 1 and BH 261 in the present discussion. We also note that `Gran 1` was already reported and characterised in Gran et al. (2019), but we will include it in the present paper because we perform a complete analysis of its properties. Our algorithm was able to recover all but 5 of the confirmed GCs listed in the Kharchenko et al. (2016) catalogue as described in Gran et al. (2019). Not surprisingly, given that Gaia works at visible wavelengths, the 5 missed clusters are all very close to the Galaxy midplane, at $|b| \leq 2.5$ deg, in regions heavily affected by crowding and extinction.

4.1.5 Known clusters from the literature

A crossmatch with 10 arcmin tolerance was performed between the new cluster centroids and other GC catalogues from the literature (Harris, 1996; Harris, 2010; Kharchenko et al., 2016, online versions) in order to identify already known clusters. We found three matches within the imposed angular separation with our candidates in the Kharchenko et al. (2016) catalogue.

Of those three, the properties of `Gran 1` differ significantly from the possible literature match, although it is located only 38.72 arcsec away from ESO 456-29 (or ESO 456-SC29), discovered by the ESO/Uppsala photometric plates survey (Holmberg et al., 1974; Holmberg et al., 1978; Lauberts, 1982) as a star cluster. However, its nature was questioned by Dias et al. (2002) and Dias et al. (2014) who changed its classification to "dubious open cluster". Despite this fact, Kharchenko et al. (2016) and Bica et al. (2019) still consider ESO 456-29 as an open cluster. Moreover, Kharchenko et al. (2016) derived a distance to the candidate cluster of ~ 3 kpc and PMs of $\mu_\alpha \cos \delta = -3.38 \pm 4.15$ mas yr^{-1}, $\mu_\delta = -6.25 \pm 4.72$ mas yr^{-1}. This PM is also different from the value of $\mu_\alpha \cos \delta = 0.558 \pm 4.15$ mas yr^{-1}, $\mu_\delta = -2.96 \pm 4.72$ mas yr^{-1} quoted in the online-catalogue by Dias et al. (2014).

In order to verify these measurements, Fig. 4.1 shows the VPD of the selected stars from both catalogues (Dias et al., 2014; Kharchenko et al., 2013) as quoted in the original papers (left panel) and as resulting from a match with Gaia (right panel; 1 arcsec tolerance in the match). Note that we show all the stars from Dias et al. (2014) with the ESO 456-29 designation, but only the ones with at least 80% probability of being cluster members according to Kharchenko et al. (2013).

As Fig. 4.1 shows, neither Dias et al. nor Kharchenko et al. recover the cluster in the VPD; only with additional data from Gaia EDR3 a total of nine stars (eight from the Dias, and one from the Kharchenko catalogues) are located within the PM centre derived by us. With the additional Gaia EDR3 data, most of the putative cluster members identified by Dias et al. (2014) and Kharchenko et al. (2013) are now classified as field stars. Since

the original cluster centre proposed by Lauberts (1982) agrees with the one derived in this work within the (arguably large) errors, `Gran 1` may indeed be ESO 456-29. However, in Sec. 4.1.7 we show that our derived properties differ significantly from those presented in past works, reason why we will maintain the `Gran 1` designation, already introduced in Gran et al. (2019). Nonetheless, as for many GCs, we consider both names equally valid (i.e., `Gran 1` = ESO 456-29).

One of our derived cluster candidate is 50.58 arcsec away from the known GC BH 261 (also known as ESO 456-78 or AL 3), discovered by Andrews and Lindsay (1967) and analysed by Lauberts (1982), van den Bergh and Hagen (1975), and Ortolani et al. (2006) and Barbuy et al. (2021). A first CMD was presented by Ortolani et al. (2006) describing BH 261 by its prominent HB with respect to the field stars, deriving a distance of 6.0 ± 0.5 kpc and a metallicity of -1.3 ± 0.3 dex. However, the Ortolani et al. (2006) observations could not optimally decontaminate the cluster RGB nor turn-off (TO) point. Bonatto and Bica (2008) and Rossi et al. (2015) later attempted a characterisation of the cluster properties, however, the low number of members and high reddening in the area led to inconclusive results. Also, Barbuy et al. (2021) tried to constrain the cluster metallicity by means of near-IR spectra. However, no [Fe/H] measurement was performed due to the limited wavelength range, adopting the same Ortolani et al. (2006) metallicity value of -1.3 dex. H. Baumgardt catalogue of MW GCs[2] (Baumgardt et al., 2020; Baumgardt and Vasiliev, 2021) reports a distance of 6.12 ± 0.26 kpc, which is an average of the 4 independent literature measurements. They do not report Gaia EDR3 parallax, nor kinematic distance measurement. As we have an improved decontamination procedure based on the Gaia EDR3 PMs, we are able to isolate members down to the sub-giant branch (SGB) level, to better constrain BH 261 distance and metallicity. Sec. 4.1.7 presents our derived properties for this cluster.

Lastly, one of our detected overdensities is located 36.82 arcsec away from the known

---

[2]`https://people.smp.uq.edu.au/HolgerBaumgardt/globular/`
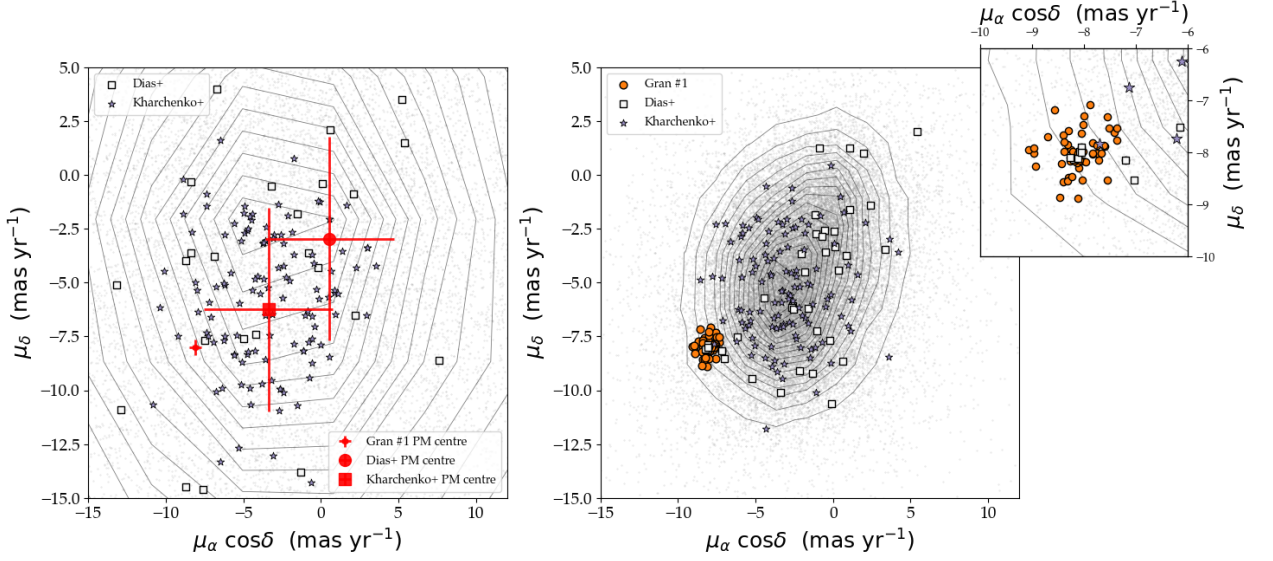
Figure 4.1: **(Left)**: VPD of the Kharchenko et al. (2013) stars within 10 arcmin from the centre we derived for `Gran 1`. Background grey points represent all the field stars while the contours mark different density levels. Squares and stars are the putative cluster members of ESO 456-29 from Dias+ (Dias et al., 2014), and Kharchenko+ (Kharchenko et al., 2013), respectively. The red point, circle and square with error bars represent the derived PM centroid of the cluster, for the authors indicated in the labels. **(Right)**: Same as the left panel, now with the PM, for the same stars, from the Gaia EDR3 catalogue. Orange circles are the members of `Gran 1` derived in the present work, while squares and stars are the cluster members from the Dias+ (Dias et al., 2014), and Kharchenko+ (Kharchenko et al., 2013) catalogues, respectively. Both panels are in the same scale. Finally, the inset is a zoom-in version of the VPD, that we include because eight stars in Dias et al. (2014) and one from Kharchenko et al. (2013) are within our derived PM centre of the cluster. As can be seen, only with Gaia data this cluster could be detected.

GC Djorg 1 (Djorgovski, 1987). Due to the high extinction present towards the cluster, only a few studies have focused on it (Ortolani et al., 1995; Davidge, 2000; Valenti et al., 2010). Recently, Vásquez et al. (2018) determined its radial velocity (RV), Vasiliev (2019a) its PM and Ortolani et al. (2019) presented the first decontaminated CMD showing a prominent HB. Unfortunately, our analysis could not detect the HB of the cluster, which is below the detection limit of both Gaia or VVV data. Additionally, our derived CMD shows more scatter in comparison with other discovered clusters. Nevertheless, the PM overdensity that we detect matches the previous Vasiliev (2019a) determination. We include Fig. 5.4 with both BH 261 and Djorg 1 within the Appendix 5.1.3 for completeness to show our results.

4.1.6 Other cluster candidate

In addition to the five GCs that we present in Sec. 4.1.7, we have selected one candidate for which we are not able to decipher whether it is real cluster or only stellar field overdensity. The positional properties of the candidate C1 is presented in Table 4.1. In this case, coordinates and PMs are clustered, but the CMD do not display a narrow cluster-like sequence.

For the C1 overdensity, our conclusion that this is not a real cluster is based on follow-up spectroscopy (see Sec. 4.1.11), which does not display coherent kinematics lacking a clear peak in the RV distribution of its Gaia-selected members, which can be seen in Fig. 5.7. Appendix 5.1.3 presents coordinates, PMs and CMD for C1.

4.1.7 A new population of GCs towards the MW bulge

Following Harris (2010) and Baumgardt and Hilker (2018), we decided to split our cluster characterisation into three categories: photometric, structural and dynamical.

4.1.8 Photometric properties of the discovered clusters

For each selected cluster, the algorithm returns the median coordinates (RA, Dec) and PMs ($\mu_\alpha \cos\delta$, μ_δ) calculated from the putative cluster members, i.e., those stars having at least nine neighbours. At this point, we expand the selection criteria by including all the stars within 2 arcmin from the cluster centre in the sky and within 1 mas yr^{-1} from the cluster centroid in the VPD. It is worth mentioning that while the initial cluster search was performed on the Gaia DR2, during this analysis the new EDR3 became available (Gaia Collaboration, Brown, et al., 2021), and therefore we repeated the search on it. Note that, while the clustering algorithm recovered the same five clusters, more members and tighter PM distribution were found with the EDR3 data.

As shown in the CMDs (see Figures 4.3, 4.4, 5.1, and 5.2), by including all the stars within a small circle around the cluster centroid in the sky and in the VPD we do not increase the contamination significantly. On the contrary, we need this step in order to include possible members in the cluster outskirts, that are ignored by the clustering code because we run it with a strong requirement of spatial concentration. The cluster centroids are listed in Table 4.1.

Note that `Gran 5` was selected due to the presence of a prominent RC, as shown in Fig. 5.1 and 5.2. However, being located very close to the Galactic plane, it is affected by high absolute and differential extinction, broadening its CMD sequences. Moreover, the upper RGB (above the RC) seems to be devoid of stars, both in Gaia and VVV data. Only taking into account spectroscopic observations, we were able to confirm its cluster nature (see Sec. 4.1.11).

We also include here BH 261, Djorg 1 and the cluster candidate labelled as C1 with the parameters derived by the clustering algorithm. The position of the clusters in the sky is shown in Fig. 4.2, labelled by their IDs, as they appear in Table 4.1. The background of Fig. 4.2 is a reddening map derived from the publicly available database `STARHORSE`[3]

---

[3]Available at `https://gaia.aip.de/`

(Queiroz et al., 2018; Anders et al., 2019) within the inner 2.5 kpc from the Galactic centre (located at 8.2 kpc, Bland-Hawthorn and Gerhard, 2016). The query considers stars within our initial search box, with valid `STARHORSE` flags. A total of 2.5 million stars were used to derive the mean extinction map in the Gaia G-band (A_G). Note that all clusters except `Gran 4`, lie in high extinction regions, with a mean $A_G \gtrsim 2$ mag.

We construct optical (G, BP − RP) CMDs with the selected members as shown in the right panel of Fig. 4.3 for `Gran 3`. We include all the other cluster CMDs in Appendix 5.1.3. The spatial distribution is shown in the top left panel of the same figure, while the VPD, a key tool to identify new clusters, is shown in the bottom left panel. A radius of 10 arcmin from the cluster centre was taken to compare the cluster population with the surrounding field (grey points and contours). As this figure clearly shows, the new clusters are highly concentrated in space, move coherently in the plane of the sky and define narrow sequences in the CMD. In a few cases, the CMD also shows an HB or a RC, helping us to assign a reliable distance to the cluster. Note that our procedure does not require the cluster mean PM to be different from the mean PM of bulge field stars. Indeed, half of the new clusters have PMs similar to the bulge (see the `Gran 2` and 4 PM distribution).

For all the clusters that are inside the footprint of the VVV survey (namely, `Gran 1, 4` and 5, BH 261 and Djorg 1), we perform a match with the catalogue presented in Surot et al. (2019) to obtain deep near-IR colours for the Gaia detected stars. Figure 4.4 contains the Gaia-VVV matched stars for two clusters (`Gran 4` and BH 261). Note that, the selection is performed exclusively on the Gaia catalogue, given the importance of isolating cluster members from field stars using PMs. All the Gaia-VVV CMDs are shown in Appendix 5.2 with the same panel arrangement and symbols as in Figure 4.3. Both clusters in Figure 4.4 present clearer sequences in the optical-near-IR CMD, showing HBs, and probably hints of an asymptotic giant branch (AGB) in BH 261, starting from (G-K_s, K_s)$\sim 2.0, 13.5$ mag to $\sim 2.5, 11.$ mag. PARSEC isochrones (version 1.2S; Bressan et al., 2012; Y. Chen et al., 2015; Y. Chen et al., 2014; Tang et al., 2014; Marigo et al., 2017; Pastorelli et al., 2019) were added here just as a reference for the eye.
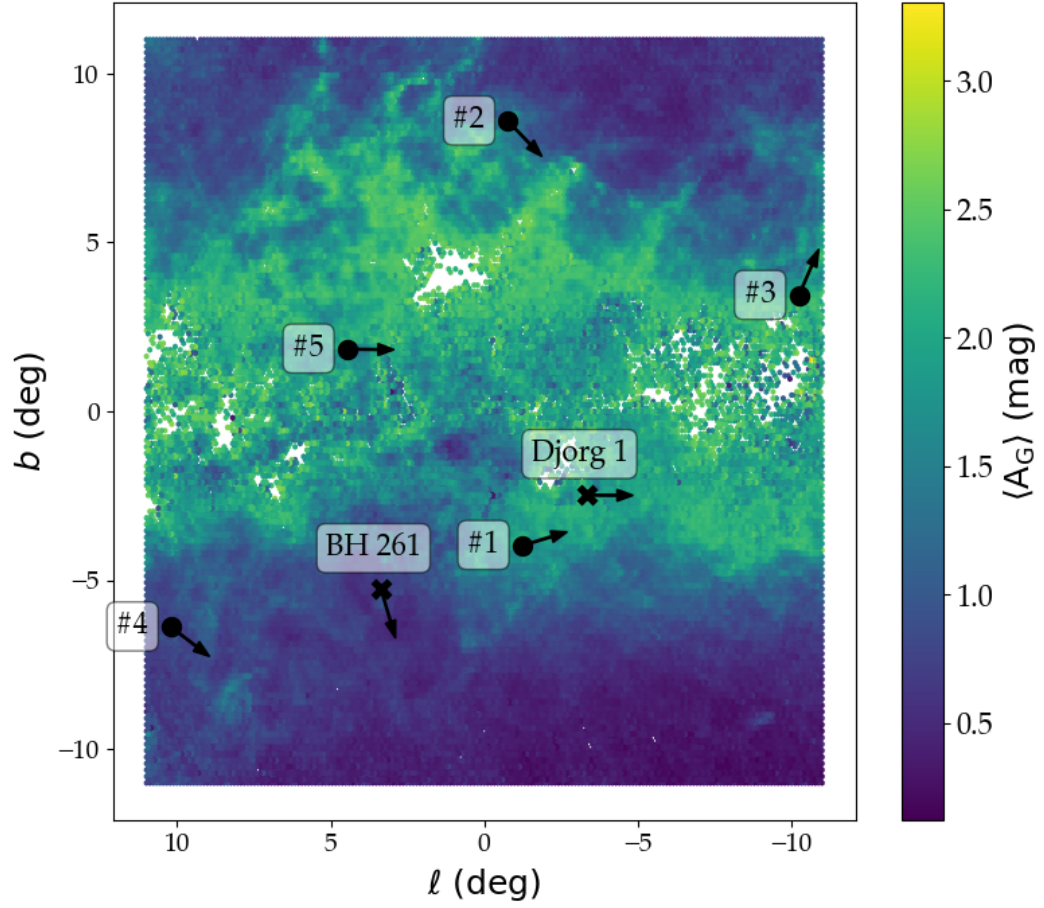
Figure 4.2: Spatial distribution of the new clusters with a `STARHORSE` mean G-band extinction map as background. The normalised 2D motion of the clusters is also shown as arrows. The numbers in the labels are the same as in Table 4.1. The location of BH 261 and Djorg 1 within the bulge area are marked with crosses.
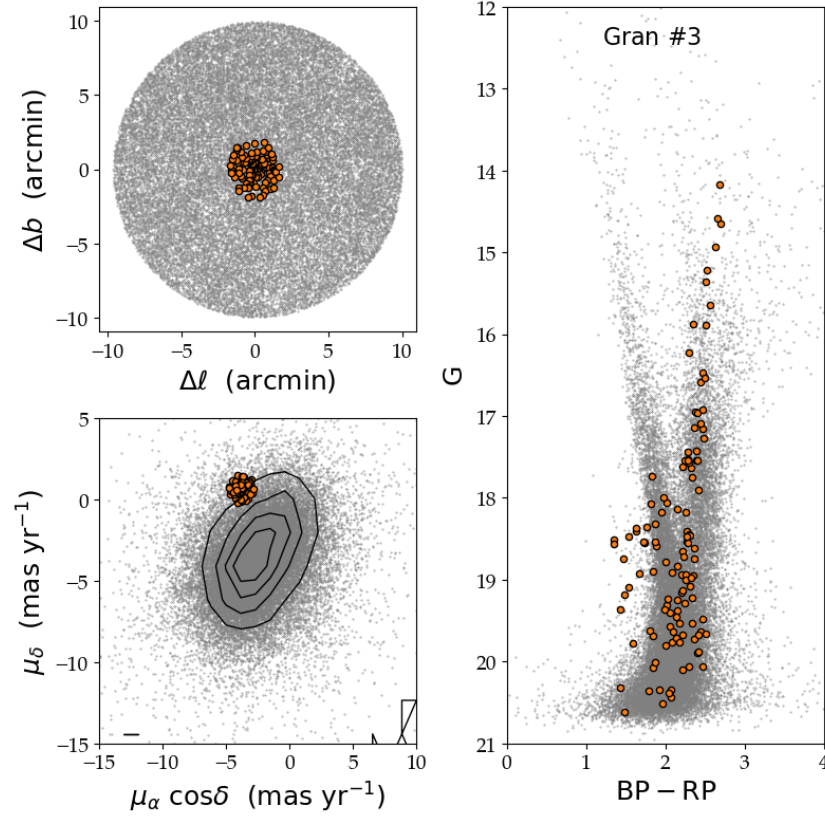
Figure 4.3: **(Upper left)**: Spatial distribution of `Gran` 3 members. Orange coloured circles represent the cluster stars while grey small points account for the foreground/background sources within 10 arcmins from the cluster centre. **(Lower left)**: Gaia VPD for the same sources as in other panels. Contours were calculated for the field population (cluster subtracted) to account for the high number of bulge stars that move with similar values and saturate a scatter plot. Note that in this case, the `Gran` 3 members are located in the outskirt of the dominant bulge distribution of stars. **(Right)**: Gaia CMD of `Gran` 3 with the same star sample as described in Sec. 4.1.8. The cluster shows a clear and narrow RGB as well as an HB at $G \sim 18.5$ mag, which is confirmed in Sec. 4.1.11. At magnitudes below $G = 19$ mag, where bulge and disk sequences merge with those of the cluster, there may be more contamination in the CMD of the cluster members.

Table 4.1: Positional parameters from the newly discovered GCs and discarded candidates. The numbered GC names are maintained across the whole article. The coordinates are in the Gaia J2016 reference frame as they were taken directly from the available catalogue using median values. The reported number of stars considered in N_{members} accounts for the constraints adopted in Sec. 4.1.2. Parameters for BH 261, Djorg 1, and `C1` are also listed under their respective groups.

GC	ℓ	b	RA	Dec	$\mu_\alpha \cos\delta$	μ_δ	$\mu_\ell \cos b$	μ_b	N_{members}
	(deg)	(deg)	(deg)	(deg)	(mas yr^{-1})	(mas yr^{-1})	(mas yr^{-1})	(mas yr^{-1})	(number)
Gran 1	-1.233	-3.977	269.651	-32.020	-8.10	-8.01	-10.94	3.03	57
Gran 2	-0.771	8.587	257.890	-24.849	0.19	-2.57	-1.86	-1.76	102
Gran 3	-10.244	3.424	256.256	-35.496	-3.78	0.66	-1.76	3.71	118
Gran 4	10.198	-6.388	278.113	-23.114	0.46	-3.49	-2.88	-2.01	155
Gran 5	4.459	1.838	267.228	-24.170	-5.32	-9.20	-10.55	-0.10	76
Cluster candidates									
C1	-3.589	4.174	260.151	-29.673	-2.90	-6.11	-6.61	-1.07	113
Known clusters analysed									
BH 261	3.359	-5.272	273.527	-28.638	3.55	-3.60	-1.55	-4.80	99
Djorg 1	-3.324	-2.485	266.871	-33.066	-4.67	-8.41	-9.66	-0.04	149

We searched for RR Lyrae variables near the clusters. To this goal, we used the Gaia and OGLE catalogues (Soszyński et al., 2019; Gaia Collaboration, Eyer, et al., 2019), finding one confirmed dynamical member of `Gran 4` located within ~ 1.3 arcmin from its centre. The variable star was found in both catalogues, however we used the period derived by the OGLE team, which is measured from 105 epochs in the I-band, compared to the 15 G-band epochs of Gaia. The RR Lyrae star (`OGLE-BLG-RRLYR-62550` or `Gaia DR2 4077796986282497664`), with a typical RRab-type saw shaped light curve and a period of ~ 0.610087 days, allows us to determine a robust distance to the cluster. Using the PL relations described in Catelan et al. (2004) and Alonso-García et al. (2015) for the near-IR bands of VVV, the approximate cluster metallicity derived from the isochrones (~ -2.4 dex), and the Cardelli extinction law (Cardelli et al., 1989), we derived a distance of 20.69 ± 0.14 kpc for the RRL in `Gran 4`. This value is consistent with the approximate distance of ~ 22.5 kpc, obtained by matching the isochrone to the cluster HB. Clearly, this

is not a bulge GC as it is located on the far side of the Galaxy.

BH 261, on the other hand, shows a rather broad HB, a feature that might be enhanced due to a population of blue straggler (BS) stars. This hypothesis was already considered by Ortolani et al. (2006), suggesting the presence of a non-negligible BS population within the cluster. Given the large PM difference of this cluster with respect to bulge stars, field contamination would be very unlikely. Based on the (G-K_s, K_s) CMD presented in Fig. 4.4, and using the SGB and the slope of the RGB we were able to estimate a distance of ~ 9.50 kpc and a metallicity of ~ -2.4 dex, similar to that of `Gran 4`.

Given the low-metallicity of BH 261, we used the α-enhanced isochrones from the PGPUC (Valcarce et al., 2012) database, finding the best match with [Fe/H]=-2.4 dex and αFe = 0.2 dex. We use the Wang and X. Chen (2019) relations to convert the E(G$-K_s$) reddening into the A_{K_s} extinction. Previous estimates reported a distance for this cluster of d=6.12 kpc, versus the 9.12 kpc derived here. Imposing this shorter distance is not compatible with the low metallicity we find. A reasonable fit could still be achieved for this distance and a higher metallicity [Fe/H]=-1.3 dex. We show all three fits in Fig. 5.5. We favor a larger distance and lower metallicity because the fit is better in the lower RGB, and SGB, and also because a shorter distance would imply unreasonably high dynamical mass (by a factor of 5), mass-to-light ratio and velocity dispersion (both doubled), compared to the typical values in (Baumgardt and Hilker, 2018; Baumgardt et al., 2019). Note that these are estimates and should be confirmed with both high-resolution spectroscopy and deeper photometry.

For `Gran 2` and `Gran 3` we have distance determinations by means of spectra taken with MUSE@VLT, which will be presented in Sec. 4.1.11.

Finally, we include in this list `Gran 5` and the candidate cluster `C1`. While the first was confirmed, the latter was eventually ruled out, both based on MUSE spectroscopic follow-up (Sec 4.1.11). Nonetheless, we consider important to show how several pieces of evidence favoured its existence as a cluster, in order to illustrate how difficult it is to positively confirm such objects. `Gran 5` and `C1` were selected based on the visual inspection

of their CMD and its clumped PM using the Gaia DR2. Photometry and PMs from the updated Gaia EDR3 catalogue showed that their CMDs are diffuse and probably affected by differential reddening, especially in the case of `Gran 5`. However, we determined a distance using the assumed RC located at $(J - K_s, K_s) \sim (1.00, 12.85)$, as shown in Fig. 5.2. Using the same approach as in Minniti et al. (2011b) and Gran et al. (2016), we estimated a distance of ~ 6.82 kpc, i.e., in the near side of the Galactic bulge. The cluster nature is later confirmed by the spectroscopic measurements, while we also refine the distance determination.

For `C1`, in addition to a dubious CMD with rather broad sequences, we also have MUSE spectroscopic observations. These allowed us to finally discard this candidate, as the putative cluster members selected from Gaia PMs do not clump in RV. In fact, in Fig. 5.6 we could not identify any RV peak when considering all stars detected within the MUSE field of view. We cannot stress this point enough to warn the reader that even prominent overdensities can be stochastic fluctuations of bulge stars. The PMs (or RVs in one of our cases) are a key piece of information to unveil the true nature of these candidates. Given the uncertain nature of these candidates, in the following sections we will focus our analysis on the confirmed clusters.

Individual distances and reddening values for optical and near-IR colours are reported in Table 4.2. Note that we use the Cardelli et al. (1989) relation to convert the reddening into a K_s-band extinction using $A_{K_s} = 0.689 \times E\left(J - K_s\right)$ to properly define an isochrone distance. Additionally, we use $A_G = 2.0 \times E\left(BP - RP\right)$ derived in Andrae et al., 2018 to convert optical reddening to extinction.

Another parameter that we can derive from photometry is the integrated luminosity of each cluster. In order to compare with previous studies, we convert the Gaia G magnitudes into the Johnson V system using the publicly available colour transformation in the Calibration models of the Gaia documentation webpage.[4] When deriving the integrated light

---

[4]`https://gea.esac.esa.int/archive/documentation/GEDR3/Data_processing/chap_cu5pho/cu5pho_sec_photSystem/cu5pho_ssec_photRelations.html`
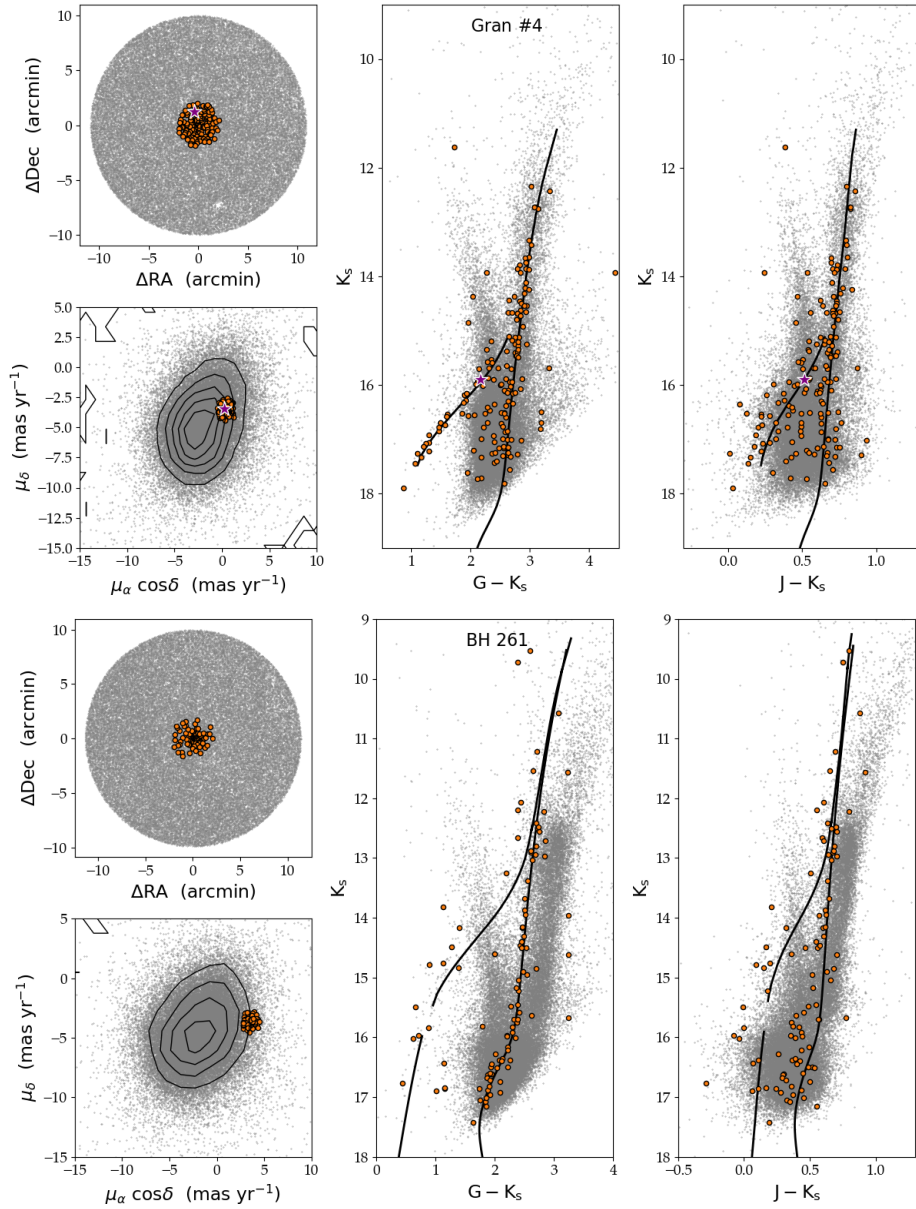
Figure 4.4: (**Upper four panels**): Spatial distribution, VPD, and near-IR-optical ($G-K_s$ and $J-K_s$) CMD for the `Gran 4` GC with identical panel distribution as in Figure 4.3. A PARSEC isochrone of 12 Gyr and [Fe/H]~ -2.4 dex is presented as a reference. The cluster member RR Lyrae star is marked with a star in all the panels. (**Lower four panels**): Same as in the upper panels, but for BH 261. Note that we draw the AGB phase in the CMD, since the possible association of some stars to that stage, as two parallel sequences can be appreciated in both near-IR-optical CMDs at $K_s \gtrsim 13$ mag. The selected isochrone is a composition of a PGPUC (SGB, RGB and HB) and a PARSEC (AGB) models as it is described in Sec. 4.1.8. Both isochrones are for a metallicity of -2.4 dex and shifted by a distance modulus of 14.80 mag.

of the cluster, we need to take into account also the stars that might not be included in the Gaia catalogues due to their incompleteness. In order to account for these missing stars, we used the completeness analysis by Boubert et al. (2020), Boubert and Everall (2020), and Boubert et al. (2021), through the `scanninglaw` python package. We retrieved the average fraction of stars, at a given coordinate and G-magnitude, that were ignored by the Gaia selection function. We performed this correction at the position of each cluster, in bins of $\Delta G = 0.1$ mag, across the cluster luminosity function. Overall, the completeness of our sources for $G < 16$ mag is more than $\sim 90\%$, but it drops significantly at fainter magnitudes, reaching less than $\sim 30\%$ at $G = 21$ mag.

After this step, we transformed the corrected integrated fluxes into an apparent V magnitude (V_t, according to the Harris 2010 notation). Distances and extinctions are required to derive the absolute V magnitude of each cluster, for which we used two methods depending on whether we were able to fit an isochrone to the cluster CMD or not. In the case of `Gran 4` and BH 261, isochrones were fitted to the clusters and are shown in Figure 4.4. Isochrones were also used for `Gran 1, 2, 3` and 5 (see Sec. 4.1.11).

For completeness, Table 4.2 lists the integrated and absolute V magnitude in addition to the extinction coefficients in the G- and V- bands (A_G and A_V) and the adopted metallicities for all the clusters.

4.1.9 Structural properties of the discovered clusters

Having a clean sample of cluster members, in this section we discuss their radial profile and structural properties. We fitted the radial luminosity profile of the clusters with two sets of empirical models, a King (1962) model and an exponential one. We fitted the model parameters, namely the core (r_c) and the tidal radius (r_t) for the King profile and the scale factor in the exponential one using the SciPy `curve_fit` routine (Virtanen et al., 2020), by minimising a classical χ^2 function. Figure 4.5 shows an example of the two fitted profiles for Gran 1, while all the other fits can be seen in Appendix 5.1.3. For all the clusters the

Table 4.2: Photometric properties of the discovered GCs. Distances and optical-near-IR reddening and extinctions are based on isochrone fitting to the CMDs. The integrated magnitudes and half-light radius (r_h) of the clusters are also presented here.

GC	dm (mag)	Distance (kpc)	$EJ - K_s$ (mag)	A_{K_s} (mag)	A_G (mag)	A_V (mag)	V_t (mag)	M_V (mag)	r_h (arcmin)	[Fe/H] (dex)
Gran 1	14.60	7.94	0.45	0.24	2.70	3.38	12.41	-5.46	0.86	-1.19
Gran 2	16.10	16.60	—	—	1.90	2.37	12.56	-5.92	1.07	-2.12
Gran 3	15.40	12.02	—	—	2.60	3.25	12.63	-6.02	1.05	-2.33
Gran 4	16.84	22.49	0.20	0.14	1.20	1.50	11.81	-6.45	1.14	∼-2.4
Gran 5	13.25	4.47	0.63	0.43	3.24	4.05	12.11	-5.95	0.94	-1.56
Known clusters analysed										
BH 261	14.80	9.12	0.16	0.11	1.04	1.30	10.63	-5.56	1.09	∼-2.4
Djorg 1	—	—	—	—	—	—	—	—	1.23	—

exponential fit provides a better match to the data. In order to derive the luminosity errors σ_Σ, we used the recipe by Gehrels (1986), i.e., $\sigma_\Sigma = 1 \sqrt{N \, 0.75}$, where N is the number of stars in each bin. From the fitted profile, we derived the half-light radius (r_h) of each cluster as the middle point in the cumulative luminosity histogram of the fit. Note that we only report values for the r_h as the exponential profile were preferred for all the clusters. The values for each cluster can be found in Table 4.2.

At this point, we can compare directly the newly discovered clusters with the known population of GCs in the MW. Baumgardt et al. (2019) re-derived the r_h for almost all the known GCs in the Harris (2010) catalogue using the Gaia DR2 data to select cluster members. Using Harris (2010) absolute integrated magnitudes, we can compare the integrated luminosity and r_h of our clusters with the other MW GCs directly, as shown in Figure 4.6. The error bars were calculated as follows: the standard deviation of the recovery factor of Gaia has been used to estimate an upper limit for the cluster total integrated magnitude. On the other hand, a lower limit has been derived, assuming that up to ∼ 10% of the cluster integrated light per magnitude bin might be contamination from
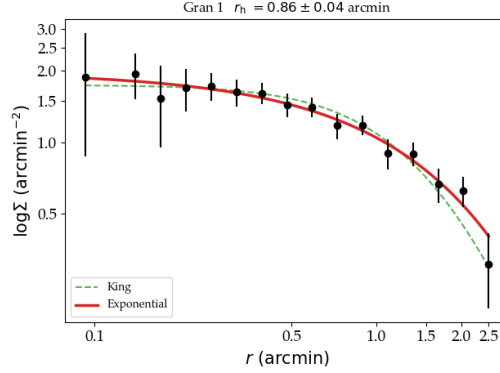
Figure 4.5: Derived fit for the King and exponential profiles of `Gran 1` as dashed green and continuous red lines, respectively. In this case, the preferred model is the exponential one, which is marked by a more pronounced line, consistent with a r_h of 0.86 arcmin.

field stars.

All our clusters are located at relatively faint absolute magnitudes, as expected for such low mass clusters that were not yet discovered (Baumgardt and Hilker, 2018). For reference, Fig. 4.6 includes the position of some well-known clusters with roughly similar r_h and/or integrated flux as the new clusters. All the discovered clusters have similar r_h, with `Gran 1` and 4 at the two extremes, with $r_h \sim 0.86$ and ~ 1.14 arcmin, respectively.

4.1.10 Dynamical properties of the discovered clusters

In this section we present the cluster velocity dispersions (σ_0) based on the PMs from Gaia EDR3. We included in the calculation only stars with uncertainties less than 1 mas yr^{-1} in both components. The intrinsic velocity dispersion of each cluster was derived as $\sigma_0^2 = \sigma_{vel}^2 - \sigma_{errors}^2$, where σ_{vel} is the standard deviation of the velocity distribution of the cluster members and σ_{errors} is the mean error of the measurements. This parameter on its own is critical to establish whether the cluster is real. Known clusters have velocity dispersions that increase with their mass, with an upper limit of ~ 20 km s^{-1} (Baumgardt and Hilker, 2018). Therefore, a higher σ_0 would suggest that a cluster is not real. In order
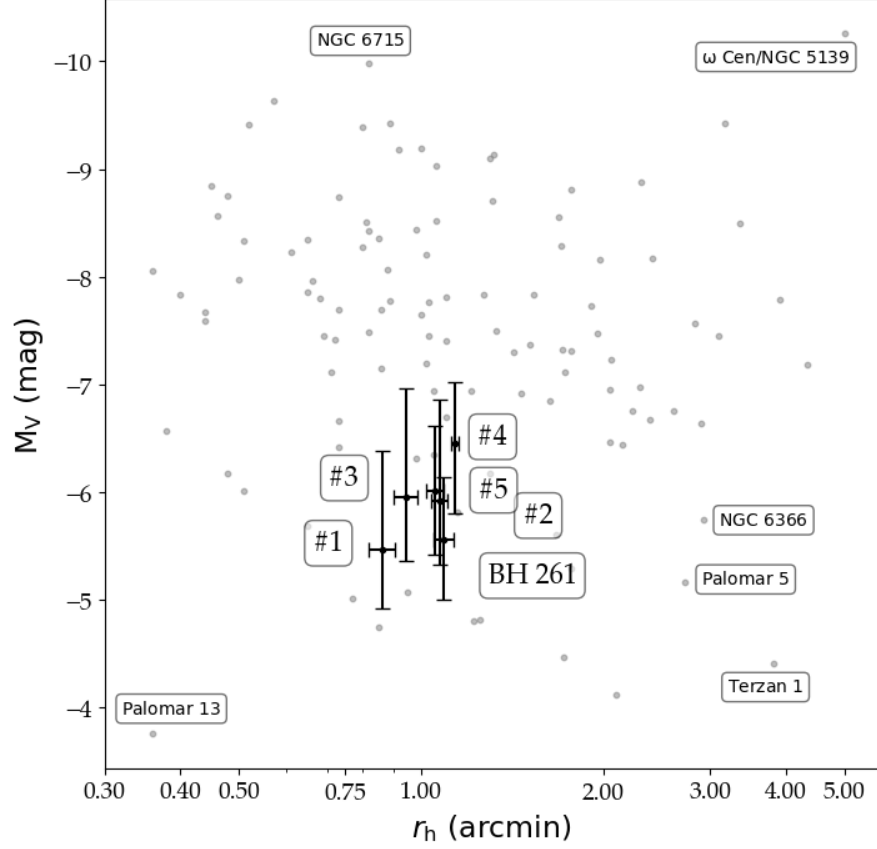
Figure 4.6: Half-light radius (r_h) and total absolute integrated magnitude (M_V) in the V-band of the known MW GCs listed in Baumgardt and Hilker (2018), shown as grey dots, and the new ones presented here as black circles with error bars, labeled with the IDs as in Table 4.1. A handful of well-known clusters at the edges of this diagram are labelled as comparison in clockwise direction: ω Cen/NGC 5139, NGC 6365, Palomar 5, Terzan 1, Palomar 13 and 3, and NGC 6715.

to obtain the velocity dispersion in km s^{-1} we must first convert the PM into a tangential velocity (v_t) using the relation $v_t = 4.74\mu d$, in which 4.74 is the equivalent in km s^{-1} of one astronomical unit in one tropical year, $\mu = \sqrt{\mu_\alpha \cos \delta^2 \; \mu_\delta^2}$ (in arcsec yr^{-1}) is the total PM, and d the distance to the cluster, expressed in parsecs. The velocity dispersions derived for the new clusters are listed in Table 4.3. Figure 4.7 compares the velocity dispersions of the new clusters with other MW GCs. The position of the new clusters is compatible with the trend defined by well-studied GCs (Harris, 2010; Baumgardt and Hilker, 2018). They stay in the upper part of the main M_V-log σ_0^2 correlation. As in Figure 4.6, we highlight some of the known clusters that stand out of the marked trend, such as, e.g., Liller 1 and Terzan 5 (Saracino et al., 2015; Ferraro et al., 2021).

Finally, we can put constraints to the clusters dynamical mass enclosed within a certain radius through the virial theorem with the estimator described by Errani et al. (2018). The latter claims that the mass of a given pressure-supported system can be described by the minimum variance estimator $M \left(< 1.8r_h \right) = 3.5 \left(1.8r_h \right) G^{-1} \langle \sigma_0^2 \rangle$, with $M \left(< 1.8r_h \right)$ being the enclosed mass within 1.8 times the half-light radius. With this relation, we can derive approximate masses for the new clusters, converting r_h from arcmin to parsecs by means of the cluster distance. Masses are listed in Table 4.3 and show good agreement with the bulk of MW GCs presented in Baumgardt and Hilker (2018). As expected from its CMD, Gran 4 is the most massive cluster in our sample, with a well-populated HB. Its mass places it among the $\sim 20\%$ most massive GCs in the MW, similar to NGC 6656/M 22. As a final remark, using masses and luminosities computed so far, we have derived estimated mass-to-light (ML) ratios for the new clusters (Table 4.3), and overall, they behave similarly to other clusters within the same M_V-log σ_0^2 regime (Baumgardt et al., 2019). However, we recognise that ML ratios larger than ~ 4 may not be valid measurements (Bianchini et al., 2017; Baumgardt et al., 2020). Several additional corrections must be performed in order to derive an accurate ML ratio, from deeper photometric observations, such as a proper completeness analysis, cluster area scaling, mass function decontamination, among others. All these corrections should account for the missing factor of $\sim 2 - 3$ in the integrated

Table 4.3: Dynamical properties of the clusters derived in Sec. 4.1.10. Cluster name, intrinsic velocity dispersion, dynamical mass within $1.8r_h$, and ML ratios are presented.

GC	σ_0	$M^{\mathrm{dyn}} < 1.8r_h$	Υ
	(km s^{-1})	($10^5 M_\odot$)	($M_\odot L_\odot^{-1}$)
Gran 1	3.96 ± 0.29	0.45 ± 0.08	3.61 ± 3.12
Gran 2	4.93 ± 0.47	1.84 ± 0.40	9.50 ± 8.51
Gran 3	4.79 ± 0.41	1.24 ± 0.25	5.84 ± 3.45
Gran 4	6.18 ± 0.33	4.16 ± 0.61	13.15 ± 7.14
Gran 5	3.68 ± 0.32	0.37 ± 0.08	1.85 ± 1.77
Known clusters analysed			
BH 261	3.79 ± 0.24	0.63 ± 0.11	4.53 ± 2.54

light magnitudes to achieve the expected ML ratios for all the GCs.

4.1.11 MUSE reconfirmation of Gran 1, 2, 3 and 5

Given the importance of the newly discovered clusters, we applied for telescope time to spectroscopically follow-up the most promising candidates and to be able to derive their full orbital parameters. MUSE (Bacon et al., 2010) observations were approved and executed during ESO P103 and P105 (June-August 2019 and April 2021; PI: F. Gran) for four of our clusters: `Gran 1, 2, 3` and `5` and one candidate: `C1`. In Wide-Field Mode (WFM), the integral field unit (IFU) field-of-view (FoV) matches the projected size of our clusters (~ 1 arcmin), providing spectra for most of the stars in a single pointing.

The observations were carried out with the GALACSI adaptive optics system (Stuik et al., 2006; Arsenault et al., 2008; Ströbele et al., 2012; Ströbele et al., 2020; Hartke et al., 2020). Standard observing blocks of one hour per cube were prepared, and the automatic ESO pipeline was used to pre-reduce the cubes with a typical image quality of $\sim 0.8 - 0.9$ arcsec per observation. Finally, all the cubes were convolved with the VRI filter response
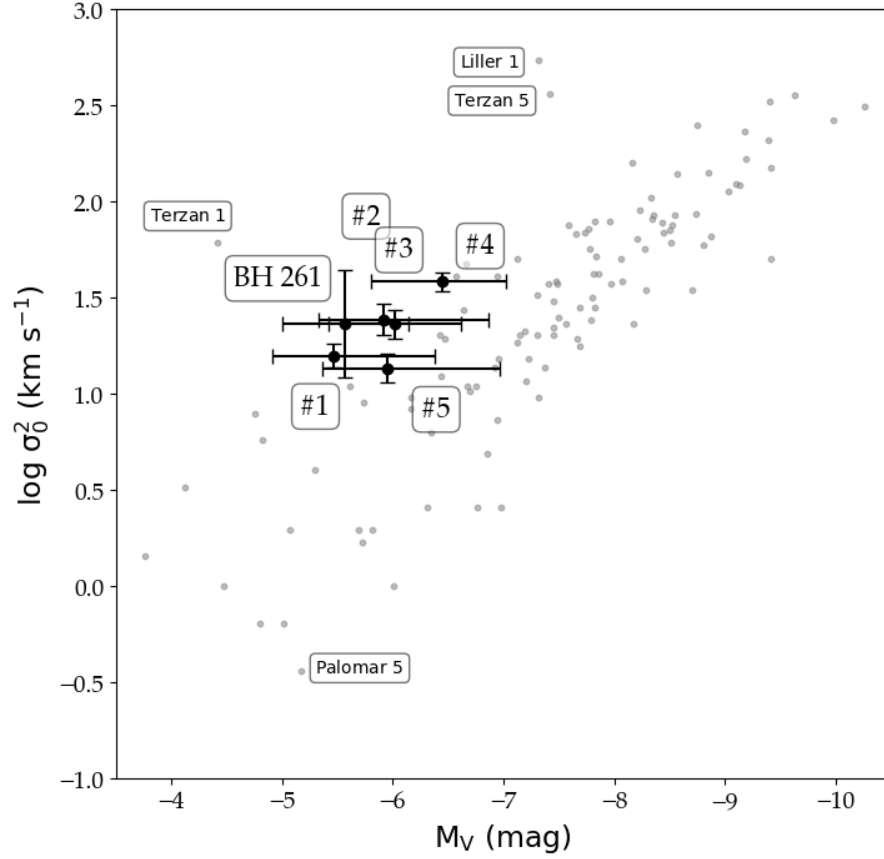
Figure 4.7: Absolute integrated magnitude (M_V) and velocity dispersion ($\log \sigma_0^2$) for our discovered clusters and the ones analysed by Baumgardt and Hilker (2018). The same symbols and numerations as in Figure 4.6 were used, showing grey points and black circles with error bars for the known MW GCs and the ones described in this study, respectively.

functions to extract images in each colour and generate CMDs.

In order to extract the spectrum of each star, in these crowded fields, we employed the widely used `PampelMuse` software (Kamann et al., 2013). By default, `PampelMuse` needs a stellar input catalogue to process the slices of each MUSE cube. To make this catalogue, we performed PSF photometry with `photutils` (Bradley et al., 2020) over the I-images and select detections above 3σ over the background. Major changes to the predefined parameters of `PampelMuse` were the use of `PSFFIT = 30` value, which implies a complete fit of the Moffat PSF model for each star, including the FWHM, β exponent, ellipticity, and position angle. Other changes involve the double extraction of the spectra, the first time with a spectral binning of 10 MUSE spaxels width, or `LAYERBIN = 10` within the `PampelMuse` routine. This binning corresponds to $\Delta\lambda \sim 12.5$ Å, and it is done to speed up the extraction process of the whole raw spectrum. During the first run, the FWHM is derived for each binned image to properly account for its changes across the wavelength, and then this value is used to extract individual frame fluxes without binning.

After extracting all the spectra, we normalise them using the `fit_generic_spectra` routine in the Astropy affiliated package `specutils` (Astropy Collaboration, Robitaille, et al., 2013; Astropy Collaboration, A. M. Price-Whelan, et al., 2018). RVs were derived using a cross-correlation routine implemented in Czesla et al. (2019) between the cube spectra and 6 synthetic templates, with the range of temperatures and gravities expected for giant and dwarf stars. The main cross-correlation indicator was the Ca triplet (CaT) lines at 8498, 8542 and 8662 Å, lines for which we also calculate equivalent widths (EWs). Figure 4.8 shows three `Gran 2` extracted spectra at different signal-to-noise ratios (SNR). Metallicity was estimated from the spectra applying a well-known relation using the EW of CaT lines (Armandroff and Da Costa, 1991; Rutledge et al., 1997; Cenarro et al., 2001; Vásquez et al., 2015, and references therein). We employ the relation derived for the MUSE instrument by Husser et al. (2020), which also extends the applicable region below the HB. This relation only requires prior knowledge of the CaT EW and the magnitude of the HB in the Jonhson V filter, which are V = 18.48, 18.59, 18.65 and 18.04 mag for
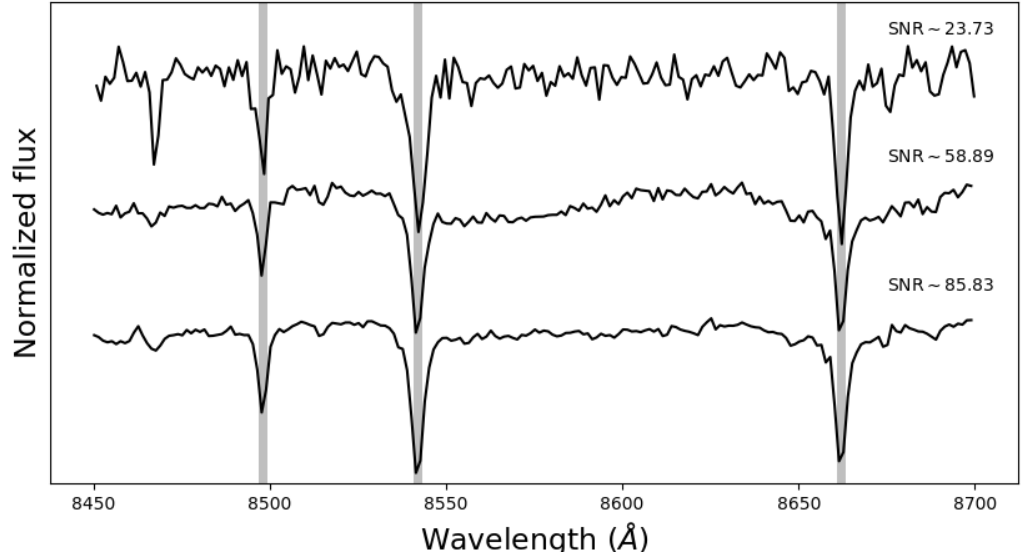
Figure 4.8: Extracted MUSE spectra of `Gran 2` around the CaT lines for three stars at different SNR regimes. Estimated SNR are given at the upper right of each spectra. Theoretical CaT lines are highlighted with grey shaded areas at at 8498, 8542 and 8662 Å.

`Gran 1, 2, 3` and 5, respectively, based on the CMD. In order to derive the reduced EW (W') of each star, we use

$$W' = \Sigma EW_{85428662}\ 0.0442V - V_{HB} - 0.058V - V_{HB}{}^2,$$

where $\Sigma EW_{85428662}$ is the sum of the EWs of the two more prominent Calcium lines at 8542 and 8662 Å, respectively. Additionally, to derive the calibrated metallicity from W' we have to apply the following relation, also derived in Husser et al. (2020)

$$\left[FeH\right] = -2.52 - 0.04W'\ 0.07W'^2.$$

At this point, we crossmatched the cluster members selected with Gaia with the stars for which we could extract a spectrum from MUSE. Figure 4.9 and 4.10 show the derived EWs and RVs for `Gran 1, 2, 3` and 5. Cluster members selected having PMs and consistent with a single RV peak are shown as orange circles. A few more stars having RV consistent with the cluster mean value (within ± 5 km s^{-1}) are shown with purple squares. All the other field stars are shown as small grey points. In the left panels, for `Gran 1, 2, 3` and `Gran 5`, we notice that PM-selected stars follow the expected trend for a cluster in the $\Sigma EW_{85428662}$-(V-V$_{HB}$) plane (c.f., Husser et al., 2020). To illustrate the errors on the EW determination, we include, as a black point with error bars, the mean uncertainty for all the stars detected in the MUSE cube. Using this trend, we can confidently extend the selection of members for those stars having RVs and EWs consistent with the cluster. The selection was performed extending three times the standard deviation of the intercept of the fitted line. The new members included allowed us to refine the mean cluster RV, adding significance to the derived value. Notice that the RV peak is narrow, also confirmed with a low standard deviation as listed in Table 4.4, as expected for a real GC. Particular attention is needed on the `Gran 3` case, given the slightly broader distribution of the RV peak, also noticeable in Table 4.4 with a higher velocity dispersion by ~ 1 km s^{-1} more than the other two observed clusters. Moreover, in all the cluster RV histograms, a 4.2 km s^{-1} binning was used. The same method applied to the candidate cluster `C1`, did not yield a

clear RV peak. Therefore, considering that the CMD of this candidate is also very sparse, we conclude that this overdensity is not a real cluster.

Mean RVs and metallicities of each cluster, calculated with the information from Figure 4.9 and 4.10, are reported in Table 4.4. We found that both `Gran` 2 and 3 clusters are metal-poor, consistent with the extended HBs seen in their CMDs. Using the relation by Husser et al. (2020), we derive a metallicity for `Gran` 1, 2, 3 and 5 of FeH $= -1.19 \pm 0.19$, -2.07 ± 0.17, -2.37 ± 0.18 and -1.56 ± 0.17 dex, respectively. Note that uncertainties in [Fe/H] are in agreement with broad error estimates for a mono-metallic population of stars, as found by Husser et al. (2020) in other MW GCs.

Figure 4.11 and 4.12 show an optical CMD for bonafide cluster members, where V and I images were obtained from the MUSE pipeline, by convolving the datacubes with the filter passbands. The optical VI magnitudes shown here are calibrated, and give the same distance modulus derived above from the Gaia (G, BP-RP) CMD. As the figure shows, a RC can be identified for `Gran` 1 and 5, a feature that is seen in other GCs at this metallicity; the HB for `Gran` 2 is entirely horizontal, as expected for the V filter; and the SGB of `Gran` 3 is correctly defined and follows with great precision the selected isochrone. We include in the Gaia CMD the PM selected stars not present within the MUSE FoV to compare the real members with our initial selection.

Because we have both their tangential and radial velocities, we are able to determine for the first time estimated orbital parameters for `Gran` 1, 2, 3 and 5. We used the galactic dynamics python package `gala` (Adrian M. Price-Whelan, 2017; A. Price-Whelan et al., 2020) allowing us to simulate the MW potential in a realistic manner, and therefore integrate the orbit of these four clusters within it. The MW potential includes a halo, a disk and a bulge using the recommended `MWPotential2014` parameters described in Bovy (2015). Additionally, we included a rotating bar, with the parameters given in Shen and Zheng (2020). We then integrated test particles with the `Gran` 1, 2, 3 and 5 space velocities to trace their orbits through the Galaxy. Integration times were short (~ 100 Myr) to visualise the clusters immediate response to the Galactic potential, as shown in
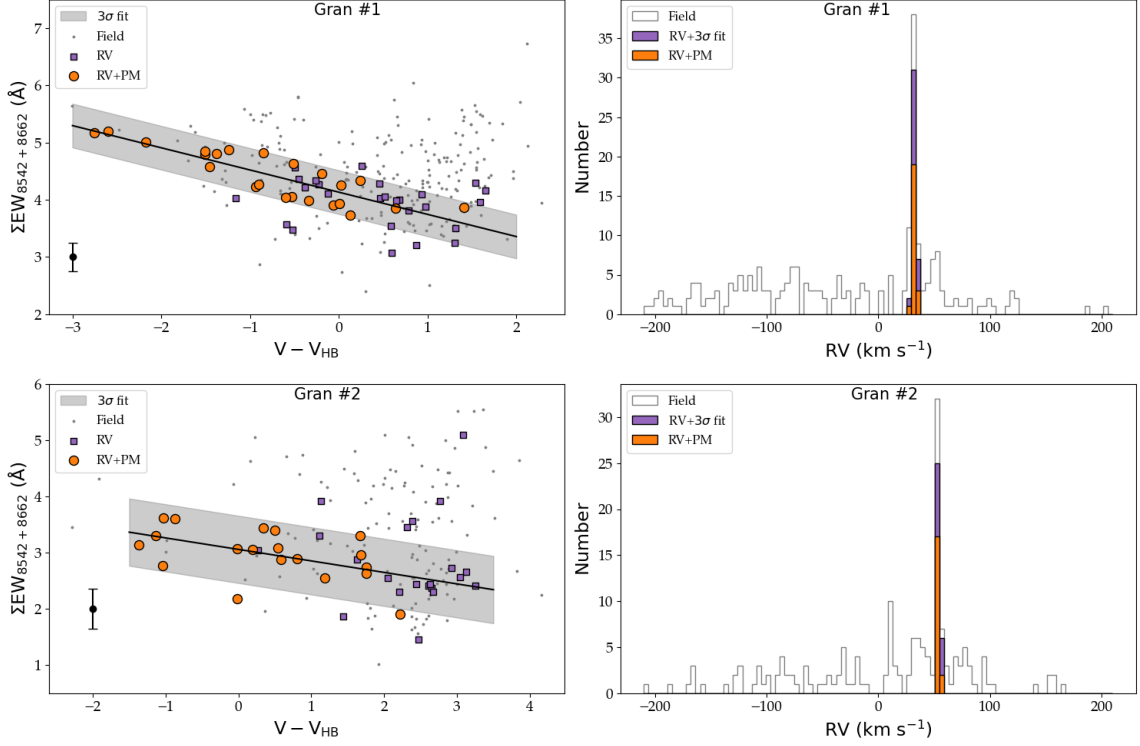
Figure 4.9: (**Upper left panel**): EW of the two most prominent lines in the CaT versus the V magnitude normalised to the HB level for the GC `Gran 1`. Circular orange symbols represent the PM-selected stars matched with the MUSE extracted spectra, purple squares show the stars selected by RV within 5 km s^{-1} from the cluster value, and grey points represent the field stars present in the cube. The error bars of the black point represent the mean EW error for the stars in the MUSE field. The line fitted to the PM-selected stars is also shown with a shaded area and is equivalent to 3 times the intercept uncertainty. (**Upper right panel**): RV histogram of all the sources in the MUSE cube colour-coded by a selection procedure: orange for the PM, purple of the stars with RV that lie within the shaded area, and grey for the field stars in the FoV. (**Upper middle left and upper middle right panels**): Same as in the upper panels but for `Gran 2`. (**Lower middle left and lower middle right panels**): Same as in the upper panels but for `Gran 3`. (**Lower left and lower right panels**): Same as in the upper panels but for `Gran 5`.
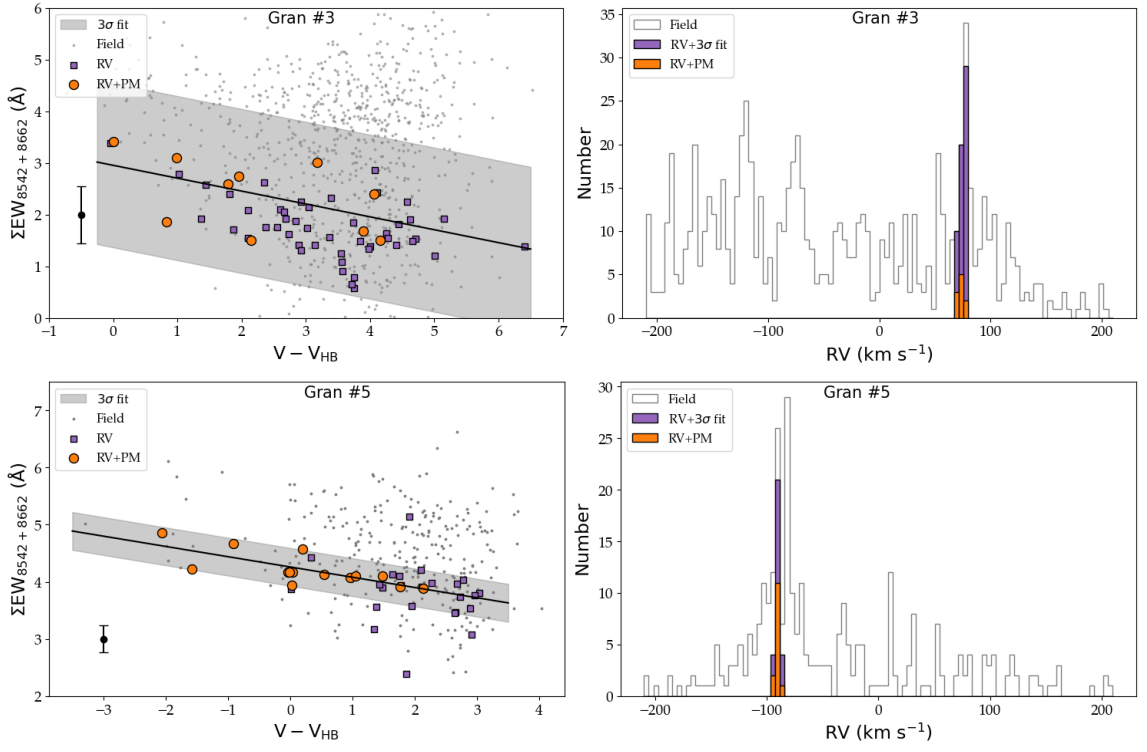
Figure 4.10: Same as Figure 4.9 but for `Gran 3` and 5.
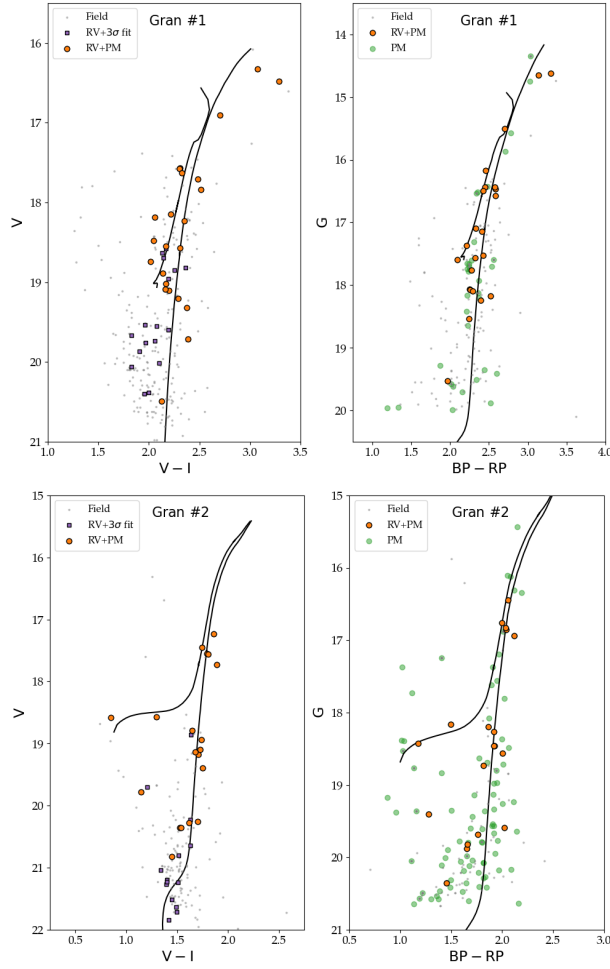
Figure 4.11: (**Upper left and upper middle left**): CMDs of `Gran` 1 with the MUSE and Gaia colours. Orange circles, purple squares and grey points stand for the PM-selected stars with available RVs, the MUSE stars with RVs similar to the cluster that also are located within the shaded area of Fig 4.9 and 4.10, and the field stars that do not correspond to the other two groups. The Gaia CMD includes the same stars with MUSE counterparts as orange circles, the Gaia-only PM selected stars as shaded green circles, and the field stars with MUSE detections. The selected PARSEC isochrones are identical for all the diagrams, with an age of 12 Gyr, and the determined cluster metallicity, shifted to the RC/HB. (**Upper middle right and upper right**): Same as in the left panels but for `Gran` 2. As can be expected for the V-band, the location of the stars at V$\sim$ 18.5 mags reveals the HB for this cluster. There are also hints of two BS stars off the isochrone. (**Lower left and lower middle left**): Same as in the left panels but for `Gran` 3. The cluster SGB is clearly visible by its characteristic shape at (V-I, V) $\sim$ (2.0, 21.5) mag. (**Lower middle right and lower right**): Same as in the left panels but for `Gran` 5. The cluster RC is visible at V$\sim$18 mag or G$\sim$17 mag.
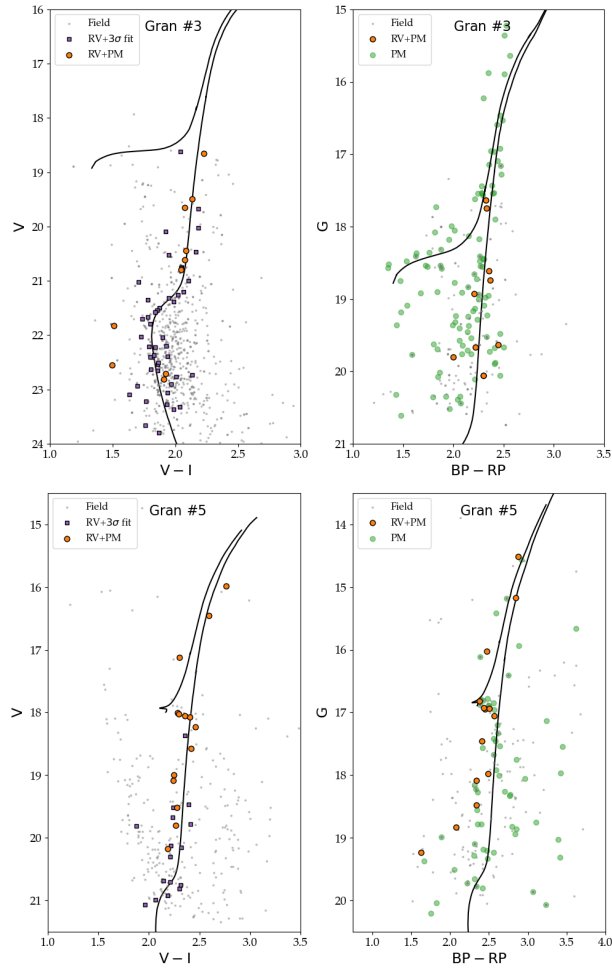
Figure 4.12: Same as Figure 4.11, but for `Gran 3` and 5.

Figure 4.13 and 4.14. A more extended integration time was also performed to calculate orbital properties such as the maximum z excursion length, the amplitude of the orbits, and the total energy and angular momentum (see Table 4.4). Note that integrated orbital properties were derived using mean cluster coordinates, PMs, and RVs. More precise values can be achieved considering its uncertainties and different Galaxy models, however, the presented values serve as a first estimate of the cluster properties.

Recently, major discoveries have been made describing some of the processes involved in the formation of the MW. Starting with the formal discovery and analysis of the Gaia-Enceladus/Sausage merger event (Belokurov et al., 2018; Helmi et al., 2018; Myeong et al., 2019), more evidence has been collected to describe the early merging history of the MW using its GCs (Myeong et al., 2018; Kruijssen et al., 2019a; Woody and Schlaufman, 2021). Following the Massari et al. (2019) definition of the different groups in the orbital energy space (E_{tot}-L_z), we assigned the most probable classification to our MUSE observed clusters. Take in consideration that orbital motions could be slightly different using another Galaxy model. According to the z-axis angular momentum and total energy of the derived orbit, we estimated that `Gran 1` belongs to the Main Progenitor or the so-called "low-energy" group, while `Gran 2, 3` and `5` appears to be related to the Gaia-Enceladus/Sausage structure. `Gran 5`, could also be related to the "low-energy" group, since its orbital parameters are located in the limits of both classifications.

4.1.12   Summary

We have detected and analysed seven new cluster candidates located towards the Galactic bulge, resulting in the discovery of five new GCs, dynamically confirmed through PMs or RVs.

All five of them exhibit narrow sequences in the CMD, coherent motion in PM-space and compact on-sky projections.

Based on the computed distances and orbits, when available, we concluded that three of
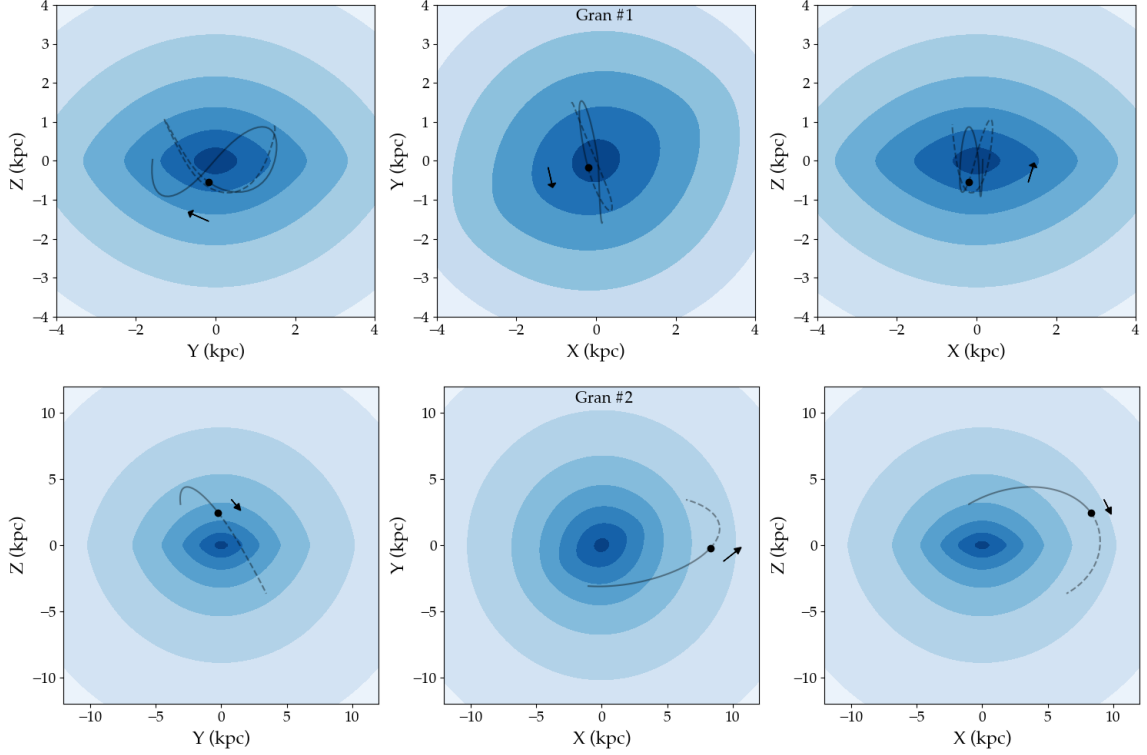
Figure 4.13: (**Upper panels**): Galactocentric cartesian projection (YZ, XY and XZ planes from left to right) of the orbit derived for `Gran 1`. An arrow represents the actual direction of the cluster in time. Backwards and forward orbit integrations through ~100 Myr are presented in solid and dashed lines, respectively. The background model contours comprise the equipotential levels of the synthetic built galaxy. The bar is clearly marked in the central parts of the projections. (**Upper middle panels**): The same as in the upper panels but for the orbit that describes `Gran 2` in the Galactocentric cartesian projection. (**Lower middle panels**): The same as in the upper panels but for the orbit that describes `Gran 3` in the Galactocentric cartesian projection. (**Lower panels**): The same as in the upper panels but for the orbit that describes `Gran 5` in the Galactocentric cartesian projection. Note that the cluster orbit is completely constrained up to a maximum Z excursion of ~0.13 kpc. As it is evident in this case from both YZ and XZ projections, the orbit is entirely confined within the Galactic plane.
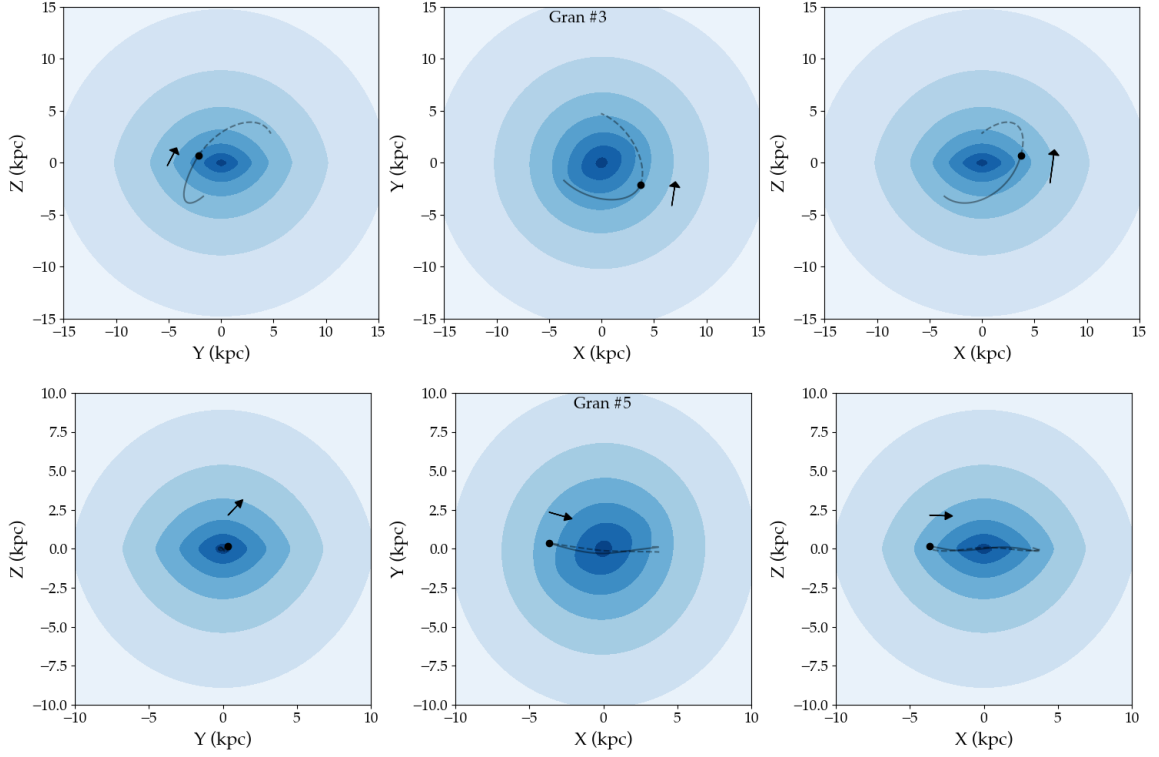
Figure 4.14: Same as Figure 4.13, but for `Gran 3` and 5.

Table 4.4: Chemodynamical parameters derived from the MUSE data. The level of the HB in each cluster is represented by V_{HB}, while the orbit eccentricity, maximum Z excursion, pericenter and apocenter radius, angular momentum in the z direction and total orbital energy, are presented by e, z_{max}, r_{peri}, r_{apo}, L_z, E_{tot}, respectively.

GC	RV	[Fe/H]	V_{HB}	e	z_{max}	r_{peri}	r_{apo}	L_z	E_{tot}
	(km s^{-1})	(dex)	(mag)		(kpc)	(kpc)	(kpc)	(kpc^2 Myr^{-1})	(kpc^2 Myr^{-2})
Gran 1	32.30 ± 1.87	-1.19 ± 0.19	19.08	0.76	0.38	0.31	2.22	0.03	-0.21
Gran 2	53.22 ± 1.67	-2.07 ± 0.17	18.59	0.34	5.44	4.59	9.24	0.79	-0.16
Gran 3	74.32 ± 2.70	-2.37 ± 0.18	18.65	0.08	3.88	4.66	5.47	0.69	-0.17
Gran 5	-90.40 ± 1.93	-1.56 ± 0.17	18.04	0.90	0.13	0.20	3.75	-0.04	-0.19

them are halo GCs (`Gran 2, 3` and 4), while `Gran 3` and 5 present bulge-like properties. MUSE cubes have been analysed to extract RVs, metallicities and orbital properties of `Gran 1, 2, 3` and 5, reconfirming their cluster nature, initially derived with Gaia PMs. With $[Fe/H] \lesssim -2$ dex and distances greater than ~ 12 kpc, `Gran 2` and 3 are clearly part of the fairly unexplored regions of the Galaxy that lie behind the bulge. Our preliminary analysis indicates that `Gran 1` is located in between the Main Progenitor and the "low-energy" group, `Gran 2` and 3 present dynamical signatures similar to the ones exhibited by the Gaia-Enceladus/Sausage structure, while `Gran 5` could be part of the Main Progenitor or the "low-energy" group.

This work proves that new GCs can be discovered in the far side of the MW, even with optical surveys and behind high extinction regions produced by the disk and bulge.

The new clusters, especially `Gran 1`, lie in the lower part of the MW GC luminosity function, an under-represented regime, as discussed in Baumgardt and Hilker (2018). Their velocity dispersions are comparable with typical known GCs, representing a low-luminosity population of objects that had escaped detection until now.

4.1.13   General software, funding acknowledgements

Data Availability: all the data used in this study is publicly available.

5

General appendix for all the chapters

5.1 General appendix for all the subsections

5.1.1 Appendix 1: APOGEE view of the globular cluster NGC 6544

Table 5.1: Identifiers and stellar parameters, $[\alpha/\text{Fe}]$, [Fe/H] and elemental abundances from the NGC 6544 members. Median values, standard deviation and mean ASPCAP errors are also derived.

APOGEE ID	Type	T_{eff} (K)	$\log g$ (dex)	V_{HELIO} (km s^{-1})	SNR	[Fe/H] (dex)	$[\alpha/\text{Fe}]$ (dex)	[C/Fe] (dex)	[N/Fe] (dex)	[O/Fe] (dex)	[Na/Fe] (dex)	[Mg/Fe] (dex)	[Al/Fe] (dex)	[Si/Fe] (dex)	[K/Fe] (dex)	[Ca/Fe] (dex)	[Ce/Fe] (dex)
2M18070312-2501429	lrgb	4949.61	2.42	-41.9	119.35	-1.47	0.16	0.23	0.47	0.23	0.11	0.17	0.30	0.22	0.75	0.23	-0.25
2M18070657-2500417	agb	4797.31	1.49	-30.9	291.71	-1.55	0.11	-0.14	0.53	0.21	—	0.12	0.25	0.16	0.42	0.24	0.28
2M18071190-2458586	lrgb	4929.79	2.27	-39.2	70.09	-1.41	0.23	0.42	0.12	0.52	0.34	0.27	0.23	0.20	-0.05	0.53	—
2M18071347-2458525	urgb	4782.61	1.95	-39.7	169.30	-1.48	0.18	-0.15	0.55	0.21	0.50	0.24	0.11	0.24	0.16	0.18	-0.17
2M18071474-2454595	lrgb	4943.43	2.17	-37.9	205.98	-1.54	0.26	0.10	0.17	0.57	0.44	0.23	-0.20	0.22	0.24	0.19	-0.79
2M18071492-2457397	agb	4819.18	1.71	-34.2	152.02	-1.62	0.29	-0.23	-0.23	0.28	—	0.31	-0.26	0.29	0.39	0.18	-0.13
2M18071622-2457231	urgb	4688.18	1.76	-51.4	206.36	-1.60	0.27	-0.27	0.21	0.37	—	0.40	-0.20	0.26	0.80	0.28	0.06
2M18071727-2504387	lrgb	5018.44	2.42	-36.6	94.82	-1.44	0.14	0.14	0.55	0.33	0.57	0.17	0.07	0.13	-0.47	0.21	0.14
2M18071947-2500517	lrgb	4986.75	2.27	-50.6	224.29	-1.46	0.23	0.10	-0.08	0.53	-0.59	0.26	-0.25	0.19	0.19	0.24	0.22
2M18072003-2502407	lrgb	5074.18	2.50	-38.5	114.17	-1.52	0.24	0.16	0.33	0.50	—	0.37	0.06	0.20	0.63	0.21	-0.84
2M18072114-2458359	lrgb	4861.69	2.23	-37.7	115.97	-1.39	0.20	0.08	0.49	0.19	0.62	0.26	0.52	0.33	0.39	0.30	-0.16
2M18072123-2502436	lrgb	5112.84	2.65	-30.5	117.47	-1.37	0.16	0.17	0.92	—	—	0.26	0.39	0.20	-0.04	-0.01	—
2M18072204-2501100	urgb	4674.79	1.73	-37.5	159.89	-1.44	0.21	-0.20	0.09	0.30	-0.13	0.22	-0.26	0.22	0.07	0.21	-0.17
2M18072226-2500325	urgb	4470.25	1.39	-38.2	492.25	-1.44	0.13	-0.36	0.83	0.19	—	0.13	0.22	0.16	0.42	0.22	0.39
2M18072230-2458509	agb	4896.84	1.74	-33.4	323.80	-1.76	0.31	-0.03	—	0.39	0.11	0.30	-0.21	0.28	0.42	0.10	—
2M18072402-2458088	lrgb	5099.30	2.51	-37.2	79.06	-1.37	0.20	0.25	0.71	—	—	0.22	0.25	0.27	0.39	0.11	—
2M18072492-2458004	agb	5062.54	1.90	-36.8	82.36	-1.71	0.21	0.06	0.03	0.21	—	0.32	0.23	0.29	—	-0.01	0.61
2M18072612-2457497	lrgb	4972.73	2.32	-42.4	99.79	-1.45	0.18	0.20	0.41	0.33	—	0.27	0.10	0.19	-0.34	0.27	-0.39
2M18072927-2502396	lrgb	4912.17	2.20	-40.2	109.95	-1.44	0.13	0.02	0.62	0.13	—	0.19	0.35	0.21	0.67	0.32	-0.93
2M18072970-2456359	urgb	4316.64	1.19	-47.1	650.68	-1.43	0.19	-0.40	0.71	0.21	0.16	0.16	-0.06	0.20	0.29	0.14	-0.53
2M18073271-2500281	lrgb	4885.97	2.16	-40.1	72.44	-1.43	0.23	-0.07	0.65	0.23	0.47	0.25	0.22	0.29	0.07	0.06	-0.97
2M18073312-2457396	lrgb	5029.56	2.35	-40.7	129.57	-1.49	0.24	0.09	-0.09	0.58	—	0.20	-0.21	0.24	0.30	0.22	0.96
2M18074298-2452101	urgb	4756.59	1.85	-36.7	226.44	-1.47	0.20	-0.09	0.09	0.31	-0.46	0.19	-0.11	0.20	0.37	0.10	0.36
Cluster median		—	—	-38.17	129.57	-1.46	0.20	0.06	0.44	0.30	0.25	0.24	0.10	0.22	0.33	0.21	-0.16
Cluster 1σ		—	—	5.10	138.04	0.10	0.05	0.20	0.31	0.14	0.38	0.07	0.23	0.05	0.31	0.11	0.52
ASPCAP mean error		113.57	0.09	0.06	—	0.02	0.02	0.05	0.07	0.05	0.13	0.03	0.03	0.02	0.10	0.06	0.11

5.1.2 Appendix 2: Globular cluster candidates in the Galactic bulge: Gaia and VVV view of the latest discoveries

Diagnostic plots of the candidate GCs found in Gaia (left side) and VVV (right side). Each panel contains the sky position (upper left), VPD (lower left), and CMD (right) for the inner 1 arcmin (highlighted in orange) and the field stars within 10 arcmins from the nominal cluster centre up to G = 19 mag. All the 93 candidate clusters but one (Minni 02) were located in the Gaia DR2 catalogue and 53 were located in our VVV catalogue. We recall that PMs are available from VVV only within latitudes $|b| < 3°$, plus a few fields where they were calculated specifically for other projects. For simplicity, this Appendix was moved to the online version due its length (100+ figures or 1800+ subplots). It can be found here in the official Open Access article: `https://www.aanda.org/articles/aa/full_html/2019/08/aa34986-18/aa34986-18.html#app`

5.1.3 Appendix 3: Hidden in the haystack: low-luminosity globular clusters towards the Milky Way bulge

Gaia (BP-RP, G) recovered CMDs of the discovered GCs.

Gaia-VVV (G-K_s, K_s) CMDs of the analysed clusters in the VVV footprint

Radial profiles of the clusters

Known GCs: BH 261 and Djorg 1

GC candidate `C1`
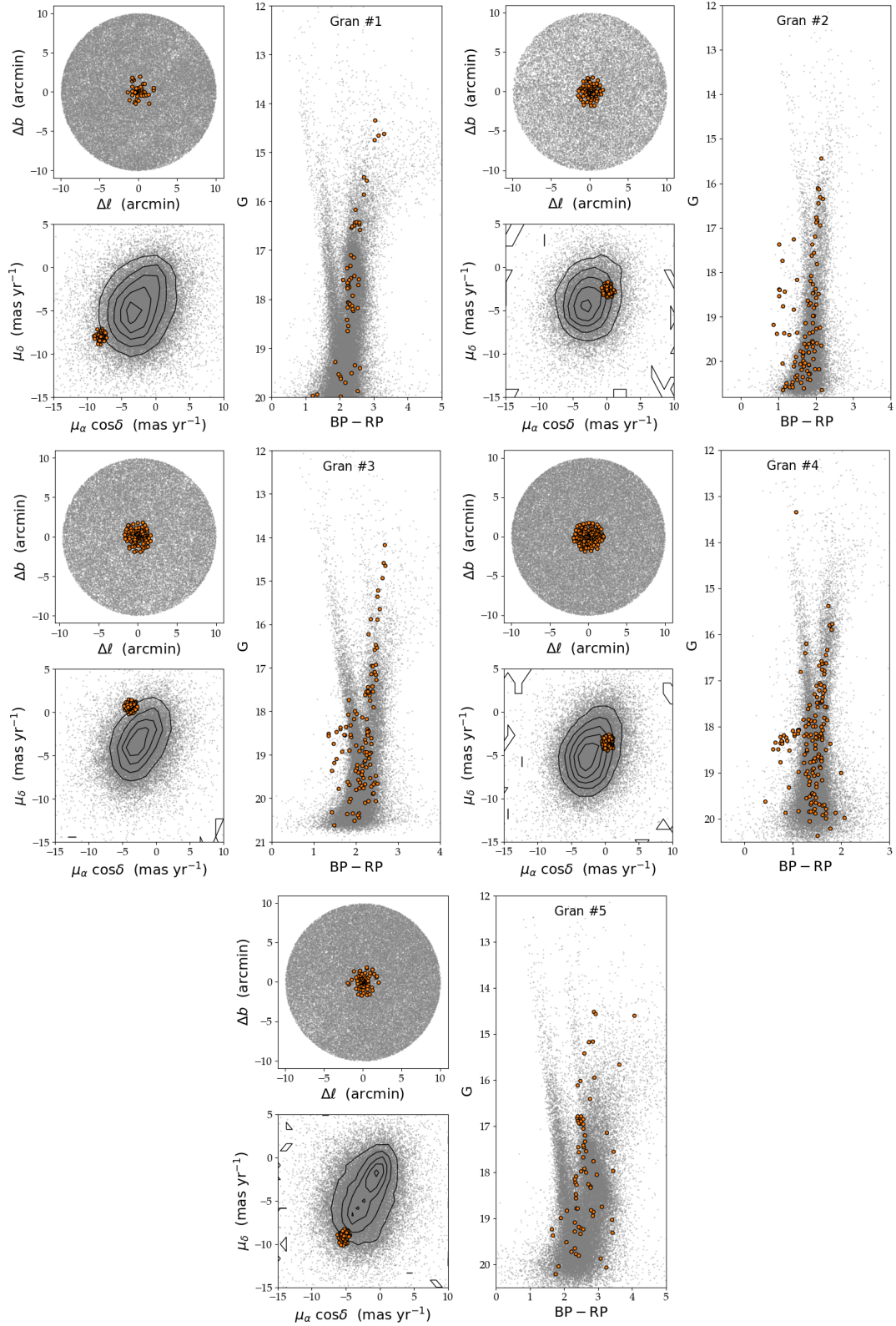
Figure 5.1: Gaia CMDs selected using only PM information. The panels follow the same structure and content as in Fig. 4.3.
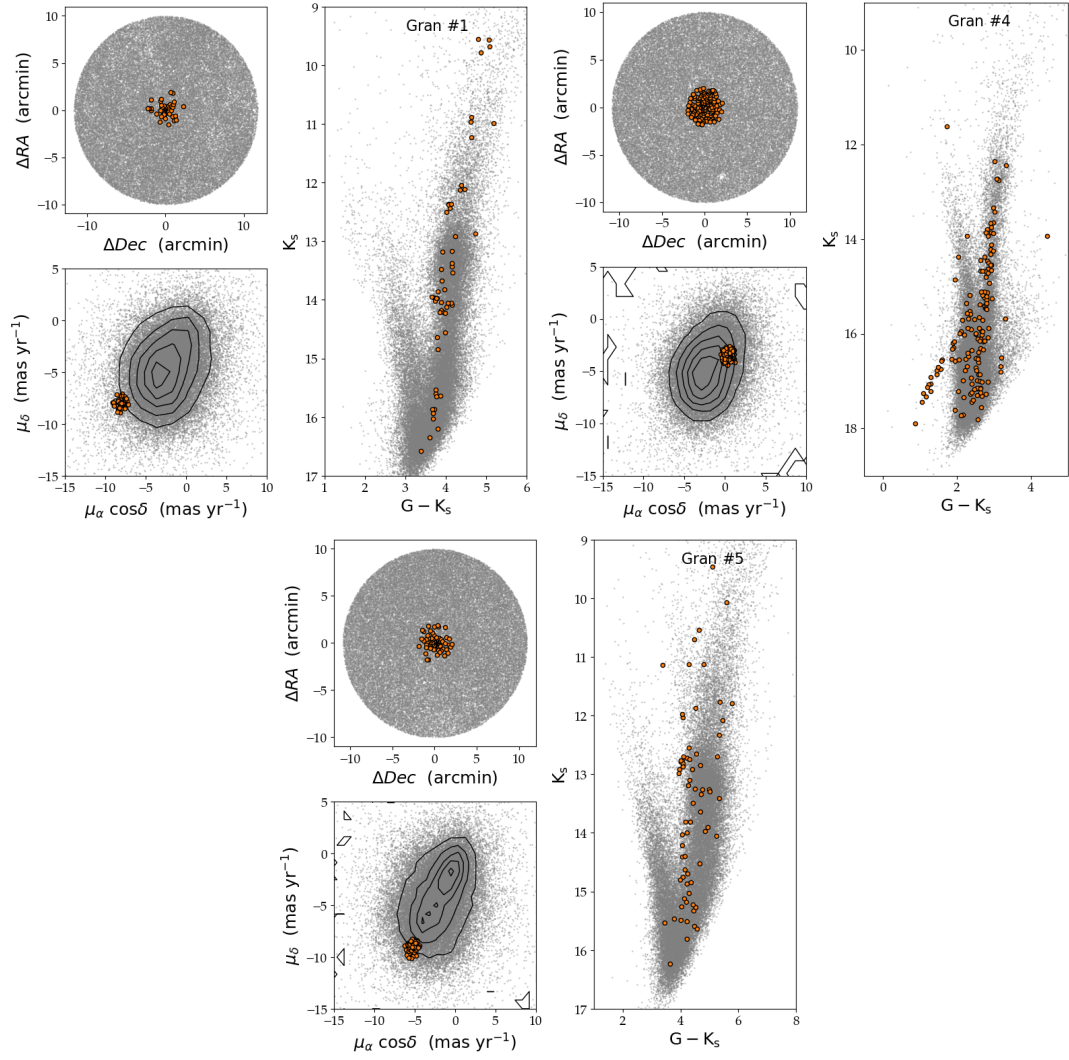
Figure 5.2: Optical-near-IR CMDs for the clusters within the VVV area. The panels follow the same structure and content as in Fig. 4.4.
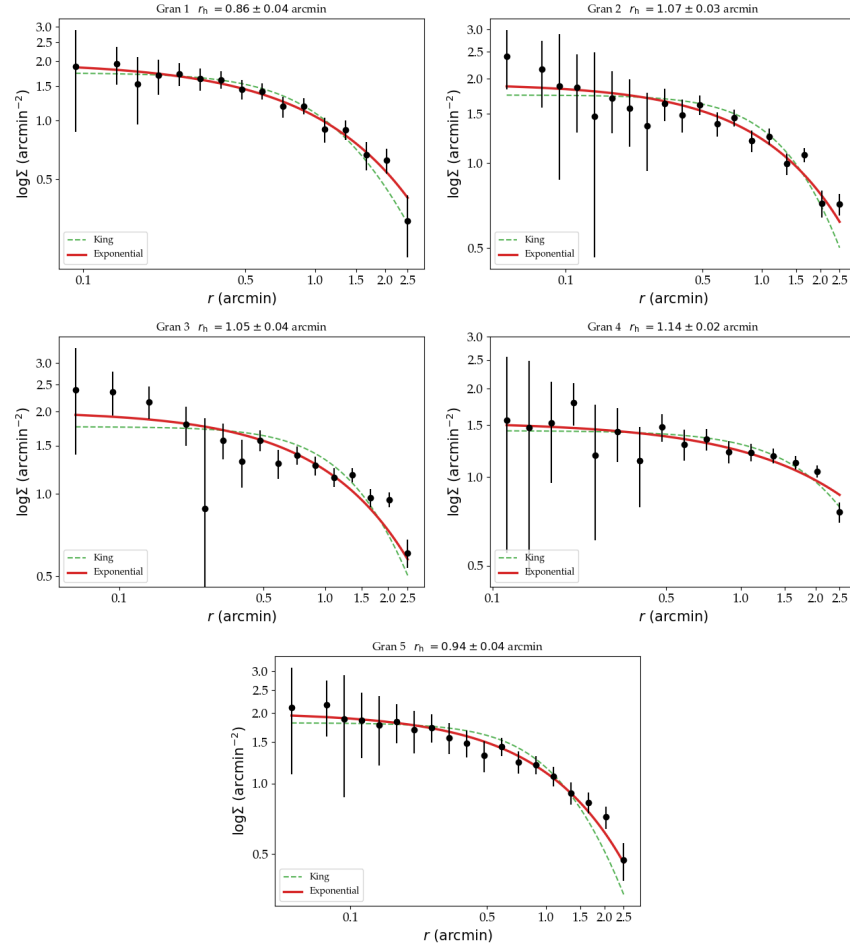
Figure 5.3: Radial luminosity profiles of the discovered clusters `Gran 1-2-3-4-5`. As explained in Sec. 4.1.8 and Fig. 4.5, the exponential profile is preferred in all the cases.
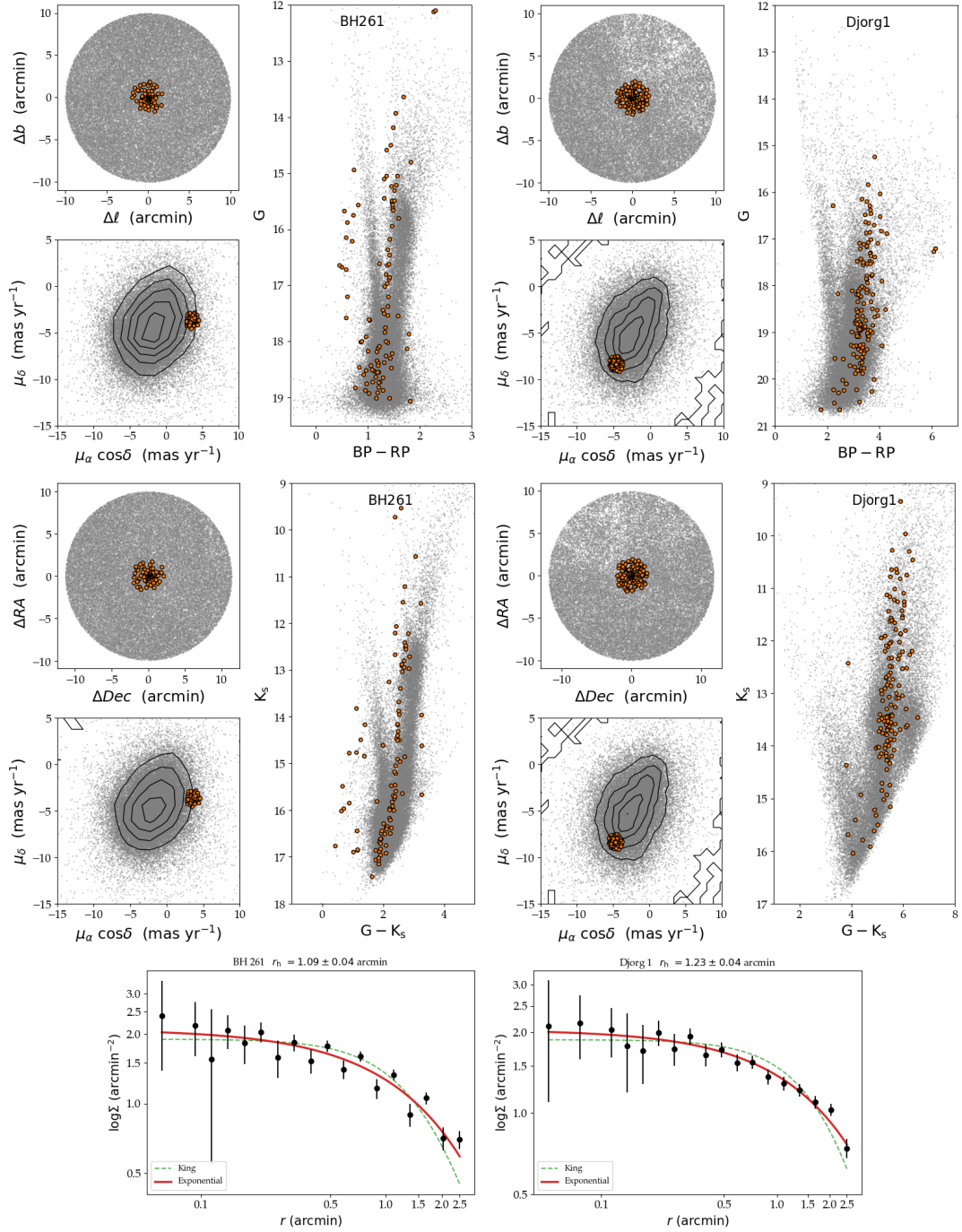
Figure 5.4: Gaia recovered CMDs for the GC BH 261 and Djorg 1 using only PM information. The panels follow the same structure and content of the Fig. 4.3, Fig. 4.4, and Fig. 4.5 for the upper, middle and lower pair of panels, respectively.
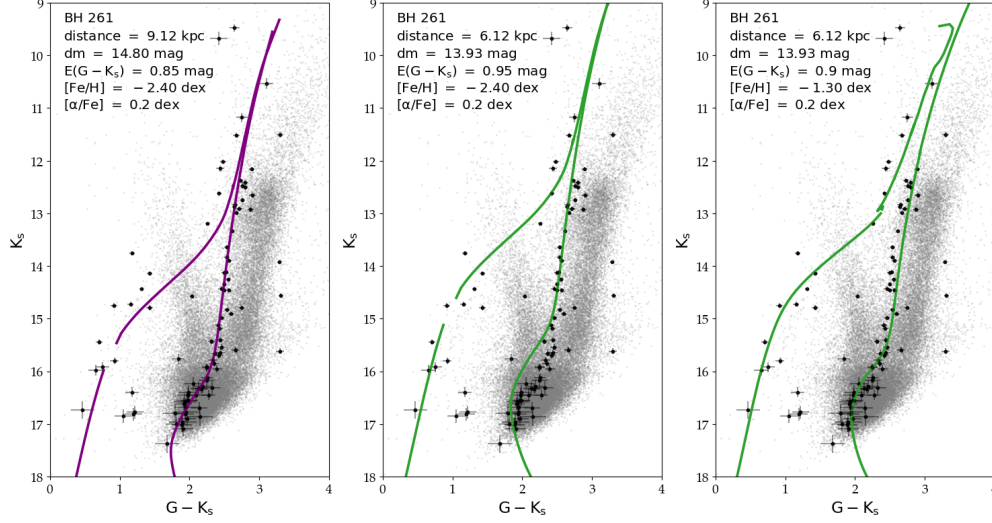
Figure 5.5: Isochrone comparison for the GC BH 261. (**Left panel**): Derived distance and metallicity of this work for the cluster (9.12 kpc and −2.4 dex) traced by a combination of a PGPUC (SGB, RGB and HB stages) and PARSEC (AGB phase) isochrones. Detailed information regarding the distance modulus, extinction value, metallicity and α-enhancement values can be found in the text within each panel. Black points with error bars and grey background represent the Gaia PM-selected cluster members and the field stars within 10 arcmin of the cluster centre, respectively. (**Middle panel**): Same as the left panel, but using the literature distance to fit the FeH = −2.4 dex isochrone. The extinction value was shifted to fit the RGB stars present in the cluster. (**Right panel**): Same as the left panel, but using the Ortolani et al. (2006) derived metallicity (−1.3 dex) and distance (6.12 kpc).
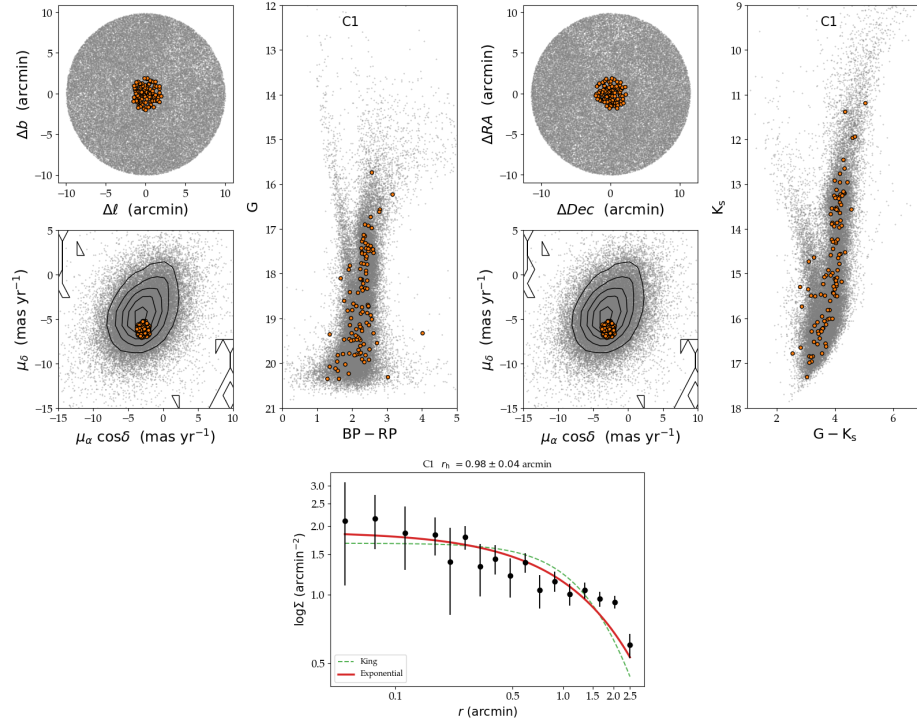
Figure 5.6: Gaia, Gaia-VVV CMDs, and radial profile of the discarded GC candidate C1. The panels follow the same structure and content of the Fig. 4.3, Fig. 4.4, and Fig. 4.5 for the upper, middle and lower pair of panels, respectively.
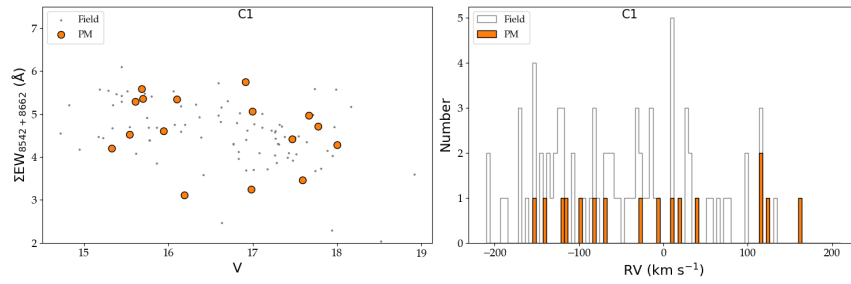
Figure 5.7: (**Left panel**): EW of the two most prominent lines in the CaT versus the V magnitude for `C1`. Circular orange symbols represent the PM-selected stars matched with the MUSE extracted spectra and grey points represent the field stars present in the cube. Note that no clear relation between the EW and V-magnitude is observed, contrary to the expected GC behaviour. (**Right panel**): RV histogram of all the sources in the MUSE cube colour-coded by a selection procedure: orange for the PM and grey for the field stars in the FoV. No RV peak is seen within the 16 matched Gaia PM-selected stars.

REFERENCES

Ahumada, R. et al. (July 2020). "The 16th Data Release of the Sloan Digital Sky Surveys: First Release from the APOGEE-2 Southern Survey and Full Release of eBOSS Spectra". In: ApJS 249.1, 3, p. 3. DOI: 10.3847/1538-4365/ab929e. arXiv: 1912.02905 [astro-ph.GA].

Alcaino, G. (Apr. 1983). "The globular cluster NGC 6544". In: A&AS 52, pp. 105–113.

Alonso-García, J. et al. (Mar. 2015). "Variable Stars in the VVV Globular Clusters. I. 2MASS-GC 02 and Terzan 10". In: AJ 149.3, 99, p. 99. DOI: 10.1088/0004-6256/149/3/99. arXiv: 1411.1696 [astro-ph.SR].

Anders, F. et al. (Aug. 2019). "Photo-astrometric distances, extinctions, and astrophysical parameters for Gaia DR2 stars brighter than G = 18". In: A&A 628, A94, A94. DOI: 10.1051/0004-6361/201935765. arXiv: 1904.11302 [astro-ph.GA].

Andrae, R. et al. (Aug. 2018). "Gaia Data Release 2. First stellar parameters from Apsis". In: A&A 616, A8, A8. DOI: 10.1051/0004-6361/201732516. arXiv: 1804.09374 [astro-ph.SR].

Andrews, A. D. and E. M. Lindsay (Dec. 1967). "New Southern Clusters and Nebulous Ovals". In: *Irish Astronomical Journal* 8, p. 126.

Armandroff, T. E. and G. S. Da Costa (Apr. 1991). "Metallicities for Old Stellar Systems from CA II Triplet Strengths in Member Giants". In: AJ 101, p. 1329. DOI: 10.1086/115769.

Arsenault, R. et al. (July 2008). "ESO adaptive optics facility". In: *Adaptive Optics Systems*. Ed. by Norbert Hubin, Claire E. Max, and Peter L. Wizinowich. Vol. 7015. Society of Photo-Optical Instrumentation Engineers (SPIE) Conference Series, 701524, p. 701524. DOI: 10.1117/12.790359.

Astropy Collaboration, A. M. Price-Whelan, et al. (Sept. 2018). "The Astropy Project: Building an Open-science Project and Status of the v2.0 Core Package". In: AJ 156.3, 123, p. 123. DOI: 10.3847/1538-3881/aabc4f. arXiv: 1801.02634 [astro-ph.IM].

Astropy Collaboration, T. P. Robitaille, et al. (Oct. 2013). "Astropy: A community Python package for astronomy". In: A&A 558, A33, A33. DOI: 10.1051/0004-6361/201322068. arXiv: 1307.6212 [astro-ph.IM].

Bacon, R. et al. (July 2010). "The MUSE second-generation VLT instrument". In: *Ground-based and Airborne Instrumentation for Astronomy III*. Ed. by Ian S. McLean, Suzanne K. Ramsay, and Hideki Takami. Vol. 7735. Society of Photo-Optical Instrumentation Engineers (SPIE) Conference Series, 773508, p. 773508. DOI: 10.1117/12.856027.

Bailin, J. (Nov. 2019). "Globular Cluster Intrinsic Iron Abundance Spreads. I. Catalog". In: ApJS 245.1, 5, p. 5. DOI: 10.3847/1538-4365/ab4812. arXiv: 1909.11731 [astro-ph.GA].

Barbuy, B. et al. (Sept. 2018). "Chemodynamical History of the Galactic Bulge". In: ARA&A 56, pp. 223–276. DOI: 10.1146/annurev-astro-081817-051826. arXiv: 1805.01142 [astro-ph.GA].

— (Apr. 2021). "Gemini/Phoenix H-band analysis of the globular cluster AL 3". In: A&A 648, A16, A16. DOI: 10.1051/0004-6361/202039761. arXiv: 2102.12674 [astro-ph.SR].

Bastian, N. and C. Lardo (Sept. 2018). "Multiple Stellar Populations in Globular Clusters". In: ARA&A 56, pp. 83–136. DOI: 10.1146/annurev-astro-081817-051839. arXiv: 1712.01286 [astro-ph.SR].

Baumgardt, H. et al. (Feb. 2019). "Mean proper motions, space orbits, and velocity dispersion profiles of Galactic globular clusters derived from Gaia DR2 data". In: MNRAS 482.4, pp. 5138–5155. DOI: 10.1093/mnras/sty2997. arXiv: 1811.01507 [astro-ph.GA].

Baumgardt, H. et al. (Nov. 2020). "Absolute V-band magnitudes and mass-to-light ratios of Galactic globular clusters". In: *PASA* 37, e046, e046. DOI: 10.1017/pasa.2020.38. arXiv: 2009.09611 [astro-ph.GA].

Baumgardt, H. and M. Hilker (Aug. 2018). "A catalogue of masses, structural parameters, and velocity dispersion profiles of 112 Milky Way globular clusters". In: MNRAS 478.2, pp. 1520–1557. DOI: 10.1093/mnras/sty1057. arXiv: 1804.08359 [astro-ph.GA].

Baumgardt, H. and E. Vasiliev (Aug. 2021). "Accurate distances to Galactic globular clusters through a combination of Gaia EDR3, HST, and literature data". In: MNRAS 505.4, pp. 5957–5977. DOI: 10.1093/mnras/stab1474. arXiv: 2105.09526 [astro-ph.GA].

Bechtol, K. et al. (July 2015). "Eight New Milky Way Companions Discovered in First-year Dark Energy Survey Data". In: ApJ 807, 50, p. 50. DOI: 10.1088/0004-637X/807/1/50. arXiv: 1503.02584.

Bellini, A. et al. (Aug. 2017). "The State-of-the-art HST Astro-photometric Analysis of the Core of ω Centauri. III. The Main Sequence's Multiple Populations Galore". In: ApJ 844.2, 164, p. 164. DOI: 10.3847/1538-4357/aa7b7e. arXiv: 1706.07063 [astro-ph.SR].

Belokurov, V. et al. (Mar. 2010). "Big Fish, Little Fish: Two New Ultra-faint Satellites of the Milky Way". In: ApJ 712, pp. L103–L106. DOI: 10.1088/2041-8205/712/1/L103. arXiv: 1002.0504.

— (July 2014). "ATLAS lifts the Cup: discovery of a new Milky Way satellite in Crater". In: MNRAS 441, pp. 2124–2133. DOI: 10.1093/mnras/stu626. arXiv: 1403.3406.

— (July 2018). "Co-formation of the disc and the stellar halo". In: MNRAS 478.1, pp. 611–619. DOI: 10.1093/mnras/sty982. arXiv: 1802.03414 [astro-ph.GA].

Benjamin, R. A. et al. (Aug. 2003). "GLIMPSE. I. An SIRTF Legacy Project to Map the Inner Galaxy". In: PASP 115.810, pp. 953–964. DOI: 10.1086/376696. arXiv: astro-ph/0306274 [astro-ph].

Bianchini, P. et al. (Aug. 2017). "The relation between the mass-to-light ratio and the relaxation state of globular clusters". In: MNRAS 469.4, pp. 4359–4369. DOI: 10.1093/mnras/stx1114. arXiv: 1705.02310 [astro-ph.GA].

Bica, E. et al. (June 2016). "Globular Clusters in the Galactic Bulge". In: *PASA* 33, e028, e028. DOI: 10.1017/pasa.2015.47. arXiv: 1510.07834 [astro-ph.SR].

— (June 2018). "A New Globular Cluster in the Area of VVVX". In: *PASA* 35, e025, e025. DOI: 10.1017/pasa.2018.24.

— (Jan. 2019). "A Multi-band Catalog of 10978 Star Clusters, Associations, and Candidates in the Milky Way". In: AJ 157.1, 12, p. 12. DOI: 10.3847/1538-3881/aaef8d. arXiv: 1812.10292 [astro-ph.GA].

Bisterzo, S. et al. (Nov. 2011). "The s-process in low-metallicity stars - II. Interpretation of high-resolution spectroscopic observations with asymptotic giant branch models". In: MNRAS 418.1, pp. 284–319. DOI: 10.1111/j.1365-2966.2011.19484.x. arXiv: 1108.0500 [astro-ph.SR].

— (May 2014). "Galactic Chemical Evolution and Solar s-process Abundances: Dependence on the ^{13}C-pocket Structure". In: ApJ 787.1, 10, p. 10. DOI: 10.1088/0004-637X/787/1/10. arXiv: 1403.1764 [astro-ph.SR].

Bland-Hawthorn, J. and O. Gerhard (Sept. 2016). "The Galaxy in Context: Structural, Kinematic, and Integrated Properties". In: ARA&A 54, pp. 529–596. DOI: 10.1146/annurev-astro-081915-023441. arXiv: 1602.07702 [astro-ph.GA].

Blanton, M. R. et al. (July 2017). "Sloan Digital Sky Survey IV: Mapping the Milky Way, Nearby Galaxies, and the Distant Universe". In: AJ 154.1, 28, p. 28. DOI: 10.3847/1538-3881/aa7567. arXiv: 1703.00052 [astro-ph.GA].

Boch, T. and P. Fernique (May 2014). "Aladin Lite: Embed your Sky in the Browser". In: *Astronomical Data Analysis Software and Systems XXIII*. Ed. by N. Manset and P. Forshay. Vol. 485. Astronomical Society of the Pacific Conference Series, p. 277.

Bonatto, C. and E. Bica (Mar. 2008). "Structural parameters of 11 faint Galactic globular clusters derived with 2MASS". In: A&A 479.3, pp. 741–750. DOI: 10.1051/0004-6361:20078687. arXiv: 0711.1434 [astro-ph].

Bonnarel, F. et al. (Apr. 2000). "The ALADIN interactive sky atlas. A reference tool for identification of astronomical sources". In: A&AS 143, pp. 33–40. DOI: 10.1051/aas:2000331.

Borissova, J. et al. (Sept. 2014). "New galactic star clusters discovered in the VVV survey. Candidates projected on the inner disk and bulge". In: A&A 569, A24, A24. DOI: 10.1051/0004-6361/201322483. arXiv: 1406.7051 [astro-ph.GA].

Boubert, D. et al. (Sept. 2020). "Completeness of the Gaia-verse - I. When and where were Gaia's eyes on the sky during DR2?" In: MNRAS 497.2, pp. 1826–1841. DOI: 10.1093/mnras/staa2050. arXiv: 2004.14433 [astro-ph.IM].

— (Feb. 2021). "Completeness of the Gaia-verse III: using hidden states to infer gaps, detection efficiencies, and the scanning law from the DR2 light curves". In: MNRAS 501.2, pp. 2954–2968. DOI: 10.1093/mnras/staa3791. arXiv: 2011.10578 [astro-ph.GA].

Boubert, D. and A. Everall (Oct. 2020). "Completeness of the Gaia verse II: what are the odds that a star is missing from Gaia DR2?" In: MNRAS 497.4, pp. 4246–4261. DOI: 10.1093/mnras/staa2305. arXiv: 2005.08983 [astro-ph.GA].

Bovy, J. (Feb. 2015). "galpy: A python Library for Galactic Dynamics". In: ApJS 216.2, 29, p. 29. DOI: 10.1088/0067-0049/216/2/29. arXiv: 1412.3451 [astro-ph.GA].

Bowen, I. S. and A. H. Vaughan (Jan. 1973). "The optical design of the 40-in. telescope and of the Irénée DuPont telescope at Las Campanas Observatory, Chile." In: Appl. Opt. 12, pp. 1430–1434. DOI: 10.1364/AO.12.001430.

Bradley, Larry et al. (Sept. 2020). *astropy/photutils: 1.0.0*. Version 1.0.0. DOI: 10.5281/zenodo.4044744. URL: https://doi.org/10.5281/zenodo.4044744.

Bressan, A. et al. (Nov. 2012). "PARSEC: stellar tracks and isochrones with the PAdova and TRieste Stellar Evolution Code". In: MNRAS 427.1, pp. 127–145. DOI: 10.1111/j.1365-2966.2012.21948.x. arXiv: 1208.4498 [astro-ph.SR].

Brown, A. G. A. (Feb. 2021). "Microarcsecond Astrometry: Science Highlights from Gaia". In: *arXiv e-prints*, arXiv:2102.11712, arXiv:2102.11712. arXiv: 2102.11712 [astro-ph.IM].

Camargo, D. (June 2018). "Five New Globular Clusters Discovered in the Galactic Bulge". In: ApJ 860, L27, p. L27. DOI: 10.3847/2041-8213/aacc68.

Cantat-Gaudin, T. et al. (Apr. 2019). "Gaia DR2 unravels incompleteness of nearby cluster population: new open clusters in the direction of Perseus". In: A&A 624, A126, A126. DOI: 10.1051/0004-6361/201834453. arXiv: 1810.05494 [astro-ph.GA].

— (Aug. 2020). "Painting a portrait of the Galactic disc with its stellar clusters". In: A&A 640, A1, A1. DOI: 10.1051/0004-6361/202038192. arXiv: 2004.07274 [astro-ph.GA].

Cantat-Gaudin, T. and F. Anders (Jan. 2020). "Clusters and mirages: cataloguing stellar aggregates in the Milky Way". In: A&A 633, A99, A99. DOI: 10.1051/0004-6361/201936691. arXiv: 1911.07075 [astro-ph.SR].

Cardelli, J. A. et al. (Oct. 1989). "The relationship between infrared, optical, and ultraviolet extinction". In: ApJ 345, pp. 245–256. DOI: 10.1086/167900.

Carlberg, R. G. (Apr. 2020). "Dynamical Simulations of the First Globular Clusters". In: ApJ 893.2, 116, p. 116. DOI: 10.3847/1538-4357/ab80bf. arXiv: 2001.00838 [astro-ph.GA].

Carretta, E. et al. (Dec. 2009a). "Intrinsic iron spread and a new metallicity scale for globular clusters". In: A&A 508.2, pp. 695–706. DOI: 10.1051/0004-6361/200913003. arXiv: 0910.0675 [astro-ph.GA].

— (Oct. 2009b). "Na-O anticorrelation and HB. VII. The chemical composition of first and second-generation stars in 15 globular clusters from GIRAFFE spectra". In: A&A 505, pp. 117–138. DOI: 10.1051/0004-6361/200912096. arXiv: 0909.2938.

Carretta, E. et al. (May 2013). "Potassium in Globular Cluster Stars: Comparing Normal Clusters to the Peculiar Cluster NGC 2419". In: ApJ 769.1, 40, p. 40. DOI: 10.1088/0004-637X/769/1/40. arXiv: 1303.4740 [astro-ph.GA].

Cassisi, S. and M. Salaris (Mar. 2013). *Old Stellar Populations: How to Study the Fossil Record of Galaxy Formation*.

Castro-Ginard, A. et al. (July 2019). "Hunting for open clusters in Gaia DR2: the Galactic anticentre". In: A&A 627, A35, A35. DOI: 10.1051/0004-6361/201935531. arXiv: 1905.06161 [astro-ph.GA].

— (Mar. 2020). "Hunting for open clusters in Gaia DR2: 582 new open clusters in the Galactic disc". In: A&A 635, A45, A45. DOI: 10.1051/0004-6361/201937386. arXiv: 2001.07122 [astro-ph.GA].

Catelan, M. et al. (Oct. 2004). "The RR Lyrae Period-Luminosity Relation. I. Theoretical Calibration". In: ApJS 154.2, pp. 633–649. DOI: 10.1086/422916. arXiv: astro-ph/0406067 [astro-ph].

Cenarro, A. J. et al. (Sept. 2001). "Empirical calibration of the near-infrared Ca ii triplet - I. The stellar library and index definition". In: MNRAS 326.3, pp. 959–980. DOI: 10.1046/j.1365-8711.2001.04688.x. arXiv: astro-ph/0109157 [astro-ph].

Chambers, K. C. et al. (Dec. 2016). "The Pan-STARRS1 Surveys". In: *arXiv e-prints*, arXiv:1612.05560, arXiv:1612.05560. arXiv: 1612.05560 [astro-ph.IM].

Chen, Y. et al. (Nov. 2014). "Improving PARSEC models for very low mass stars". In: MNRAS 444.3, pp. 2525–2543. DOI: 10.1093/mnras/stu1605. arXiv: 1409.0322 [astro-ph.SR].

— (Sept. 2015). "PARSEC evolutionary tracks of massive stars up to 350 M$_\odot$ at metallicities $0.0001 \leq Z \leq 0.04$". In: MNRAS 452.1, pp. 1068–1080. DOI: 10.1093/mnras/stv1281. arXiv: 1506.01681 [astro-ph.SR].

Churchwell, E. et al. (Mar. 2009). "The Spitzer/GLIMPSE Surveys: A New View of the Milky Way". In: PASP 121.877, p. 213. DOI: 10.1086/597811.

Cirasuolo, M. et al. (Sept. 2011). "MOONS: The Multi-Object Optical and Near-infrared Spectrograph". In: *The Messenger* 145, pp. 11–13.

Clement, C. M. et al. (Nov. 2001). "Variable Stars in Galactic Globular Clusters". In: AJ 122.5, pp. 2587–2599. DOI: 10.1086/323719. arXiv: astro-ph/0108024 [astro-ph].

Cohen, R. E. et al. (July 2014). "Photometric and Structural Properties of NGC 6544: A Combined VVV-Hubble Space Telescope Study". In: AJ 148, 18, p. 18. DOI: 10.1088/0004-6256/148/1/18.

— (Jan. 2017). "Near-infrared photometry of globular clusters towards the Galactic bulge: observations and photometric metallicity indicators". In: MNRAS 464, pp. 1874–1902. DOI: 10.1093/mnras/stw2435. arXiv: 1609.07824 [astro-ph.SR].

— (Aug. 2018). "Deep Hubble Space Telescope Imaging of Globular Clusters toward the Galactic Bulge: Observations, Data Reduction, and Color-magnitude Diagrams". In: AJ 156.2, 41, p. 41. DOI: 10.3847/1538-3881/aac889. arXiv: 1805.11150 [astro-ph.GA].

Contreras Ramos et al. (Aug. 2018). "The VVV Survey RR Lyrae Population in the Galactic Center Region". In: ApJ 863.1, 79, p. 79. DOI: 10.3847/1538-4357/aacf90. arXiv: 1807.04303 [astro-ph.GA].

Contreras Ramos, R. et al. (Dec. 2017). "Proper motions in the VVV Survey: Results for more than 15 million stars across NGC 6544". In: A&A 608, A140, A140. DOI: 10.1051/0004-6361/201731462. arXiv: 1709.07919 [astro-ph.GA].

Contreras Ramos, Rodrigo et al. (Aug. 2018). "The Orbit of the New Milky Way Globular Cluster FSR1716 = VVV-GC05". In: ApJ 863.1, 78, p. 78. DOI: 10.3847/1538-4357/aacd09. arXiv: 1807.02065 [astro-ph.GA].

Cunha, K. et al. (Aug. 2017). "Adding the s-Process Element Cerium to the APOGEE Survey: Identification and Characterization of Ce II Lines in the H-band Spectral Window". In: ApJ 844.2, 145, p. 145. DOI: 10.3847/1538-4357/aa7beb.

Czesla, S. et al. (June 2019). *PyA: Python astronomy-related packages*. ascl: 1906.010.

Davidge, T. J. (Jan. 2000). "A Near-Infrared Photometric Study of the Low-Latitude Globular Clusters Liller 1, Djorgovski 1, HP 1, and NGC 6528". In: ApJS 126.1, pp. 105–126. DOI: 10.1086/313292. arXiv: astro-ph/9909408 [astro-ph].

de Jong, R. S. et al. (Mar. 2019). "4MOST: Project overview and information for the First Call for Proposals". In: *The Messenger* 175, pp. 3–11. DOI: 10.18727/0722-6691/5117. arXiv: 1903.02464 [astro-ph.IM].

Dias, W. S. et al. (July 2002). "New catalogue of optically visible open clusters and candidates". In: A&A 389, pp. 871–873. DOI: 10.1051/0004-6361:20020668. arXiv: astro-ph/0203351 [astro-ph].

— (Apr. 2014). "Proper motions of the optically visible open clusters based on the UCAC4 catalog". In: A&A 564, A79, A79. DOI: 10.1051/0004-6361/201323226.

Djorgovski, S. (June 1987). "Discovery of Three Obscured Globular Clusters". In: ApJ 317, p. L13. DOI: 10.1086/184903.

Eisenstein, D. J. et al. (Sept. 2011). "SDSS-III: Massive Spectroscopic Surveys of the Distant Universe, the Milky Way, and Extra-Solar Planetary Systems". In: AJ 142, 72, p. 72. DOI: 10.1088/0004-6256/142/3/72. arXiv: 1101.1529 [astro-ph.IM].

Errani, R. et al. (Dec. 2018). "Systematics in virial mass estimators for pressure-supported systems". In: MNRAS 481.4, pp. 5073–5090. DOI: 10.1093/mnras/sty2505. arXiv: 1805.00484 [astro-ph.GA].

Ester, M. et al. (1996). "A density-based algorithm for discovering clusters in large spatial databases with noise". In: AAAI Press, pp. 226–231.

Evans, D. W. et al. (Aug. 2018). "Gaia Data Release 2. Photometric content and validation". In: A&A 616, A4, A4. DOI: 10.1051/0004-6361/201832756. arXiv: 1804.09368 [astro-ph.IM].

Fernández-Alvar, E. et al. (Jan. 2018). "Disentangling the Galactic Halo with APOGEE. II. Chemical and Star Formation Histories for the Two Distinct Populations". In: ApJ 852.1, 50, p. 50. DOI: 10.3847/1538-4357/aa9ced. arXiv: 1711.06225 [astro-ph.GA].

Fernández-Trincado, J. G. et al. (Dec. 2016). "Discovery of a Metal-poor Field Giant with a Globular Cluster Second-generation Abundance Pattern". In: ApJ 833.2, 132, p. 132. DOI: 10.3847/1538-4357/833/2/132. arXiv: 1604.01279 [astro-ph.GA].

— (Sept. 2017). "Atypical Mg-poor Milky Way Field Stars with Globular Cluster Second-generation-like Chemical Patterns". In: ApJ 846.1, L2, p. L2. DOI: 10.3847/2041-8213/aa8032. arXiv: 1707.03108 [astro-ph.GA].

Ferraro, F. R. et al. (Jan. 2021). "A new class of fossil fragments from the hierarchical assembly of the Galactic bulge". In: *Nature Astronomy* 5, pp. 311–318. DOI: 10.1038/s41550-020-01267-y. arXiv: 2011.09966 [astro-ph.GA].

Flewelling, H. A. et al. (Nov. 2020). "The Pan-STARRS1 Database and Data Products". In: ApJS 251.1, 7, p. 7. DOI: 10.3847/1538-4365/abb82d. arXiv: 1612.05243 [astro-ph.IM].

Forbes, D. A. and T. Bridges (May 2010). "Accreted versus in situ Milky Way globular clusters". In: MNRAS 404.3, pp. 1203–1214. DOI: 10.1111/j.1365-2966.2010.16373.x. arXiv: 1001.4289 [astro-ph.GA].

Forbes, Duncan A. et al. (Feb. 2018). "Globular cluster formation and evolution in the context of cosmological galaxy assembly: open questions". In: *Proceedings of the Royal Society of London Series A* 474.2210, 20170616, p. 20170616. DOI: 10.1098/rspa.2017.0616. arXiv: 1801.05818 [astro-ph.GA].

Gaia Collaboration, T. Antoja, et al. (May 2021). "Gaia Early Data Release 3. The Galactic anticentre". In: A&A 649, A8, A8. DOI: 10.1051/0004-6361/202039714. arXiv: 2101.05811 [astro-ph.GA].

Gaia Collaboration, A. G. A. Brown, et al. (Aug. 2018). "Gaia Data Release 2. Summary of the contents and survey properties". In: A&A 616, A1, A1. DOI: 10.1051/0004-6361/201833051. arXiv: 1804.09365 [astro-ph.GA].

— (May 2021). "Gaia Early Data Release 3. Summary of the contents and survey properties". In: A&A 649, A1, A1. DOI: 10.1051/0004-6361/202039657. arXiv: 2012.01533 [astro-ph.GA].

Gaia Collaboration, L. Eyer, et al. (Mar. 2019). "Gaia Data Release 2. Variable stars in the colour-absolute magnitude diagram". In: A&A 623, A110, A110. DOI: 10.1051/0004-6361/201833304. arXiv: 1804.09382 [astro-ph.SR].

Gaia Collaboration, A. Helmi, et al. (Aug. 2018). "Gaia Data Release 2. Kinematics of globular clusters and dwarf galaxies around the Milky Way". In: A&A 616, A12, A12. DOI: 10.1051/0004-6361/201832698. arXiv: 1804.09381 [astro-ph.GA].

Gaia Collaboration, T. Prusti, et al. (Nov. 2016). "The Gaia mission". In: A&A 595, A1, A1. DOI: 10.1051/0004-6361/201629272. arXiv: 1609.04153 [astro-ph.IM].

Gallart, C. et al. (July 2019). "Uncovering the birth of the Milky Way through accurate stellar ages with Gaia". In: *Nature Astronomy* 3, pp. 932–939. DOI: 10.1038/s41550-019-0829-5. arXiv: 1901.02900 [astro-ph.GA].

García Pérez, A. E. et al. (June 2016). "ASPCAP: The APOGEE Stellar Parameter and Chemical Abundances Pipeline". In: AJ 151, 144, p. 144. DOI: 10.3847/0004-6256/151/6/144. arXiv: 1510.07635 [astro-ph.SR].

García-Hernández, D. A. et al. (Dec. 2015). "Clear Evidence for the Presence of Second-generation Asymptotic Giant Branch Stars in Metal-poor Galactic Globular Clusters". In: ApJ 815.1, L4, p. L4. DOI: 10.1088/2041-8205/815/1/L4. arXiv: 1511.05714 [astro-ph.SR].

Garro, E. R. et al. (Oct. 2020). "VVVX-Gaia discovery of a low luminosity globular cluster in the Milky Way disk". In: A&A 642, L19, p. L19. DOI: 10.1051/0004-6361/202039233. arXiv: 2010.02113 [astro-ph.GA].

Gehrels, N. (Apr. 1986). "Confidence Limits for Small Numbers of Events in Astrophysical Data". In: ApJ 303, p. 336. DOI: 10.1086/164079.

Gran, F. et al. (July 2016). "Mapping the outer bulge with RRab stars from the VVV Survey". In: A&A 591, A145, A145. DOI: 10.1051/0004-6361/201527511. arXiv: 1604.01336 [astro-ph.GA].

Gran, F. et al. (Aug. 2019). "Globular cluster candidates in the Galactic bulge: Gaia and VVV view of the latest discoveries". In: A&A 628, A45, A45. DOI: 10.1051/0004-6361/201834986. arXiv: 1904.10872 [astro-ph.GA].

— (July 2021a). "APOGEE view of the globular cluster NGC 6544". In: MNRAS 504.3, pp. 3494–3508. DOI: 10.1093/mnras/stab1051. arXiv: 2104.05865 [astro-ph.GA].

— (Sept. 2021b). "Hidden in the Haystack: Low-luminosity globular clusters towards the Milky Way bulge". In: MNRAS. DOI: 10.1093/mnras/stab2463. arXiv: 2108.11922 [astro-ph.GA].

Gratton et al. (Sept. 2004). "Abundance Variations Within Globular Clusters". In: ARA&A 42.1, pp. 385–440. DOI: 10.1146/annurev.astro.42.053102.133945.

— (Feb. 2012). "Multiple populations in globular clusters. Lessons learned from the Milky Way globular clusters". In: A&A Rev. 20, 50, p. 50. DOI: 10.1007/s00159-012-0050-3. arXiv: 1201.6526 [astro-ph.SR].

Gratton, R. A. et al. (Nov. 2019). "What is a globular cluster? An observational perspective". In: A&A Rev. 27.1, 8, p. 8. DOI: 10.1007/s00159-019-0119-3. arXiv: 1911.02835 [astro-ph.SR].

Green, G. M. et al. (Mar. 2014). "Measuring Distances and Reddenings for a Billion Stars: Toward a 3D Dust Map from Pan-STARRS 1". In: ApJ 783.2, 114, p. 114. DOI: 10.1088/0004-637X/783/2/114. arXiv: 1401.1508 [astro-ph.GA].

— (Dec. 2019). "A 3D Dust Map Based on Gaia, Pan-STARRS 1, and 2MASS". In: ApJ 887.1, 93, p. 93. DOI: 10.3847/1538-4357/ab5362. arXiv: 1905.02734 [astro-ph.GA].

Green, Gregory M. (2018). "dustmaps: A Python interface for maps of interstellar dust". In: *Journal of Open Source Software* 3.26, p. 695. DOI: 10.21105/joss.00695. URL: https://doi.org/10.21105/joss.00695.

Gunn, J. E. et al. (Apr. 2006). "The 2.5 m Telescope of the Sloan Digital Sky Survey". In: AJ 131, pp. 2332–2359. DOI: 10.1086/500975. eprint: astro-ph/0602326.

Hajdu, G. et al. (June 2020). "On the optimal calibration of VVV photometry". In: *Experimental Astronomy* 49.3, pp. 217–238. DOI: 10.1007/s10686-020-09661-0. arXiv: 1908.06160 [astro-ph.IM].

Halley, Edmund (Jan. 1717). "Considerations on the Change of the Latitudes of Some of the Principal Fixt Stars. By Edmund Halley, R. S. Sec." In: *Philosophical Transactions of the Royal Society of London Series I* 30, pp. 736–738. DOI: 10.1098/rstl.1717.0025.

Harris, W. E. (Oct. 1996). "A Catalog of Parameters for Globular Clusters in the Milky Way". In: AJ 112, p. 1487. DOI: 10.1086/118116.

— (Dec. 2010). "A New Catalog of Globular Clusters in the Milky Way". In: *arXiv e-prints*, arXiv:1012.3224, arXiv:1012.3224. arXiv: 1012.3224 [astro-ph.GA].

Hartke, J. et al. (Dec. 2020). "MUSE+GALACSI: the first years". In: *Society of Photo-Optical Instrumentation Engineers (SPIE) Conference Series*. Vol. 11448. Society of Photo-Optical Instrumentation Engineers (SPIE) Conference Series, 114480V, p. 114480V. DOI: 10.1117/12.2560793.

Hasselquist, S. et al. (Dec. 2016). "Identification of Neodymium in the Apogee H-Band Spectra". In: ApJ 833.1, 81, p. 81. DOI: 10.3847/1538-4357/833/1/81.

Helmi, A. et al. (Oct. 2018). "The merger that led to the formation of the Milky Way's inner stellar halo and thick disk". In: Nature 563.7729, pp. 85–88. DOI: 10.1038/s41586-018-0625-x. arXiv: 1806.06038 [astro-ph.GA].

Holmberg, E. B. et al. (Jan. 1974). "The ESO/Uppsala survey of the ESO (B) atlas of the southern sky. I." In: A&AS 18, p. 463.

— (Nov. 1978). "The ESO/Uppsala survey of the ESO(B) Atlas of the Southern Sky. VI." In: A&AS 34, pp. 285–340.

Horta, D. et al. (Apr. 2020). "The chemical compositions of accreted and in situ galactic globular clusters according to SDSS/APOGEE". In: MNRAS 493.3, pp. 3363–3378. DOI: 10.1093/mnras/staa478. arXiv: 2001.03177 [astro-ph.GA].

Horta, D. et al. (Jan. 2021). "Evidence from APOGEE for the presence of a major building block of the halo buried in the inner Galaxy". In: MNRAS 500.1, pp. 1385–1403. DOI: 10.1093/mnras/staa2987. arXiv: 2007.10374 [astro-ph.GA].

Hughes, M. E. et al. (Jan. 2020). "The [α/Fe]-[Fe/H] relation in the E-MOSAICS simulations: its connection to the birth place of globular clusters and the fraction of globular cluster field stars in the bulge". In: MNRAS 491.3, pp. 4012–4022. DOI: 10.1093/mnras/stz3341. arXiv: 1912.01660 [astro-ph.GA].

Hunt, E. L. and S. Reffert (Feb. 2021). "Improving the open cluster census. I. Comparison of clustering algorithms applied to Gaia DR2 data". In: A&A 646, A104, A104. DOI: 10.1051/0004-6361/202039341. arXiv: 2012.04267 [astro-ph.GA].

Hunter, J. D. (2007). "Matplotlib: A 2D graphics environment". In: *Computing In Science & Engineering* 9.3, pp. 90–95. DOI: 10.1109/MCSE.2007.55.

Husser, T-O. et al. (Mar. 2020). "A stellar census in globular clusters with MUSE. Extending the CaT-metallicity relation below the horizontal branch and applying it to multiple populations". In: A&A 635, A114, A114. DOI: 10.1051/0004-6361/201936508. arXiv: 2001.07725 [astro-ph.SR].

Ibata, R. A. et al. (Feb. 2001). "Galactic Halo Substructure in the Sloan Digital Sky Survey: The Ancient Tidal Stream from the Sagittarius Dwarf Galaxy". In: ApJ 547.2, pp. L133–L136. DOI: 10.1086/318894. arXiv: astro-ph/0004255 [astro-ph].

— (Oct. 2018). "Phlegethon, a Nearby 75°-long Retrograde Stellar Stream". In: ApJ 865.2, 85, p. 85. DOI: 10.3847/1538-4357/aadba3. arXiv: 1806.01195 [astro-ph.GA].

Iben, Icko (Oct. 1968). "Age and Initial Helium Abundance of Stars in the Globular Cluster M15". In: Nature 220.5163, pp. 143–146. DOI: 10.1038/220143a0.

Iliadis, C. et al. (Feb. 2016). "On Potassium and Other Abundance Anomalies of Red Giants in NGC 2419". In: ApJ 818.1, 98, p. 98. DOI: 10.3847/0004-637X/818/1/98. arXiv: 1601.01359 [astro-ph.SR].

Ivans, I. I. et al. (Sept. 2001). "New Analyses of Star-to-Star Abundance Variations among Bright Giants in the Mildly Metal-poor Globular Cluster M5". In: AJ 122.3, pp. 1438–1463. DOI: 10.1086/322108. arXiv: astro-ph/0106249 [astro-ph].

Jönsson, H. et al. (Sept. 2018). "APOGEE Data Releases 13 and 14: Stellar Parameter and Abundance Comparisons with Independent Analyses". In: AJ 156.3, 126, p. 126. DOI: 10.3847/1538-3881/aad4f5. arXiv: 1807.09784 [astro-ph.SR].

— (Sept. 2020). "APOGEE Data and Spectral Analysis from SDSS Data Release 16: Seven Years of Observations Including First Results from APOGEE-South". In: AJ 160.3, 120, p. 120. DOI: 10.3847/1538-3881/aba592. arXiv: 2007.05537 [astro-ph.GA].

Kamann, S. et al. (Jan. 2013). "Resolving stellar populations with crowded field 3D spectroscopy". In: A&A 549, A71, A71. DOI: 10.1051/0004-6361/201220476. arXiv: 1211.0445 [astro-ph.IM].

Kharchenko, N. V. et al. (Oct. 2013). "Global survey of star clusters in the Milky Way. II. The catalogue of basic parameters". In: A&A 558, A53, A53. DOI: 10.1051/0004-6361/201322302. arXiv: 1308.5822 [astro-ph.GA].

— (Jan. 2016). "Global survey of star clusters in the Milky Way. V. Integrated JHK$_S$ magnitudes and luminosity functions". In: A&A 585, A101, A101. DOI: 10.1051/0004-6361/201527292.

Kim, D. and H. Jerjen (Jan. 2015). "A Hero's Little Horse: Discovery of a Dissolving Star Cluster in Pegasus". In: ApJ 799, 73, p. 73. DOI: 10.1088/0004-637X/799/1/73. arXiv: 1411.3063.

King, I. (Oct. 1962). "The structure of star clusters. I. an empirical density law". In: AJ 67, p. 471. DOI: 10.1086/108756.

Kisku, S. et al. (Feb. 2021). "An enquiry on the origins of N-rich stars in the inner Galaxy based on APOGEE chemical compositions". In: MNRAS. DOI: 10.1093/mnras/stab525. arXiv: 2102.06720 [astro-ph.GA].

Koposov, S. et al. (Nov. 2007). "The Discovery of Two Extremely Low Luminosity Milky Way Globular Clusters". In: ApJ 669, pp. 337–342. DOI: 10.1086/521422. arXiv: 0706.0019.

Koposov, S. E. et al. (Sept. 2017). "Gaia 1 and 2. A pair of new Galactic star clusters". In: MNRAS 470, pp. 2702–2709. DOI: 10.1093/mnras/stx1182. arXiv: 1702.01122.

Kruijssen, J. M. D. et al. (July 2019a). "The formation and assembly history of the Milky Way revealed by its globular cluster population". In: MNRAS 486.3, pp. 3180–3202. DOI: 10.1093/mnras/sty1609. arXiv: 1806.05680 [astro-ph.GA].

— (July 2019b). "The formation and assembly history of the Milky Way revealed by its globular cluster population". In: MNRAS 486.3, pp. 3180–3202. DOI: 10.1093/ mnras/sty1609. arXiv: 1806.05680 [astro-ph.GA].

Kruijssen, J. M. D. (June 2019). "The minimum metallicity of globular clusters and its physical origin - implications for the galaxy mass-metallicity relation and observations of proto-globular clusters at high redshift". In: MNRAS 486.1, pp. L20–L25. DOI: 10.1093/mnrasl/slz052. arXiv: 1904.09987 [astro-ph.GA].

Kundu, R. et al. (Feb. 2019a). "Search for extra-tidal RR Lyrae stars in Milky Way globular clusters from Gaia DR2". In: MNRAS 483.2, pp. 1737–1743. DOI: 10.1093/mnras/ sty3239. arXiv: 1811.11130 [astro-ph.GA].

— (Nov. 2019b). "The tale of the Milky Way globular cluster NGC 6362 - I. The orbit and its possible extended star debris features as revealed by Gaia DR2". In: MNRAS 489.4, pp. 4565–4573. DOI: 10.1093/mnras/stz2500. arXiv: 1909.02016 [astro-ph.GA].

Laevens, B. P. M. et al. (May 2014). "A New Distant Milky Way Globular Cluster in the Pan-STARRS1 3π Survey". In: ApJ 786, L3, p. L3. DOI: 10.1088/2041-8205/786/1/L3. arXiv: 1403.6593.

— (Apr. 2015a). "A New Faint Milky Way Satellite Discovered in the Pan-STARRS1 3π Survey". In: ApJ 802, L18, p. L18. DOI: 10.1088/2041-8205/802/2/L18. arXiv: 1503.05554.

Laevens, B. P. M. et al. (Nov. 2015b). "Sagittarius II, Draco II and Laevens 3: Three New Milky Way Satellites Discovered in the Pan-STARRS 1 3π Survey". In: ApJ 813, 44, p. 44. DOI: 10.1088/0004-637X/813/1/44. arXiv: 1507.07564.

Lapenna, E. et al. (Dec. 2014). "Non-local Thermodynamical Equilibrium Effects on the Iron Abundance of Asymptotic Giant Branch Stars in 47 Tucanae". In: ApJ 797.2, 124, p. 124. DOI: 10.1088/0004-637X/797/2/124.

— (Nov. 2015). "Chemical Analysis of Asymptotic Giant Branch Stars in M62". In: ApJ 813.2, 97, p. 97. DOI: 10.1088/0004-637X/813/2/97. arXiv: 1509.08917 [astro-ph.SR].

Laporte, C. F. P. et al. (Feb. 2022). "Kinematics beats dust: unveiling nested substructure in the perturbed outer disc of the Milky Way". In: MNRAS 510.1, pp. L13–L17. DOI: 10.1093/mnrasl/slab109. arXiv: 2103.12737 [astro-ph.GA].

Lardo, C. et al. (Dec. 2012). "Carbon and nitrogen abundances of stellar populations in the globular cluster M 2". In: A&A 548, A107, A107. DOI: 10.1051/0004-6361/201220129. arXiv: 1210.2566 [astro-ph.SR].

Lauberts, A. (1982). *ESO/Uppsala survey of the ESO(B) atlas*.

Leaman, R. et al. (Nov. 2013). "The bifurcated age-metallicity relation of Milky Way globular clusters and its implications for the accretion history of the galaxy". In: MNRAS 436.1, pp. 122–135. DOI: 10.1093/mnras/stt1540. arXiv: 1309.0822 [astro-ph.GA].

Leigh, N. et al. (May 2012). "Quantifying the universality of the stellar initial mass function in old star clusters". In: MNRAS 422, pp. 1592–1600. DOI: 10.1111/j.1365-2966.2012.20735.x. arXiv: 1202.2851 [astro-ph.SR].

Lindegren, L. et al. (Aug. 2018). "Gaia Data Release 2. The astrometric solution". In: A&A 616, A2, A2. DOI: 10.1051/0004-6361/201832727. arXiv: 1804.09366 [astro-ph.IM].

— (May 2021). "Gaia Early Data Release 3. The astrometric solution". In: A&A 649, A2, A2. DOI: 10.1051/0004-6361/202039709. arXiv: 2012.03380 [astro-ph.IM].

Luque, E. et al. (June 2017). "The Dark Energy Survey view of the Sagittarius stream: discovery of two faint stellar system candidates". In: MNRAS 468, pp. 97–108. DOI: 10.1093/mnras/stx405. arXiv: 1608.04033.

Mackey, A. D. and G. F. Gilmore (Dec. 2004). "Comparing the properties of local globular cluster systems: implications for the formation of the Galactic halo". In: MNRAS 355.2, pp. 504–534. DOI: 10.1111/j.1365-2966.2004.08343.x. arXiv: astro-ph/0408404 [astro-ph].

Mainzer, A. et al. (Apr. 2011). "Preliminary Results from NEOWISE: An Enhancement to the Wide-field Infrared Survey Explorer for Solar System Science". In: ApJ 731.1, 53, p. 53. DOI: 10.1088/0004-637X/731/1/53. arXiv: 1102.1996 [astro-ph.EP].

Majewski, S. R. et al. (Sept. 2017). "The Apache Point Observatory Galactic Evolution Experiment (APOGEE)". In: AJ 154, 94, p. 94. DOI: 10.3847/1538-3881/aa784d. arXiv: 1509.05420 [astro-ph.IM].

Marigo, P. et al. (Jan. 2017). "A New Generation of PARSEC-COLIBRI Stellar Isochrones Including the TP-AGB Phase". In: ApJ 835.1, 77, p. 77. DOI: 10.3847/1538-4357/835/1/77. arXiv: 1701.08510 [astro-ph.SR].

Massari, D. et al. (Oct. 2019). "Origin of the system of globular clusters in the Milky Way". In: A&A 630, L4, p. L4. DOI: 10.1051/0004-6361/201936135. arXiv: 1906.08271 [astro-ph.GA].

Masseron, T. et al. (May 2016). *BACCHUS: Brussels Automatic Code for Characterizing High accUracy Spectra*. ascl: 1605.004.

— (Feb. 2019). "Homogeneous analysis of globular clusters from the APOGEE survey with the BACCHUS code. I. The northern clusters". In: A&A 622, A191, A191. DOI: 10.1051/0004-6361/201834550. arXiv: 1812.08817 [astro-ph.SR].

McLaughlin, D. E. and R. P. van der Marel (Dec. 2005). "Resolved Massive Star Clusters in the Milky Way and Its Satellites: Brightness Profiles and a Catalog of Fundamental Parameters". In: ApJS 161, pp. 304–360. DOI: 10.1086/497429. eprint: astro-ph/0605132.

Mészáros, S. et al. (May 2015). "Exploring Anticorrelations and Light Element Variations in Northern Globular Clusters Observed by the APOGEE Survey". In: AJ 149, 153, p. 153. DOI: 10.1088/0004-6256/149/5/153. arXiv: 1501.05127 [astro-ph.SR].

— (Feb. 2020). "Homogeneous analysis of globular clusters from the APOGEE survey with the BACCHUS code - II. The Southern clusters and overview". In: MNRAS 492.2, pp. 1641–1670. DOI: 10.1093/mnras/stz3496. arXiv: 1912.04839 [astro-ph.SR].

Minniti, D. (Apr. 1995). "Metal-Rich Globular Clusters with R</=3 KPC: Disk or Bulge Clusters?" In: AJ 109, p. 1663. DOI: 10.1086/117393.

Minniti, D. et al. (July 2010). "VISTA Variables in the Via Lactea (VVV): The public ESO near-IR variability survey of the Milky Way". In: *New A* 15.5, pp. 433–443. DOI: 10.1016/j.newast.2009.12.002. arXiv: 0912.1056 [astro-ph.GA].

— (Mar. 2011a). "Discovery of VVV CL001. A low-mass globular cluster next to UKS 1 in the direction of the Galactic bulge". In: A&A 527, A81, A81. DOI: 10.1051/0004-6361/201015795. arXiv: 1012.2450 [astro-ph.GA].

— (June 2011b). "The Edge of the Milky Way Stellar Disk Revealed Using Clump Giant Stars as Distance Indicators". In: ApJ 733.2, L43, p. L43. DOI: 10.1088/2041-8205/733/2/L43. arXiv: 1105.3151 [astro-ph.GA].

— (Dec. 2017a). "New Metal-poor Globular Clusters in the Galactic Bulge: The Elephant Graveyard". In: *Research Notes of the American Astronomical Society* 1.1, 16, p. 16. DOI: 10.3847/2515-5172/aa9ab7.

— (Nov. 2017b). "New VVV Survey Globular Cluster Candidates in the Milky Way Bulge". In: ApJ 849.2, L24, p. L24. DOI: 10.3847/2041-8213/aa95b8.

— (Dec. 2017c). "The Elephant Graveyard: 24 New Globular Cluster Candidates in the Galactic Bulge". In: *Research Notes of the American Astronomical Society* 1.1, 54, p. 54. DOI: 10.3847/2515-5172/aaa3ed.

— (Dec. 2017d). "The Elephant Graveyard: 24 New Globular Cluster Candidates in the Galactic Bulge". In: *Research Notes of the American Astronomical Society* 1.1, 54, p. 54. DOI: 10.3847/2515-5172/aaa3ed.

Moni Bidin, C. et al. (Nov. 2011). "Three Galactic globular cluster candidates". In: A&A 535, A33, A33. DOI: 10.1051/0004-6361/201117488. arXiv: 1109.1854 [astro-ph.GA].

Mucciarelli, A. et al. (Aug. 2015a). "A Chemical Trompe-L'oeil: No Iron Spread in the Globular Cluster M22". In: ApJ 809.2, 128, p. 128. DOI: 10.1088/0004-637X/809/2/128. arXiv: 1507.01596 [astro-ph.SR].

— (Mar. 2015b). "The Origin of the Spurious Iron Spread in the Globular Cluster NGC 3201". In: ApJ 801.1, 69, p. 69. DOI: 10.1088/0004-637X/801/1/69. arXiv: 1501.01968 [astro-ph.SR].

— (Apr. 2017). "The potassium abundance in the globular clusters NGC 104, NGC 6752 and NGC 6809". In: A&A 600, A104, A104. DOI: 10.1051/0004-6361/201730410. arXiv: 1702.02953 [astro-ph.SR].

Muñoz, R. R. et al. (July 2012). "The Discovery of an Ultra-faint Star Cluster in the Constellation of Ursa Minor". In: ApJ 753, L15, p. L15. DOI: 10.1088/2041-8205/753/1/L15. arXiv: 1204.5750.

Muraveva, T. et al. (July 2015). "New Near-infrared Period-Luminosity-Metallicity Relations for RR Lyrae Stars and the Outlook for Gaia". In: ApJ 807, 127, p. 127. DOI: 10.1088/0004-637X/807/2/127. arXiv: 1505.06001 [astro-ph.SR].

Myeong, G. C. et al. (Aug. 2018). "The Sausage Globular Clusters". In: ApJ 863.2, L28, p. L28. DOI: 10.3847/2041-8213/aad7f7. arXiv: 1805.00453 [astro-ph.GA].

— (Sept. 2019). "Evidence for two early accretion events that built the Milky Way stellar halo". In: MNRAS 488.1, pp. 1235–1247. DOI: 10.1093/mnras/stz1770. arXiv: 1904.03185 [astro-ph.GA].

Nataf, D. M. et al. (July 2019). "The Relationship between Globular Cluster Mass, Metallicity, and Light-element Abundance Variations". In: AJ 158.1, 14, p. 14. DOI: 10.3847/1538-3881/ab1a27. arXiv: 1904.07884 [astro-ph.SR].

Navarrete, C. et al. (May 2015). "Updated census of RR Lyrae stars in the globular cluster ω Centauri (NGC 5139)". In: A&A 577, A99, A99. DOI: 10.1051/0004-6361/201424838. arXiv: 1501.02286 [astro-ph.SR].

Nidever, D. L. et al. (Dec. 2015). "The Data Reduction Pipeline for the Apache Point Observatory Galactic Evolution Experiment". In: AJ 150, 173, p. 173. DOI: 10.1088/0004-6256/150/6/173. arXiv: 1501.03742 [astro-ph.IM].

Nishiyama, S. et al. (May 2009). "Interstellar Extinction Law Toward the Galactic Center III: J, H, K_S Bands in the 2MASS and the MKO Systems, and 3.6, 4.5, 5.8, 8.0 μm in the Spitzer/IRAC System". In: ApJ 696.2, pp. 1407–1417. DOI: 10.1088/0004-637X/696/2/1407. arXiv: 0902.3095 [astro-ph.GA].

Ochsenbein, F. et al. (Apr. 2000). "The VizieR database of astronomical catalogues". In: A&AS 143, pp. 23–32. DOI: 10.1051/aas:2000169. arXiv: astro-ph/0002122 [astro-ph].

Oliveira, R. A. P. et al. (Mar. 2020). "The Hubble Space Telescope UV Legacy Survey of Galactic Globular Clusters. XX. Ages of Single and Multiple Stellar Populations in Seven Bulge Globular Clusters". In: ApJ 891.1, 37, p. 37. DOI: 10.3847/1538-4357/ab6f76. arXiv: 2001.08611 [astro-ph.GA].

Ortolani, S. et al. (Apr. 1995). "Two reddened globular clusters projected close to the galactic center: Palomar 6 and Djorgovski 1." In: A&A 296, p. 680.

— (Oct. 1999). "HST observations of Terzan 1: a second parameter globular cluster in the galactic bulge". In: A&A 350, pp. 840–846.

— (Aug. 2006). "AL 3 (BH 261): A New Globular Cluster in the Galaxy". In: ApJ 646.2, pp. L115–L118. DOI: 10.1086/507108. arXiv: astro-ph/0606718 [astro-ph].

— (Nov. 2012). "Kronberger 49: A New Low-mass Globular Cluster or an Unprecedented Bulge Window?" In: AJ 144, 147, p. 147. DOI: 10.1088/0004-6256/144/5/147.

— (Feb. 2019). "Halo intruders in the Galactic bulge revealed by HST and Gaia: the globular clusters Terzan 10 and Djorgovski 1". In: A&A 622, A94, A94. DOI: 10.1051/0004-6361/201834477. arXiv: 1901.03574 [astro-ph.SR].

Palma, T. et al. (Aug. 2019). "Analysis of the physical nature of 22 New VVV Survey Globular Cluster candidates in the Milky Way bulge". In: MNRAS 487.3, pp. 3140–3149. DOI: 10.1093/mnras/stz1489. arXiv: 1905.11835 [astro-ph.GA].

Pancino, E. et al. (May 2017). "Globular clusters with Gaia". In: MNRAS 467.1, pp. 412–427. DOI: 10.1093/mnras/stx079. arXiv: 1701.03003 [astro-ph.GA].

Pastorelli, G. et al. (June 2019). "Constraining the thermally pulsing asymptotic giant branch phase with resolved stellar populations in the Small Magellanic Cloud". In: MNRAS 485.4, pp. 5666–5692. DOI: 10.1093/mnras/stz725. arXiv: 1903.04499 [astro-ph.SR].

Pedregosa, F. et al. (2011). "Scikit-learn: Machine Learning in Python". In: *Journal of Machine Learning Research* 12, pp. 2825–2830.

Pérez, Fernando and Brian E. Granger (May 2007). "IPython: a System for Interactive Scientific Computing". In: *Computing in Science and Engineering* 9.3, pp. 21–29. ISSN: 1521-9615. DOI: 10.1109/MCSE.2007.53. URL: https://ipython.org.

Pérez-Villegas, A. et al. (Jan. 2020). In: MNRAS 491.3, pp. 3251–3265. DOI: 10.1093/mnras/stz3162. arXiv: 1911.05207 [astro-ph.GA].

Perryman, Michael (Oct. 2012). "The history of astrometry". In: *European Physical Journal H* 37.5, pp. 745–792. DOI: 10.1140/epjh/e2012-30039-4. arXiv: 1209.3563 [physics.hist-ph].

Pietrukowicz, P. et al. (Oct. 2015). "Deciphering the 3D Structure of the Old Galactic Bulge from the OGLE RR Lyrae Stars". In: ApJ 811.2, 113, p. 113. DOI: 10.1088/0004-637X/811/2/113. arXiv: 1412.4121 [astro-ph.GA].

Prantzos, N. et al. (July 2007). "Light nuclei in galactic globular clusters: constraints on the self-enrichment scenario from nucleosynthesis". In: A&A 470, pp. 179–190. DOI: 10.1051/0004-6361:20077205. arXiv: 0704.3331.

Price-Jones, N. et al. (Aug. 2020). "Strong chemical tagging with APOGEE: 21 candidate star clusters that have dissolved across the Milky Way disc". In: MNRAS 496.4,

pp. 5101–5115. DOI: 10.1093/mnras/staa1905. arXiv: 2004.04263 [astro-ph.GA].

Price-Whelan, A. M. et al. (June 2016). "Spending Too Much Time at the Galactic Bar: Chaotic Fanning of the Ophiuchus Stream". In: ApJ 824.2, 104, p. 104. DOI: 10.3847/0004-637X/824/2/104. arXiv: 1601.06790 [astro-ph.GA].

Price-Whelan, Adrian et al. (Oct. 2020). *adrn/gala: v1.3*. Version v1.3. DOI: 10.5281/zenodo.4159870. URL: https://doi.org/10.5281/zenodo.4159870.

Price-Whelan, Adrian M. (2017). "Gala: A Python package for galactic dynamics". In: *Journal of Open Source Software* 2.18, p. 388. DOI: 10.21105/joss.00388. URL: https://doi.org/10.21105/joss.00388.

Queiroz, A. B. A. et al. (May 2018). "StarHorse: a Bayesian tool for determining stellar masses, ages, distances, and extinctions for field stars". In: MNRAS 476.2, pp. 2556–2583. DOI: 10.1093/mnras/sty330. arXiv: 1710.09970 [astro-ph.IM].

Ramos, P. et al. (Dec. 2021). "The Sagittarius stream in Gaia eDR3 and the origin of the bifurcations". In: *arXiv e-prints*, arXiv:2112.02105, arXiv:2112.02105. arXiv: 2112.02105 [astro-ph.GA].

Reid, M. J. and A. Brunthaler (Dec. 2004). "The Proper Motion of Sagittarius A*. II. The Mass of Sagittarius A*". In: ApJ 616, pp. 872–884. DOI: 10.1086/424960. eprint: astro-ph/0408107.

Renzini, A. (Nov. 2008). "Origin of multiple stellar populations in globular clusters and their helium enrichment". In: MNRAS 391, pp. 354–362. DOI: 10.1111/j.1365-2966.2008.13892.x. arXiv: 0808.4095.

Renzini, A. et al. (Dec. 2015). "The Hubble Space TelescopeUV Legacy Survey of Galactic Globular Clusters - V. Constraints on formation scenarios". In: MNRAS 454, pp. 4197–4207. DOI: 10.1093/mnras/stv2268. arXiv: 1510.01468.

Renzini, A. (July 2017). "Finding forming globular clusters at high redshifts". In: MNRAS 469.1, pp. L63–L67. DOI: 10.1093/mnrasl/slx057. arXiv: 1704.04883 [astro-ph.GA].

Riello, M. et al. (Aug. 2018). "Gaia Data Release 2. Processing of the photometric data". In: A&A 616, A3, A3. DOI: 10.1051/0004-6361/201832712. arXiv: 1804.09367 [astro-ph.IM].

Roming, P. W. A. et al. (Oct. 2005). "The Swift Ultra-Violet/Optical Telescope". In: Space Sci. Rev. 120.3-4, pp. 95–142. DOI: 10.1007/s11214-005-5095-4. arXiv: astro-ph/0507413 [astro-ph].

Rossi, L. J. et al. (July 2015). "Proper motions and kinematics of selected bulge globular clusters". In: MNRAS 450.3, pp. 3270–3288. DOI: 10.1093/mnras/stv748. arXiv: 1504.01743 [astro-ph.GA].

Ruiz-Lara, T. et al. (May 2020). "The recurrent impact of the Sagittarius dwarf on the star formation history of the Milky Way". In: *Nature Astronomy* 4, pp. 965–973. DOI: 10.1038/s41550-020-1097-0. arXiv: 2003.12577 [astro-ph.GA].

Rutledge, G. A. et al. (Aug. 1997). "Galactic Globular Cluster Metallicity Scale from the Ca II Triplet I. Catalog". In: PASP 109, pp. 883–906. DOI: 10.1086/133958. arXiv: astro-ph/9707067 [astro-ph].

Ryu, J. and M. G. Lee (Aug. 2018). "Discovery of Two New Globular Clusters in the Milky Way". In: ApJ 863, L38, p. L38. DOI: 10.3847/2041-8213/aad8b7. arXiv: 1808.03455.

Saito, R. K. et al. (Jan. 2012). "VVV DR1: The first data release of the Milky Way bulge and southern plane from the near-infrared ESO public survey VISTA variables in the Vía Láctea". In: A&A 537, A107, A107. DOI: 10.1051/0004-6361/201118407. arXiv: 1111.5511 [astro-ph.GA].

Salaris, M. et al. (Dec. 2007). "Deep near-infrared photometry of the globular cluster 47 Tucanae. Reconciling theory and observations". In: A&A 476.1, pp. 243–253. DOI: 10.1051/0004-6361:20078445.

Saracino, S. et al. (June 2015). "GEMINI/GeMS Observations Unveil the Structure of the Heavily Obscured Globular Cluster Liller 1." In: ApJ 806.2, 152, p. 152. DOI: 10.1088/0004-637X/806/2/152. arXiv: 1505.00568 [astro-ph.SR].

Saviane, I. et al. (Apr. 2012). "Homogeneous metallicities and radial velocities for Galactic globular clusters. First CaT metallicities for twenty clusters". In: A&A 540, A27, A27. DOI: 10.1051/0004-6361/201118138. arXiv: 1202.1304.

Schiavon, R. P. et al. (Apr. 2017). "APOGEE chemical abundances of globular cluster giants in the inner Galaxy". In: MNRAS 466, pp. 1010–1018. DOI: 10.1093/mnras/stw3093. arXiv: 1611.03086.

Shen, J. and X. Zheng (Oct. 2020). "The bar and spiral arms in the Milky Way: structure and kinematics". In: *Research in Astronomy and Astrophysics* 20.10, 159, p. 159. DOI: 10.1088/1674-4527/20/10/159. arXiv: 2012.10130 [astro-ph.GA].

Shetrone, M. et al. (Dec. 2015). "The SDSS-III APOGEE Spectral Line List for H-band Spectroscopy". In: ApJS 221, 24, p. 24. DOI: 10.1088/0067-0049/221/2/24. arXiv: 1502.04080 [astro-ph.IM].

Skrutskie, M. F. et al. (Feb. 2006). "The Two Micron All Sky Survey (2MASS)". In: AJ 131.2, pp. 1163–1183. DOI: 10.1086/498708.

Smith, V. V. et al. (Mar. 2021). "The APOGEE Data Release 16 Spectral Line List". In: *arXiv e-prints*, arXiv:2103.10112, arXiv:2103.10112. arXiv: 2103.10112 [astro-ph.SR].

Sneden, C. et al. (Sept. 2008). "Neutron-capture elements in the early galaxy." In: ARA&A 46, pp. 241–288. DOI: 10.1146/annurev.astro.46.060407.145207.

Soszyński, I. et al. (Sept. 2014). "Over 38000 RR Lyrae Stars in the OGLE Galactic Bulge Fields". In: *Acta Astron.* 64.3, pp. 177–196. arXiv: 1410.1542 [astro-ph.SR].

— (Dec. 2019). "Over 78 000 RR Lyrae Stars in the Galactic Bulge and Disk from the OGLE Survey". In: *Acta Astron.* 69.4, pp. 321–337. DOI: 10.32023/0001-5237/69.4.2. arXiv: 2001.00025 [astro-ph.SR].

Souza, S. O. et al. (Feb. 2020). "Self-consistent Analysis of Stellar Clusters: An Application to HST Data of the Halo Globular Cluster NGC 6752". In: ApJ 890.1, 38, p. 38. DOI: 10.3847/1538-4357/ab6a0f. arXiv: 2001.02697 [astro-ph.SR].

Ströbele, S. et al. (July 2012). "GALACSI system design and analysis". In: *Adaptive Optics Systems III*. Ed. by Brent L. Ellerbroek, Enrico Marchetti, and Jean-Pierre Véran. Vol. 8447. Society of Photo-Optical Instrumentation Engineers (SPIE) Conference Series, 844737, p. 844737. DOI: 10.1117/12.926110.

— (Dec. 2020). "Overview on wavefront corrector technologies for astronomy and solar adaptive optics systems". In: *Society of Photo-Optical Instrumentation Engineers (SPIE) Conference Series*. Vol. 11448. Society of Photo-Optical Instrumentation Engineers (SPIE) Conference Series, 114481B, 114481B. DOI: 10.1117/12.2561224.

Stuik, R. et al. (Jan. 2006). "GALACSI The ground layer adaptive optics system for MUSE". In: *New A Rev.* 49.10-12, pp. 618–624. DOI: 10.1016/j.newar.2005.10.015.

Surot, F. et al. (Mar. 2019). "Mapping the stellar age of the Milky Way bulge with the VVV. I. The method". In: A&A 623, A168, A168. DOI: 10.1051/0004-6361/201833550. arXiv: 1902.01695 [astro-ph.GA].

— (Dec. 2020). "Mapping the stellar age of the Milky Way bulge with the VVV. III. High-resolution reddening map". In: A&A 644, A140, A140. DOI: 10.1051/0004-6361/202038346. arXiv: 2010.02723 [astro-ph.GA].

Tang, J. et al. (Dec. 2014). "New PARSEC evolutionary tracks of massive stars at low metallicity: testing canonical stellar evolution in nearby star-forming dwarf galaxies". In: MNRAS 445.4, pp. 4287–4305. DOI: 10.1093/mnras/stu2029. arXiv: 1410.1745 [astro-ph.SR].

Taylor, M. B. (Dec. 2005). "TOPCAT & STIL: Starlink Table/VOTable Processing Software". In: *Astronomical Data Analysis Software and Systems XIV*. Ed. by P. Shopbell, M. Britton, and R. Ebert. Vol. 347. Astronomical Society of the Pacific Conference Series, p. 29.

team, The pandas development (Feb. 2020). *pandas-dev/pandas: Pandas*. Version latest. DOI: 10.5281/zenodo.3509134. URL: https://doi.org/10.5281/zenodo.3509134.

The HIPPARCOS and TYCHO catalogues. Astrometric and photometric star catalogues derived from the ESA HIPPARCOS Space Astrometry Mission (Jan. 1997). Vol. 1200. ESA Special Publication.

Thévenin, F. and T. P. Idiart (Aug. 1999). "Stellar Iron Abundances: Non-LTE Effects". In: ApJ 521.2, pp. 753–763. DOI: `10.1086/307578`. arXiv: `astro-ph/9906433 [astro-ph]`.

Tonry, J. L. et al. (May 2012). "The Pan-STARRS1 Photometric System". In: ApJ 750.2, 99, p. 99. DOI: `10.1088/0004-637X/750/2/99`. arXiv: `1203.0297 [astro-ph.IM]`.

Valcarce, A. A. R. et al. (Nov. 2012). "Effects of helium enrichment in globular clusters. I. Theoretical plane with PGPUC stellar evolution code". In: A&A 547, A5, A5. DOI: `10.1051/0004-6361/201219510`. arXiv: `1208.5127 [astro-ph.SR]`.

Valenti, E. et al. (Apr. 2007). "Near-Infrared Properties of 24 Globular Clusters in the Galactic Bulge". In: AJ 133, pp. 1287–1301. DOI: `10.1086/511271`. eprint: `astro-ph/0612280`.

— (Mar. 2010). "Near-infrared properties of 12 globular clusters towards the inner bulge of the Galaxy". In: MNRAS 402, pp. 1729–1739. DOI: `10.1111/j.1365-2966.2009.15991.x`. arXiv: `0911.1264`.

van Altena, W. F. et al. (1995). *The general catalogue of trigonometric [stellar] parallaxes*.

van den Bergh, S. and G. L. Hagen (Jan. 1975). "Uniform survey of clusters in the southern Milky Way." In: AJ 80, pp. 11–16. DOI: `10.1086/111707`.

Vasiliev, E. (Apr. 2019a). "Proper motions and dynamics of the Milky Way globular cluster system from Gaia DR2". In: MNRAS 484.2, pp. 2832–2850. DOI: `10.1093/mnras/stz171`. arXiv: `1807.09775 [astro-ph.GA]`.

— (Apr. 2019b). "Proper motions and dynamics of the Milky Way globular cluster system from Gaia DR2". In: MNRAS 484.2, pp. 2832–2850. DOI: `10.1093/mnras/stz171`. arXiv: `1807.09775 [astro-ph.GA]`.

Vasiliev, E. and H. Baumgardt (Feb. 2021). "Gaia EDR3 view on Galactic globular clusters". In: *arXiv e-prints*, arXiv:2102.09568, arXiv:2102.09568. arXiv: `2102.09568` `[astro-ph.GA]`.

Vásquez, S. et al. (Aug. 2015). "Calcium triplet metallicity calibration for stars in the Galactic bulge". In: A&A 580, A121, A121. DOI: `10.1051/0004-6361/201526534`. arXiv: `1507.00425 [astro-ph.GA]`.

— (Nov. 2018). "Homogeneous metallicities and radial velocities for Galactic globular clusters. II. New CaT metallicities for 28 distant and reddened globular clusters". In: A&A 619, A13, A13. DOI: `10.1051/0004-6361/201833525`. arXiv: `1808.03834` `[astro-ph.GA]`.

Ventura, P. et al. (Dec. 2012). "Super-AGB-AGB Evolution and the Chemical Inventory in NGC 2419". In: ApJ 761.2, L30, p. L30. DOI: `10.1088/2041-8205/761/2/L30`. arXiv: `1211.3857 [astro-ph.SR]`.

Virtanen, P. et al. (2020). "SciPy 1.0: Fundamental Algorithms for Scientific Computing in Python". In: *Nature Methods* 17, pp. 261–272. DOI: `10.1038/s41592-019-0686-2`.

Walt S.; Colbert, S. C. van der and G. Varoquaux (Mar. 2011). "The NumPy Array: A Structure for Efficient Numerical Computation". In: *Computing in Science and Engineering* 13.2, pp. 22–30. ISSN: 1521-9615. DOI: `10.1109/MCSE.2011.37`. URL: `http://numpy.org`.

Wang, S. and X. Chen (June 2019). "The Optical to Mid-infrared Extinction Law Based on the APOGEE, Gaia DR2, Pan-STARRS1, SDSS, APASS, 2MASS, and WISE Surveys". In: ApJ 877.2, 116, p. 116. DOI: `10.3847/1538-4357/ab1c61`. arXiv: `1904.04575 [astro-ph.GA]`.

Watkins, L. L. et al. (Apr. 2015). "Hubble Space Telescope Proper Motion (HSTPROMO) Catalogs of Galactic Globular Cluster. II. Kinematic Profiles and Maps". In: ApJ 803, 29, p. 29. DOI: `10.1088/0004-637X/803/1/29`. arXiv: `1502.00005`.

Webb, J. J. and R. G. Carlberg (Apr. 2021). "The likelihood of undiscovered globular clusters in the outskirts of the Milky Way". In: MNRAS 502.3, pp. 4547–4557. DOI: 10.1093/mnras/stab353. arXiv: 2012.08535 [astro-ph.GA].

Webb, J. J. and N. W. C. Leigh (Nov. 2015). "Back to the future: estimating initial globular cluster masses from their present-day stellar mass functions". In: MNRAS 453, pp. 3278–3287. DOI: 10.1093/mnras/stv1780. arXiv: 1508.00577.

Wenger, M. et al. (Apr. 2000). "The SIMBAD astronomical database. The CDS reference database for astronomical objects". In: A&AS 143, pp. 9–22. DOI: 10.1051/aas:2000332. arXiv: astro-ph/0002110 [astro-ph].

Wilson, J. C. et al. (July 2010). "The Apache Point Observatory Galactic Evolution Experiment (APOGEE) high-resolution near-infrared multi-object fiber spectrograph". In: *Ground-based and Airborne Instrumentation for Astronomy III*. Vol. 7735. Proc. SPIE, 77351C, p. 77351C. DOI: 10.1117/12.856708.

— (Sept. 2012). "Performance of the Apache Point Observatory Galactic Evolution Experiment (APOGEE) high-resolution near-infrared multi-object fiber spectrograph". In: *Ground-based and Airborne Instrumentation for Astronomy IV*. Vol. 8446. Proc. SPIE, 84460H, 84460H. DOI: 10.1117/12.927140.

— (May 2019). "The Apache Point Observatory Galactic Evolution Experiment (APOGEE) Spectrographs". In: PASP 131.999, p. 055001. DOI: 10.1088/1538-3873/ab0075. arXiv: 1902.00928 [astro-ph.IM].

Woody, T. and K. C. Schlaufman (Aug. 2021). "The Age-Metallicity-Specific Orbital Energy Relation for the Milky Way's Globular Cluster System Confirms the Importance of Accretion for Its Formation". In: AJ 162.2, 42, p. 42. DOI: 10.3847/1538-3881/abff5f. arXiv: 2104.10697 [astro-ph.GA].

Wright, E. L. et al. (Dec. 2010). "The Wide-field Infrared Survey Explorer (WISE): Mission Description and Initial On-orbit Performance". In: AJ 140.6, pp. 1868–1881. DOI: 10.1088/0004-6256/140/6/1868. arXiv: 1008.0031 [astro-ph.IM].

Zasowski, G. et al. (Oct. 2013). "Target Selection for the Apache Point Observatory Galactic Evolution Experiment (APOGEE)". In: AJ 146, 81, p. 81. DOI: 10.1088/0004-6256/146/4/81. arXiv: 1308.0351.

— (Nov. 2017). "Target Selection for the SDSS-IV APOGEE-2 Survey". In: AJ 154.5, 198, p. 198. DOI: 10.3847/1538-3881/aa8df9. arXiv: 1708.00155 [astro-ph.GA].

— (Jan. 2019). "APOGEE DR14/DR15 Abundances in the Inner Milky Way". In: ApJ 870.2, 138, p. 138. DOI: 10.3847/1538-4357/aaeff4. arXiv: 1811.01097 [astro-ph.GA].

Zoccali, M. (Aug. 2019). "The Stellar Population, 3D structure, and kinematics of the Galactic bulge". In: *Boletin de la Asociacion Argentina de Astronomia La Plata Argentina* 61, pp. 137–144.